AN ELECTROSTATIC PRECIPITATOR
PERFORMANCE MODEL

RESEARCH REPORTING SERIES

Research reports of the Office of Research and Development, U. S. Environmental Protection Agency, have been grouped into series. These broad categories were established to facilitate further development and application of environmental technology. Elimination of traditional grouping was consciously planned to foster technology transfer and maximum interface in related fields. These series are:

1. ENVIRONMENTAL HEALTH EFFECTS RESEARCH
2. ENVIRONMENTAL PROTECTION TECHNOLOGY
3. ECOLOGICAL RESEARCH
4. ENVIRONMENTAL MONITORING
5. SOCIOECONOMIC ENVIRONMENTAL STUDIES
6. SCIENTIFIC AND TECHNICAL ASSESSMENT REPORTS
9. MISCELLANEOUS

This report has been assigned to the ENVIRONMENTAL PROTECTION TECHNOLOGY series. This series describes research performed to develop and demonstrate instrumentation, equipment and methodology to repair or prevent environmental degradation from point and non-point sources of pollution. This work provides the new or improved technology required for the control and treatment of pollution sources to meet environmental quality standards.

AN ELECTROSTATIC PRECIPITATOR PERFORMANCE MODEL

by

Grady B. Nichols and John P. Gooch

Southern Research Institute
2000 Ninth Avenue South
Birmingham, Alabama 35205

Control Systems Laboratory
National Environmental Research Center
Research Triangle Park, North Carolina 27711

Prepared for

OFFICE OF RESEARCH AND DEVELOPMENT
U.S. ENVIRONMENTAL PROTECTION AGENCY
WASHINGTON, D.C. 20460

July 1972

EPA REVIEW NOTICE

TABLE OF CONTENTS

-i-

LIST OF FIGURES

LIST OF FIGURES (Continued)

-v-

LIST OF TABLES

ENVIRONMENTAL PROTECTION AGENCY REVIEW NOTICE

This report has been reviewed by EPA and approved for publication. Approval does not signify that the contents necessarily reflect the views and policies of EPA, nor does the mention of trade names or commercial products constitute endorsement or recommendation for use.

ACKNOWLEDGEMENTS

ABSTRACT

The objectives of the study covered by this report were:
1) extend the precipitator computer model to include factors
not included in the first model influencing its accuracy,
2) design and build a pilot precipitator for further studies
of the factors influencing precipitation processes, 3) to
review limitations to precipitator performance due to back
corona and sparking, 4) to investigate particle concentration
profile in the interelectrode space, 5) obtain data from both
field and pilot plant tests to attempt to verify the computer
model, and 6) analyze potential for optimizing precipitator
performance by design or operating modifications.

This report reviews the design details of the pilot
precipitator and the results of particle concentration profile
studies. Discussions of measurement of resistivity and
correlations between resistivity and precipitator operation
are also reviewed.

AN ELECTROSTATIC PRECIPITATOR PERFORMANCE MODEL

INTRODUCTION

This is the final report under Contract CPA 70-166, covering a study of an electrostatic precipitator performance model. The purposes of this study were to analyze some of the critical factors limiting precipitator performance, to establish quantitative relationships between precipitator performance and these factors, and to review operating experience and costs to determine the influence of gas temperature on overall system economics and problems related to the tendency toward corrosion and fouling of the air heater and precipitator.

In carrying out this program, a small-scale precipitator was designed and constructed to permit studies to be made of precipitator fundamentals, such as the effect of charging time, relation of particle distribution in the interelectrode space to collection efficiency, reentrainment factors, etc. This report outlines the results of these fundamental studies utilizing the pilot precipitator. These studies provide a more thorough understanding of the basic precipitation process in addition to providing a basis for estimating precipitator performance based upon dust characteristics and precipitator operating parameters.

In addition to the small-scale precipitator studies, operation of several full-scale plants was reviewed, particularly the plants where unusual problems were encountered. Many of these problems involved dust resistivity, both high and low values. In attempting to correlate resistivities with precipitator performance, it was found that resistivities determined by various methods differed by such a wide margin that no analysis was possible without a better understanding of resistivity measurement techniques. Measurements were made at several power stations burning different types of coal in an effort to compare resistivities measured by several types of apparatus and to provide data for analysis of precipitator performance.

Finally, the mathematical precipitator model developed under Contract CPA 22-69-73 was upgraded by providing refinements that were not included in the initial simplified version. This model includes some input from the small- and full-scale precipitators to determine how closely the predicted and experimental values matched.

The various studies carried out under this contract can be grouped into categories which include the development of a pilot-scale precipitator model, fundamental studies of the precipitation process, reentrainment, refinement of the precipitator mathematical model, economics of collecting high resistivity dusts, and studies of problems of low temperature corrosion and fouling.

SECTION 1. DEVELOPMENT OF A PILOT-SCALE PRECIPITATOR

A. Purpose for Building

An electrostatic precipitator can be described in terms of the system input variables and subfunctions as shown in Figure 1.1. The complexity of the system precludes a detailed evaluation of each subfunction in full-scale precipitators operating on industrial processes because of both the costs and difficulty in controlling variables in industrial operations. Thus, it was desirable to construct a general purpose precipitator with sufficient flexibility to provide a means for experimentally investigating the effects of modifications to individual system subfunctions.

In addition to providing a tool for evaluating the effects of variations of the system inputs and variables, a pilot-scale precipitator provides the means for evaluating a computer systems analysis model for describing precipitator behavior. A preliminary computer model of an electrostatic precipitator system which was developed under a previous contract was modified under this program. The purpose of this modification, as described in Section 4, was to upgrade the model to more closely predict the behavior of physical precipitator systems.

Thus, the purpose for constructing a pilot-scale precipitator is twofold:

- it provides a means for evaluating the effects of modifying subsystem inputs and variables on precipitator performance, and

- it provides an easily controlled physical model to provide data for evaluating the computer systems model of an electrostatic precipitator.

B. Philosophy of Design

The pilot-scale precipitator constructed for this project is fundamentally a research tool. Therefore, the design philosophy utilized is based on the three considerations of flexibility, accuracy, and utility. The flexibility requirement is necessary because of the wide range of possible operating configurations available. The accuracy requirement is important because of the significance of the conclusions that may be drawn from the
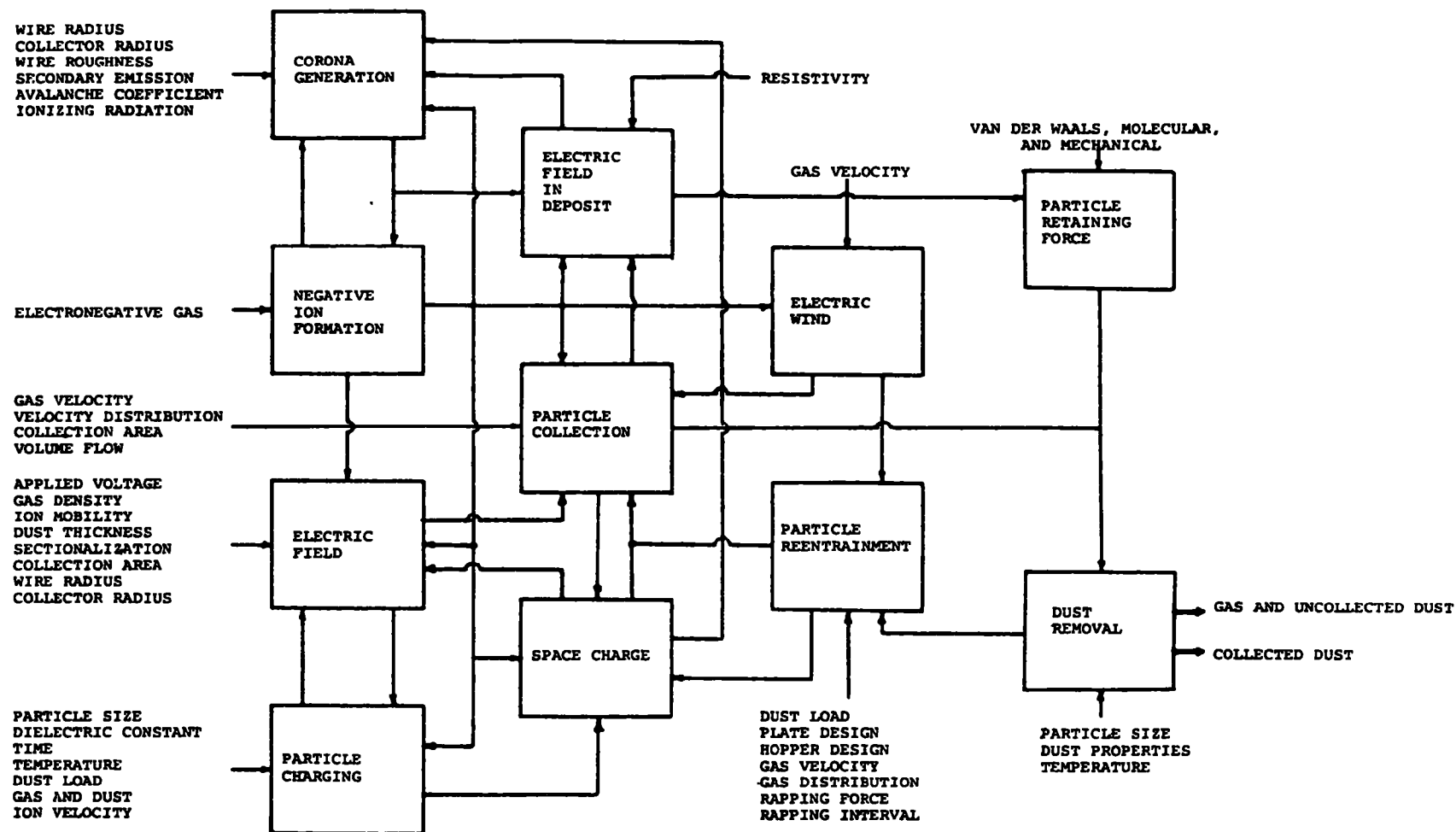
Figure 1.1. Electrostatic Precipitator System Model

experiments conducted with the apparatus, and the utility requirement is dictated by the need to minimize the manpower required to conduct tests and change conditions between tests.

In addition to the above requirements, it is important for the general configuration of the pilot unit to be similar to existing full-scale collectors. This factor is important since the pilot unit was used to evaluate a computer systems model that ultimately is planned to be used for evaluating full-scale precipitator systems.

C.   Design Requirements and Details

A precipitator system can be described in terms of the fixed and variable parameters that are associated with the mechanical and electrical components of the installation. Since this device is fundamentally a research tool, the fixed parameters were intentionally kept at a minimum, while the variable parameters were allowed as much range as was thought to be practical.

The general layout of the pilot precipitator is shown in the photograph in Figure 1.2. The electrical power supply controls are located above and to the rear of the precipitator proper. The air inlet, dust feed, and temperature controls are located at the right of the photograph; and the fan, velocity control, and measurement systems are located at the left side. The collection hoppers are shown between the precipitator support structure in the lower center.

1.   Mechanical design

The mechanical configuration of the pilot model precipitator is shown in Figure 1.3. The air is introduced into the electrical heater section (11-E) at the inlet. The gas flows into a rotary mixing section (10-C) where the dust from the dispenser system (21-B) is fed into the gas stream through a paddle wheel fan (21-D) and then into a venturi mixing chamber (13-A).

The gas stream then flows through Sections 11-C and 10-A where devices for generating a more nearly uniform gas stream are located. The gas flows from these sections through the 4-section precipitator, the rectangular-to-circular transition (10-B), the flow control orifice (1007), the velocity control unit (12-A), out through the induced draft fan (2045), and is subsequently emitted to the atmosphere.
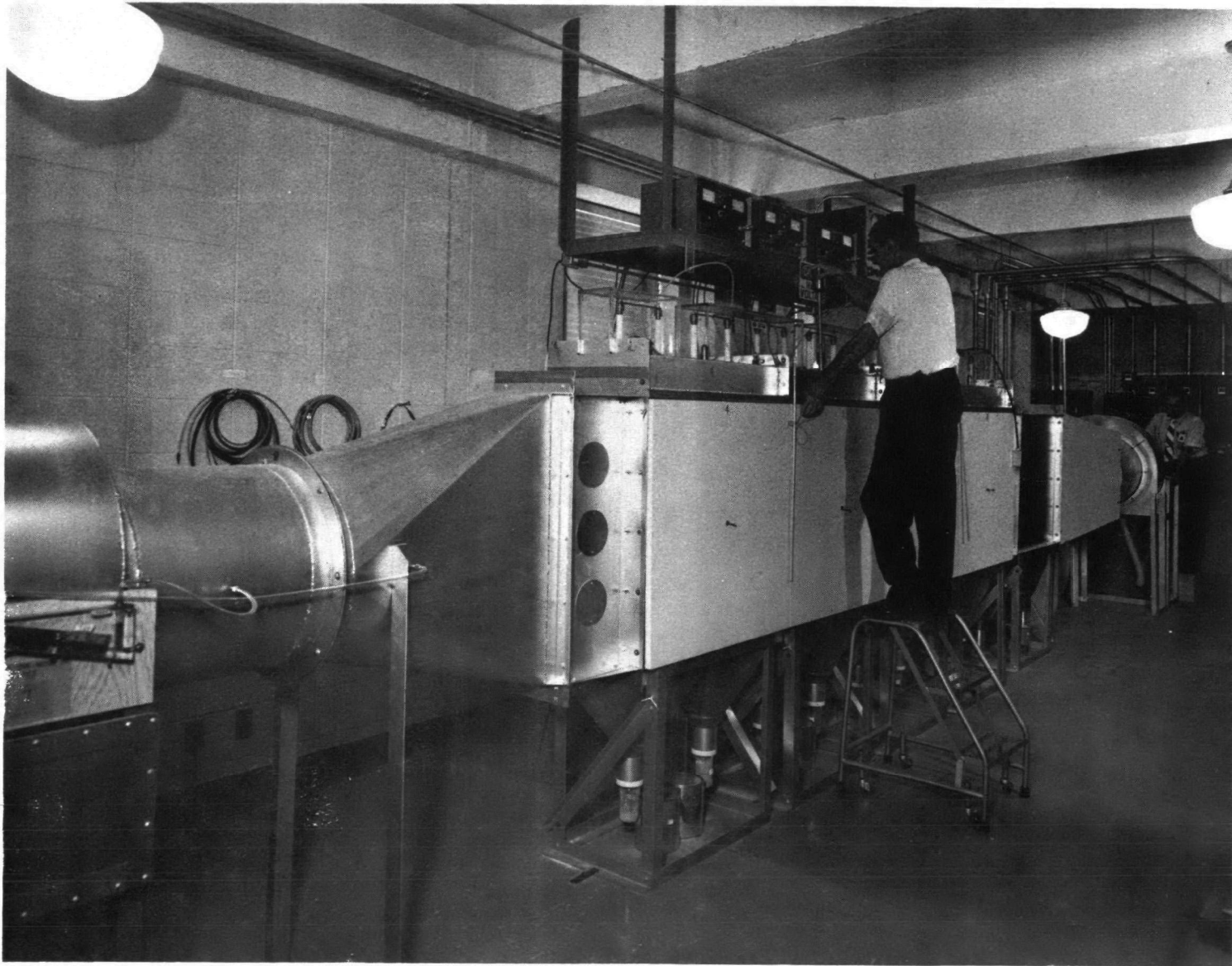
Figure 1.2.   Pilot Electrostatic Precipitator

Figure 1.3. Mechanical Configuration of the Pilot Precipitator

The gas flow characteristics of the pilot unit were determined from measurements made with a pitot tube. The necessary flow control devices were installed, to provide a nearly uniform flow; see Figure 1.4. A velocity contour map of gas flow conditions is shown in Figure 1.5. The final flow system provides a flow with a generally smooth shape and a velocity standard deviation of about 20%.

The dust is collected on the collection electrodes, rapped free from the plates, and retained in the eight collector jars below the precipitator. The collection hopper is divided into eight zones so that the characteristics of the collected dust can be determined as a function of position through the collector.

2. Electrical design

The electrode system shown in Figure 1.6 consists of corona wires suspended between collection plates spaced 10 in. apart. The corona wires are suspended from Teflon insulators with drill chucks (1504) utilized as the wire restraining device. This provides flexibility in the type of corona wire to be used. Plexiglas guard frames cover the corona lead wires for personnel protection (901).

The collection electrode system is divided into four mechanically independent plates with dimensions of 3 ft. These electrodes are suspended from spring-loaded mounting pins (1409) so that plate rapping can be easily accomplished.

Electrical power is supplied to the electrode system from three independent high voltage power supplies. These supplies are capable of providing half-wave filtered or unfiltered and full-wave filtered or unfiltered, positive or negative polarity electrical power to the electrode system. The peak voltage levels are continuously variable from 0 to 100 kV. This provides a sufficiently flexible power supply for most conditions.

The current and voltage waveforms can be displayed on an oscilloscope for routine monitoring. Meters are provided on each power supply system.
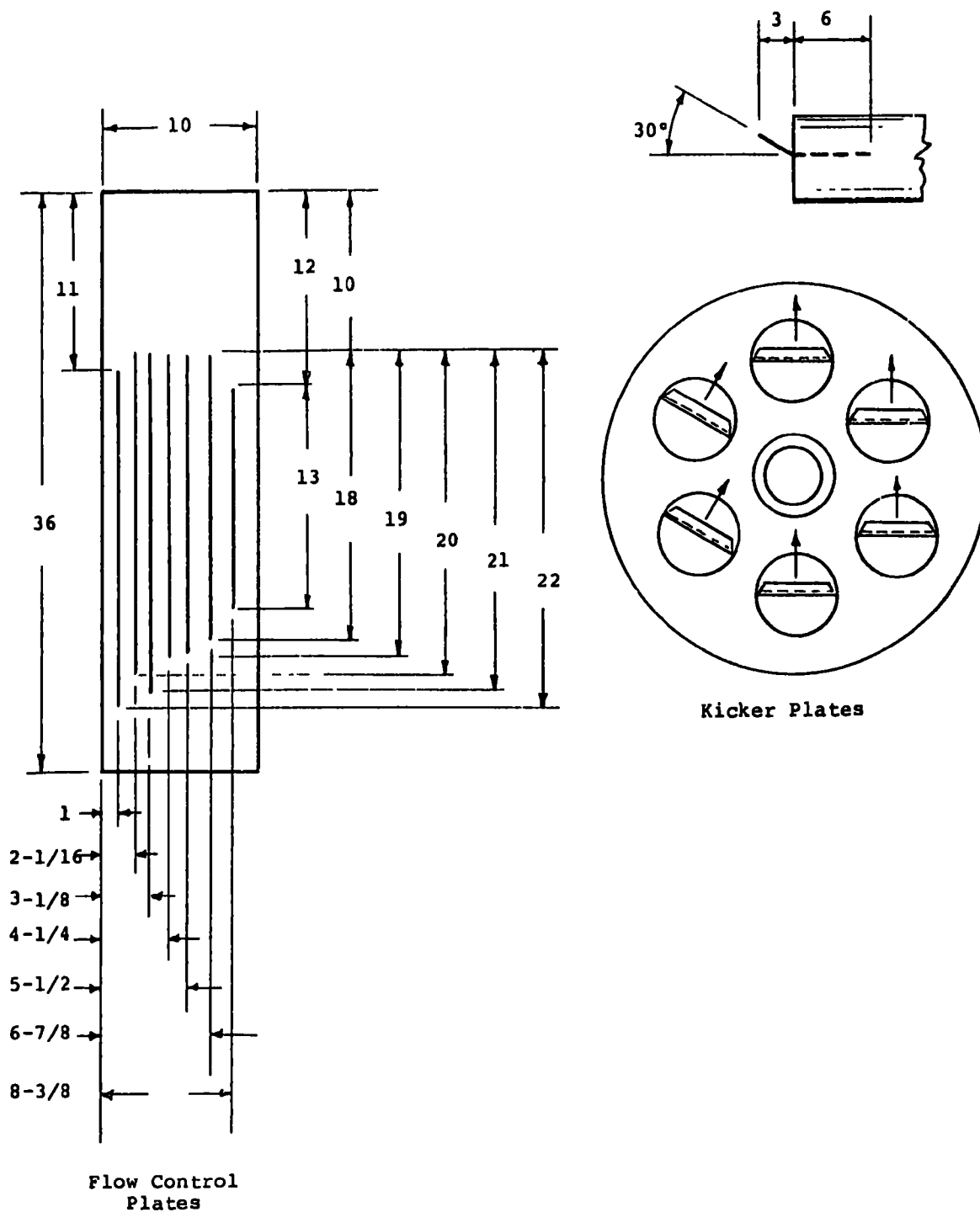
Figure 1.4. Arrangement of Flow Control Plates and
Kicker Plates
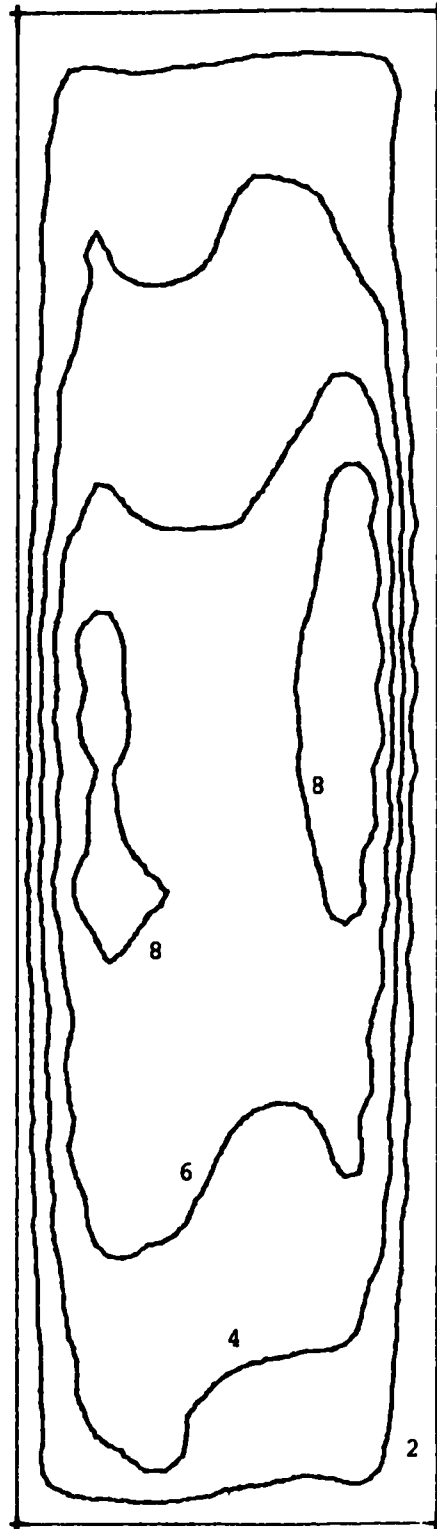
Figure 1.5.   Velocity Contours at 4.94 ft/sec
             Average Velocity

Electrode

Figure 1.6.   Details of the Collection System

D.   Design Parameters

The design parameters that are pertinent to the operation of the pilot precipitator are given in Table 1.1.

Table 1.1. Design Parameters

Collection electrode area, ft^2	72.0
Inlet cross-sectional area, ft^2	2.5
Collection electrode spacing, in.	10.0
Wire spacing, in.	9.0
Corona wire length, ft	48.0
Corona wire size, in.	0.10
Gas velocity range, ft/sec	2-20
Volume flow rate range, ft^3/sec	5-50

SECTION 2. FUNDAMENTAL STUDIES

A review of electrostatic precipitator technology was undertaken to resolve some of the questions regarding the factors influencing collection and reentrainment. Further clarification of these factors is desired to permit a more thorough understanding of the principles and to form the basis of a better precipitator model. These theoretical studies include:

- an analysis of the change in precipitation rate parameter with increasing gas velocity,

- a study of the particle concentration distribution in the interelectrode space,

- an investigation of the influence of resistivity of the dust layer on sparkover and back corona conditions, and

- verification of the theoretical concept that migration velocity was dependent upon particle charge and field.

These studies were conducted with the small-scale precipitator described in the previous section.

The collection of a monodisperse dust in a precipitator is described by the Deutsch-Anderson equation

$$\eta = 1 - \exp - \left(\frac{A}{V_g}\right) w \quad * \qquad\qquad 2.1$$

The derivation of the equation is based on the assumption that there is no reentrainment, that the particle concentration at any cross section is uniform, that the particles are spherical and monodisperse, and that particle charging occurred instantaneously. White[1] derived a similar expression for collection efficiency based upon the probability that a particle was

---

*See List of Symbols for definitions, Appendix 1.

[1]Refer to the Bibliography at the end of this section.

captured. The derivation by White assumes that particles entering the boundary zone defined by the gas flow conditions will be captured. If turbulent mixing and diffusion are sufficient to provide uniform mixing of the particles, the equation defining collection efficiency is the conventional Deutsch-Anderson equation. If, however, there is an uneven distribution of particles within a given cross section, the probability of a particle entering the boundary zone would be modified by the ratio of the particle concentration in the boundary zone to the average concentration in the cross section.

The collection concept can be illustrated by considering the boundary zone to be defined by the laminar flow region in the vicinity of the collection plate. For a given electrical migration velocity, w, the length of plate required for collection will be that defined by the vector sum of the migration velocity and the particle velocity due to gas flow. As gas velocity is increased, the distance required for collection of all of the particles in the boundary zone will increase as illustrated in Figure 2.1. Conversely, if the migration velocity is increased by increasing the particle charge or the field, the component of velocity toward the plate would increase and collection of the particles within the zone would occur in a shorter distance or a shorter time.

The thickness of the boundary layer is dependent upon gas velocity. Increasing the gas velocity in the turbulent region decreases the thickness of the laminar flow region, and hence reduces the volume of material that would be enclosed by the boundary layer as well as increasing the time required for collection. Consequently, by the Deutsch-Anderson equation alone, one would predict a decrease in collection efficiency due to an increased gas velocity. Written in another form,

$$\eta = 1 - \exp - \left(\frac{A}{A_c} \right) \frac{w}{v} \qquad\qquad 2.2$$

Thus as the gas velocity increases, there would be a corresponding decrease in efficiency. (A_c = precipitator cross-sectional area; v = gas velocity.)

Figure 2.1. Variation in Length Required for
Collection for Two Gas Velocities
with a Constant Migration Velocity
(Laminar Flow Case)

The Deutsch-Anderson equation as originally derived describes the behavior of a monodisperse aerosol in an electrostatic precipitator. For this condition, the parameter w is the terminal velocity of a charged dust particle under the influence of an electric field where this motion is opposed by the viscous drag force of the gas stream. In this report the parameter w is written with a subscript i denoting that this is the terminal velocity of the ith particle when charged to saturation as defined by equation 2.3 below. For this condition the term migration velocity applies.

In reality, the particles are not instantaneously charged to the saturation value of charge because of the non-zero charging time that exists in a real precipitator system. For this case, the collection efficiency for a monodisperse particle will be somewhat less than would occur for instantaneously charged particles. Thus, if one computes the parameter w from the Deutsch-Anderson equation from the measured performance (or integrated average of the computed performance) of an operating installation, an "effective" migration will be determined that is less than the migration velocity (w_i). This value of w is denoted as w_e, the effective migration velocity of the particle.

A third definition has evolved in the use of the Deutsch-Anderson equation in the precipitator technology community. It is used as a measure of performance of an installation collecting a polydisperse aerosol. For this special (and widely used) case, a value of the parameter w is computed from the measured performance of a real installation. If the efficiency and gas volume flow rate of an electrostatic precipitator is measured and the collection electrode area is known, the parameter w may be computed from the Deutsch-Anderson equation. The parameter w is now referred to as the precipitation rate parameter and is denoted w_p. When used in this manner, the value of w_p is strictly a measure of performance, with the dimensions of velocity, that only describes the behavior of a polydisperse dust in this particular electrostatic precipitator.

Several investigators have observed that for a precipitator collecting a polydisperse aerosol the change in efficiency with gas velocity was less than would be predicted from the Deutsch-Anderson equation. Mathematically, this would appear as though the precipitation rate parameter, w_p, increased with increasing gas velocity. Since w is defined by Detusch in terms of particle

charge and electric field, and

$$w = \frac{qE_p}{6\pi a n},$$ 2.3

it would be more appropriate to investigate other causes for the phenomenon.

Several authors have addressed themselves to this apparent anomaly in the behavior of precipitators where the theoretical considerations would predict a constant value of the parameter w independent of velocity, whereas in practice, it increased. Cooperman[2] attributed this phenomenon to a diffusional transport mechanism in the direction of the gas flow. The particulate concentration gradient in the direction of gas flow was thought to give rise to diffusional transport for the particulate that caused the mass transport to exceed the gas flow velocity. As the gas velocity increased, the concentration gradient in the direction of the flow was theorized to decrease and become less significant for higher gas velocities.

Robinson[3] relates this velocity dependent precipitation rate parameter (w_p) to an assumption that the inlet dust contains a nonprecipitable reentraining fraction. Heinrich[4] suggests that the increased turbulence transports a larger percentage of the dust particles near the corona wire in a higher field region where a larger charge is applied. Williams and Jackson[5] consider diffusion transport augmented by electrostatic particle convection as the mechaism for this behavior.

A.   Particle Concentration Distribution

A set of experiments was conducted to determine the variation in the particle concentration distribution in the cross section at the outlet of the pilot precipitator. The purpose was to determine if there was a depletion of particles near the collection electrode to account for the apparent increase in the precipitation rate parameter (w_p) with an increase in gas velocity. The particle concentration distribution was determined by the use of a laser light source with a photodetector to serve as a sensor. This device is referred to as an obscurometer and is described later. The precipitator was operated with gas velocities that covered the range from 2.5 to 11 ft/sec. Dust was fed into the precipitator at a fixed rate so that a uniform dust load as a function of time was presented to the precipitator inlet. The results of this series of tests are shown in Figure 2.2. The data are expressed as a percentage of light lost in traversing a 36 in. path.
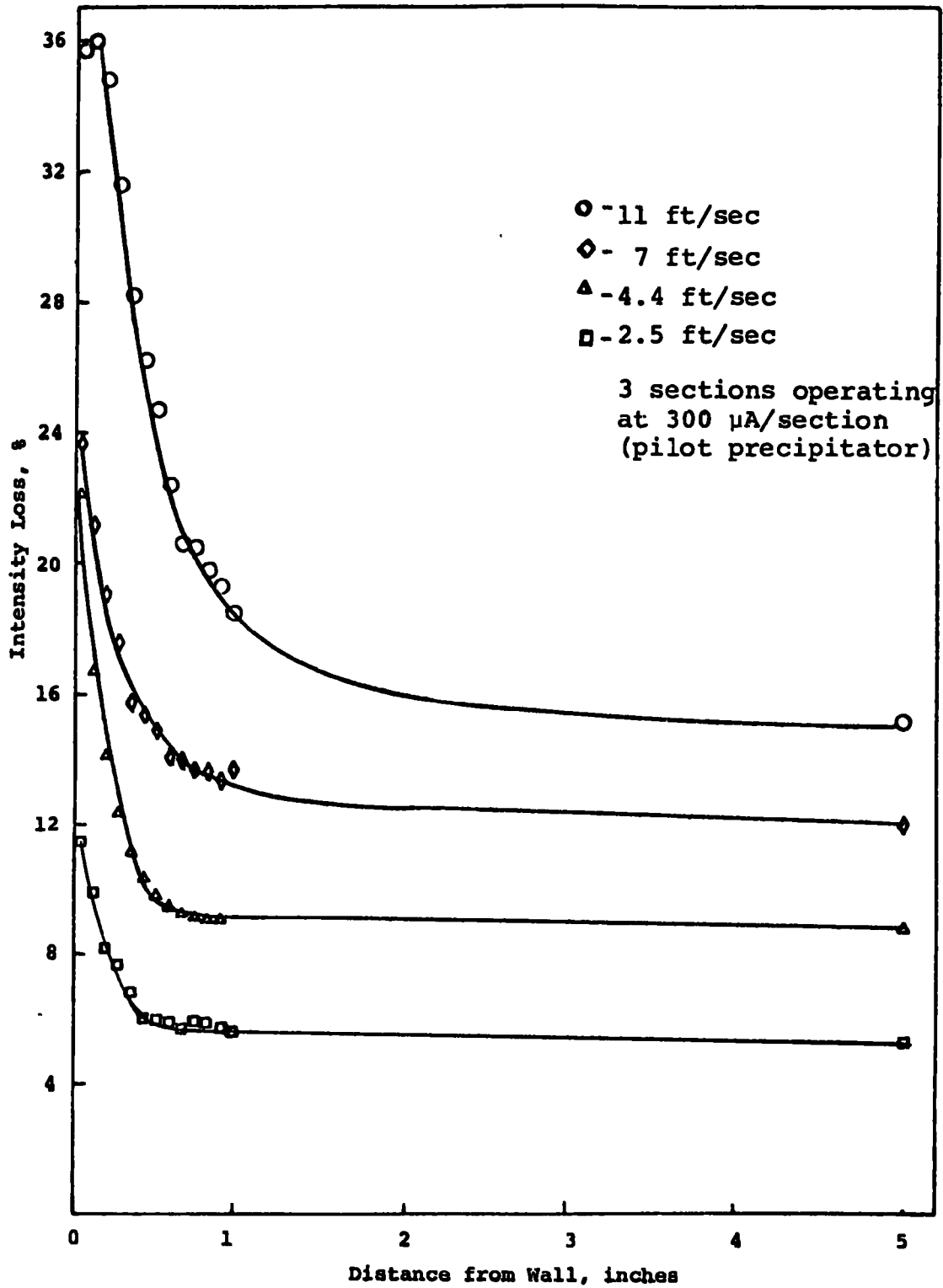
Figure 2.2. Obscuration as a Function of Distance from the Collecting Electrode for Various Gas Flow Ratios

-19-

It is to be noted that the light obscuration is not linearly related to the mass concentration of the particulate. The He-Ne laser provides a light source with a wavelength of about 0.6 μ which scatters better from the small particles, thus the light output is more nearly related to the fine particle fraction concentration than to the total mass. However, since the larger particles are preferentially collected, this should not cause too great an error in the interpretation of results for the particular experiment just described.

1.   Experimental procedure and apparatus

A sketch of the obscurometer, showing two views, is illustrated in Figure 2.3. In order to achieve good spatial resolution, particularly at very short distances from the collecting plates, a laser was used as a light source rather than a conventional collimated "white light" source. With the laser utilized in these experiments, the effective beam diameter at the point of emergence from the precipitator was about 0.08 in. The use of a lead screw, driving the entire obscurometer assembly, allowed the beam to be scanned across the precipitator in steps of slightly more than one beam diameter with good positional repeatability.

The extinction of light produced by small particles is a function of the number and size distribution of the particles within the light beam. As a consequence, if the opacity of an aerosol varies from point to point in space, either the mass concentration or size distribution, or both, must be nonuniform. If the size distribution of the particles is constant, a mass of aerosol, M, within the beam causes a fractional intensity loss, f, given by the expression

$$f = 1 - e^{-kM} = 1 - e^{-kdm} \hspace{3cm} 2.4$$

where

    d = the path length, and
    m = the mass concentration.

The value of k, the extinction coefficient per unit mass, is determined by the wavelength distribution of the light and the size distribution of the aerosol.

The obscuration measurements were made at 1/13 in. intervals within 1 in. of the precipitator plates and at 1 in. intervals over the remaining 8 in. of the duct width (10 in. total span from plate to plate). The dust feed rate was maintained as nearly constant as possible; however, it did show significant temporal

SOUTHERN RESEARCH INSTITUTE
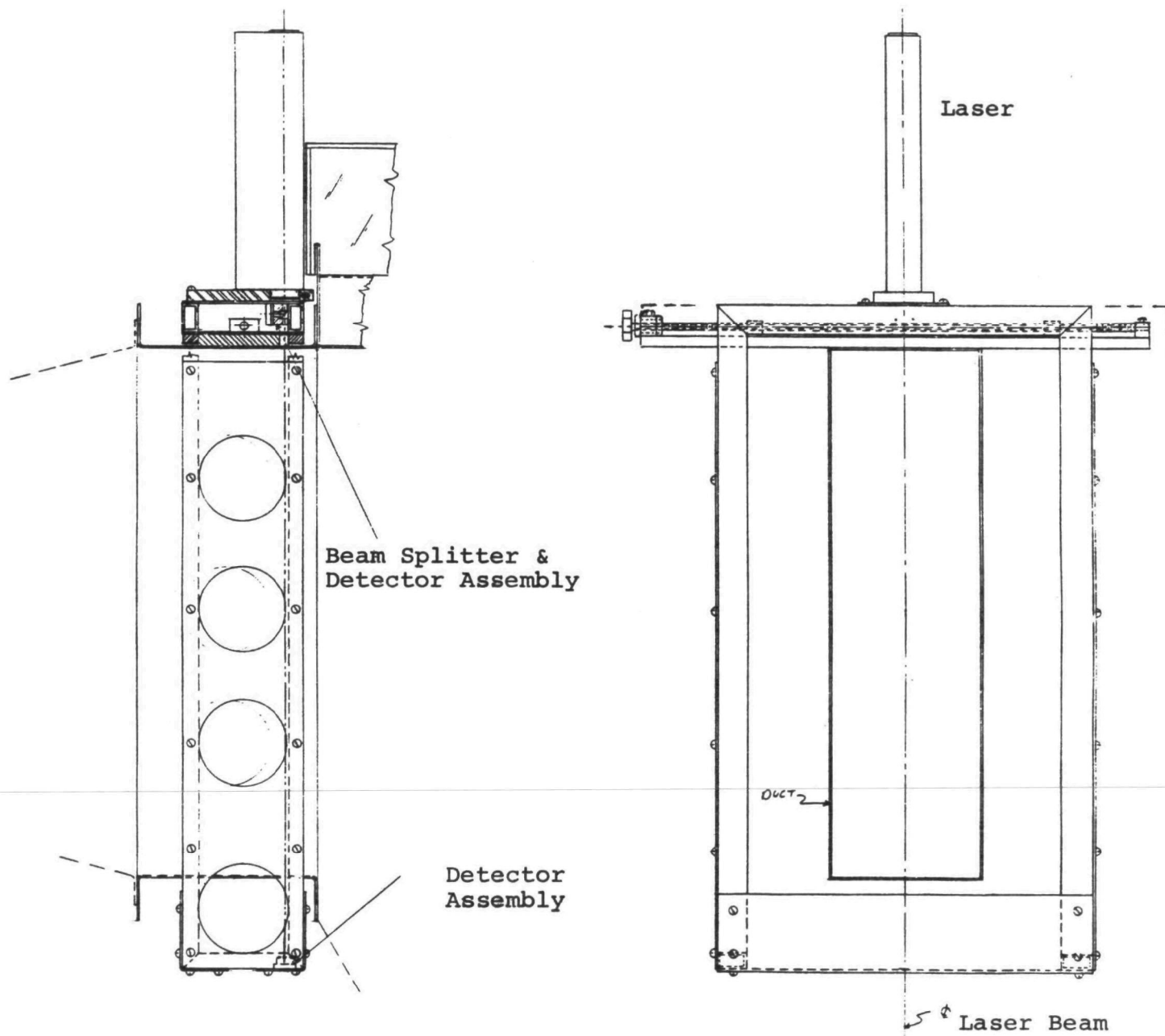
Figure 2.3.   Laser Extinction Probe Assembly

variations. In order to minimize the effect of these variations
and to average out temporal concentration variations resulting
from turbulence, from three to five scans across the duct were
made and averaged for each test condition. The sampling time at
each point on a scan was about 15 seconds.

Because the size distribution of the aerosol at the outlet
of the precipitator was unknown, and in fact probably was variable,
depending on the exact conditions for a given test (flow velocity,
current density, temperature, humidity, source of inlet dust
sample, etc.), the results are reported only in terms of the obscu-
ration produced by the aerosol.

The size distribution of the dust at the outlet was not
determined and variations due to gas velocity, humidity, etc.,
probably account for some scatter and uncertainty in the data.
However, since conditions were maintained reasonably constant,
obscuration changes are thought to be due primarily to mass
concentration changes for the fine particle fraction of the dust.
The inlet dust was similar to the MMD of 10 in Figure 2.4.

In all cases of measurements made with the precipitator
operating with the dust feed on, the obscuration was found to
increase by about a factor of 2 within the last one-half inch-to-
inch of the wall of the duct, and to increase slightly from the
center to within one inch of the wall. The shape of the opacity
curve is fairly well represented by an equation of the form

$$f = ae^{-b/x} \qquad\qquad 2.4$$

where a and b depend on operating conditions and x is the distance
from the precipitator plate to the beam center. If the size dis-
tribution were constant over the width of the duct, an equation of
this form would produce a very good fit for the resulting mass
concentration profile across the duct. It is not impossible,
however, that the mass concentration profiles would actually
increase more rapidly from the center of the duct than would be
inferred from the obscuration curves assuming a constant size dis-
tribution. This would result from the action of the precipitator
which probably tends to preferentially move larger particles from
the center of the duct toward the collection plates. As can be
seen from the curves in Figure 2.4, a much higher mass concentra-
tion of large particles is required to produce a given amount of
obscuration than is required for small particles.
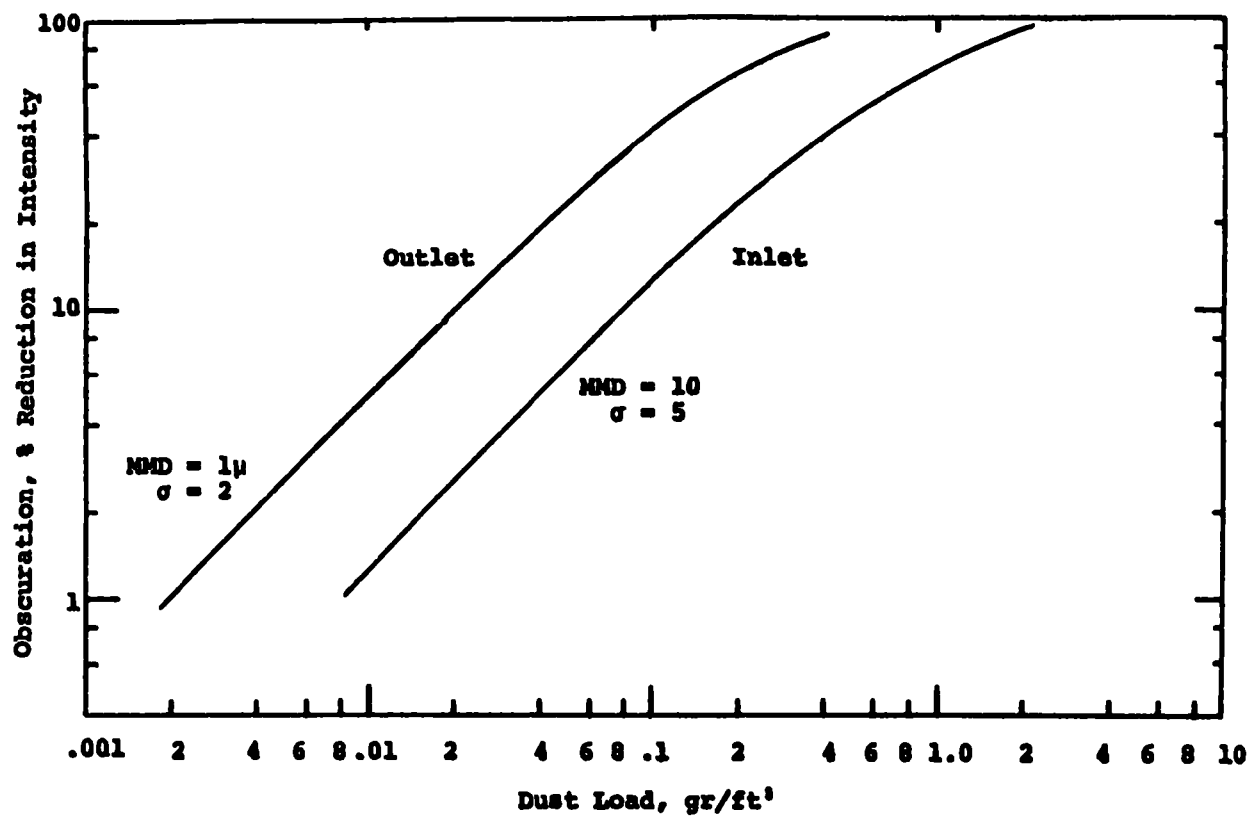
Figure 2.4   Computed Obscuration of White Light by a Varying Dust Load for Two Particle Size Distributions.

Increasing the flow velocity results in an opacity increase that varies approximately as $(v)^{+3/4}$. It is not unlikely that the mass concentration might vary more nearly as a linear function of v because of a probable shift toward a larger mean particle diameter as the precipitator efficiency drops. If the foregoing conjecture is the case, the overall inefficiency would vary as v^2 after accounting for the inlet dust loading variations induced by the velocity changes (inlet concentration is proportional to 1/v for a constant dust feed rate).

At velocities of 3.5 and 8 ft/sec, measurements were obtained at several corona currents ranging from 50 to 300 μA per section. Typical obscuration profiles for these tests are shown in Figure 2.5. Increasing collection currents leads to a flattening of the central parts of the profile, a narrowing of the high opacity region near the boundary, and a steepening of the profile near the boundary.

Following most of the foregoing tests, scans were made with the dust feed shut off, but with the collection plates unrapped. In all of the latter scans, no measurable obscuration was detected at any point across the duct, which would tend to indicate the absence of any direct erosion or scouring effects resulting solely from the air stream.

2. Conclusions

Results of the particle concentration measurements failed to explain the reasons for the increase in precipitation rate parameter in terms of increased turbulent mixing. The increase in particle concentration near the collection electrode would result in a modification of the precipitation rate because of the increased concentration of particles near the collection surface. However, the ratio of particle concentration near the collection surface to that in the interelectrode space is in the opposite direction to account for the increase in precipitation rate parameter with gas velocity.

B. Particle Size Effects

Further exploration of the cause of the increased precipitation rate parameter with gas velocity was made using the SRI model precipitator and the mathematical model. It is apparent from theoretical considerations that precipitation rate parameter varies over a wide range for various particle sizes. For large sizes, the migration velocity is so large that collection is virtually 100% for particles greater than around 10 μ. Thus, an increase in gas velocity would not materially reduce the collection of the large particles. Consequently, the increase in precipitation rate parameter with gas velocity is predictable from theory when considering a polydisperse aerosol.
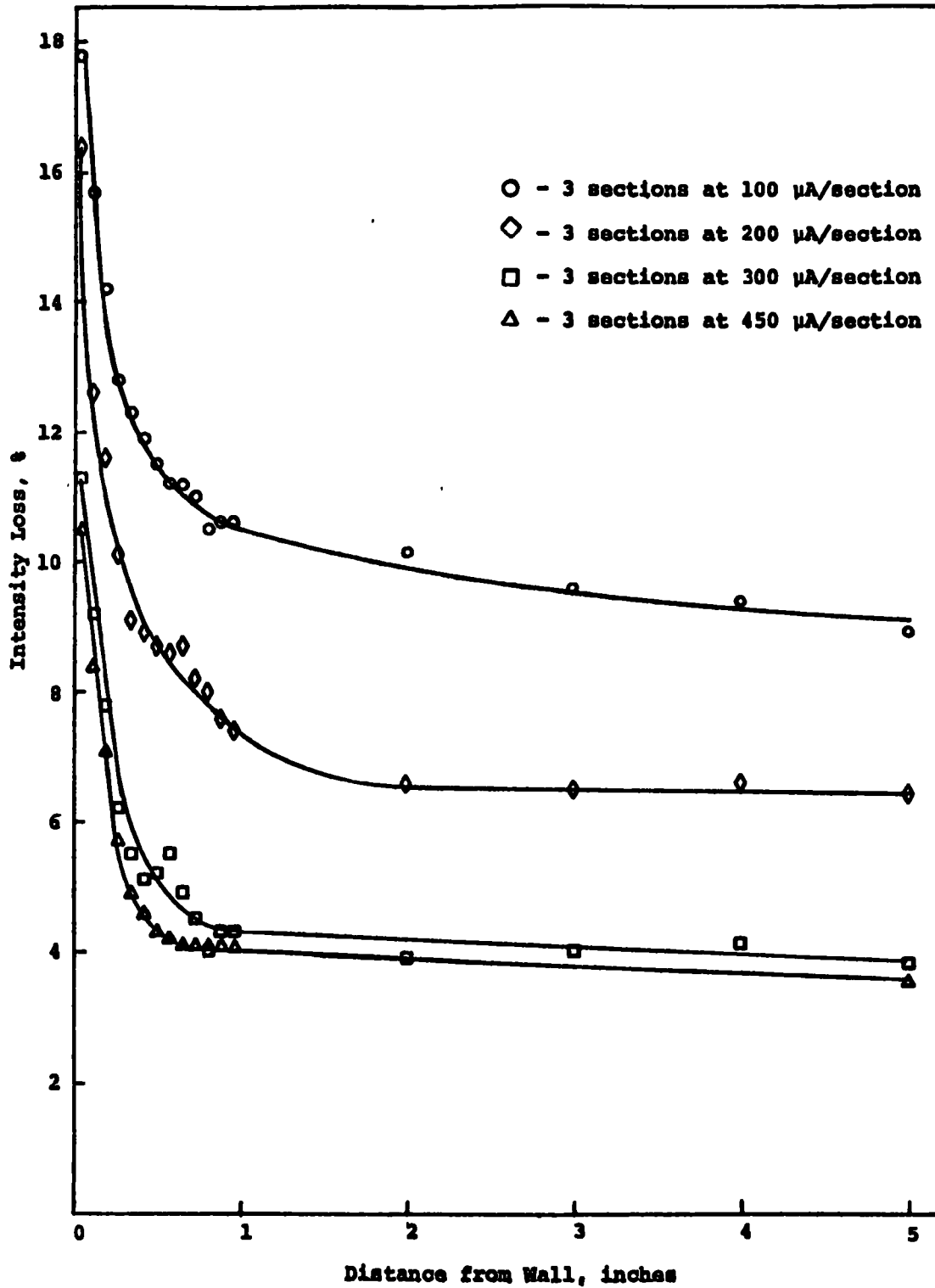
Figure 2.5. Effect of Current Density Changes on
Obscuration at a Flow Velocity of 3.5 ft/sec

This apparent anomaly is caused by the fact that the Deutsch-Anderson equation was derived for a single particle size with a constant migration velocity, while the precipitation rate parameter is obtained by measuring the collection efficiency of an installation and back-calculating.

If we are dealing with a monodisperse particle distribution where all particles have the same migration velocity, the Deutsch-Anderson equation effectively describes the behavior of the precipitator for various gas velocities. It is to be noted that in all the discussions of efficiency, the basis is for a weight or mass collecting efficiency. The behavior of a precipitator operating on a material with a range of particle sizes becomes clear if one considers the behavior of that device while collecting a material consisting of a number of mixed monodisperse particle groups. In this case, each particle size will be characterized by a mass concentration and its associated migration velocity.

The behavior of the precipitator for the dust composite can be determined by applying the Deutsch-Anderson equation to each individual particle size to determine the percentage of the weight of material removed within each size increment. The overall effect is then determined by relating the total weight of material collected to the total inlet material. Only now are we able to compute a value for the precipitation rate parameter.

The precipitation rate parameter for this same dust but for an increased gas velocity can be determined by completing the entire computation cycle for each particle size, again summing the results, and finally computing a new precipitation rate parameter. This yields a value different from that obtained by modifying only the volume flow rate for the composite system equation. This fact is illustrated by the data shown in Table 2.1.

Table 2.1. Calculated Collection Efficiency for
a Dust Composite, Based on a Charging
Field of 5 kV/cm and a Collecting
Field of 3 kV/cm

Particle size μm	Material weight %	Migration velocity cm/sec	Fractional efficiency each size range for indicated velocity ft/sec					
			4.4	5.4	6.7	8	10	12
>32.5	15	365	100	100	100	100	100	100
32.5	4	238	100	100	100	100	100	100
29.0	8	212	100	100	100	100	100	100
21.8	22	159	100	100	100	99.99	99.93	99.8
12.4	11	90.5	100	99.95	99.8	99.46	98.45	96.9
7.9	21	57.6	99.76	99.3	98.1	96.4	93.0	89.0
4.2	13	30.7	96	92.8	88.0	83.0	75.8	69.4
2.1	3	15.3	79.8	72.7	65.0	58.4	50.6	44.3
1.3	3	9.5	63	55.6	48.0	42.3	35.6	30.6
Overall efficiency:			97.76	96.9	95.5	94.0	91.81	89.45
Area-to-volume ratio, ft²/kcfm:			53	43	35	29.3	23.5	19.5
Precipitation rate parameter:			36	40.8	45.7	48.8	54.3	58.6

A plot of this variation in precipitation rate parameter as a function of gas velocity is shown in Figure 2.6. Thus we see a variation in precipitation rate parameter with gas velocity based on purely theoretical considerations for polydisperse dusts, while the collection efficiency for each size interval is based on the Deutsch-Anderson equation with a fixed migration velocity and an area-to-volume ratio depending upon the gas velocity.

The computer performance model described in Section 4 also predicts this behavior. The precipitator operating parameters for the SRI pilot plant were used as inputs to the computer mathematical model which was used to compute the charge, effective migration velocity, and collection efficiency for each size range at each position, and finally, an overall efficiency for each of a number of test conditions. These computed efficiencies were used to determine a precipitation rate parameter for each gas velocity. These data are shown in Figure 2.7.

White[1] reports similar results when collecting fine oil smokes on two types of collection electrodes. Thus, the increase in migration velocity with gas velocity is not an anomalous behavior based on diffusion phenomena or electric wind, but rather is predictable from purely theoretical considerations due to the large variation in migration velocity for a wide range of particle sizes. The primary misunderstanding comes from a misuse of the Deutsch-Anderson equation in a manner that violates the initial assumptions.

C.   Resistivity

The influence of resistivity on the performance of electrostatic precipitatiors has been rather clearly established. White,[1] Penney,[6] and others have shown that resistivity of the collected dust determines the voltage and current at which a precipitator will operate due to sparking and back corona limitations.

A review of the methods of measuring resistivity and comparison of the resistivity data measured by the various methods indicated that there were fundamental differences in the measurement methods and probably wide variation in the resistivity values obtained by the different techniques.

To resolve some of the questions regarding the measurement of resistivity, a review was made of the methods used or proposed for resistivity measurement and comparisons were made utilizing several types of resistivity probes.

1.   Types of apparatus

Dust resistivity can be measured in the flue-gas environment (in situ) or the dust sample can be measured in an environment
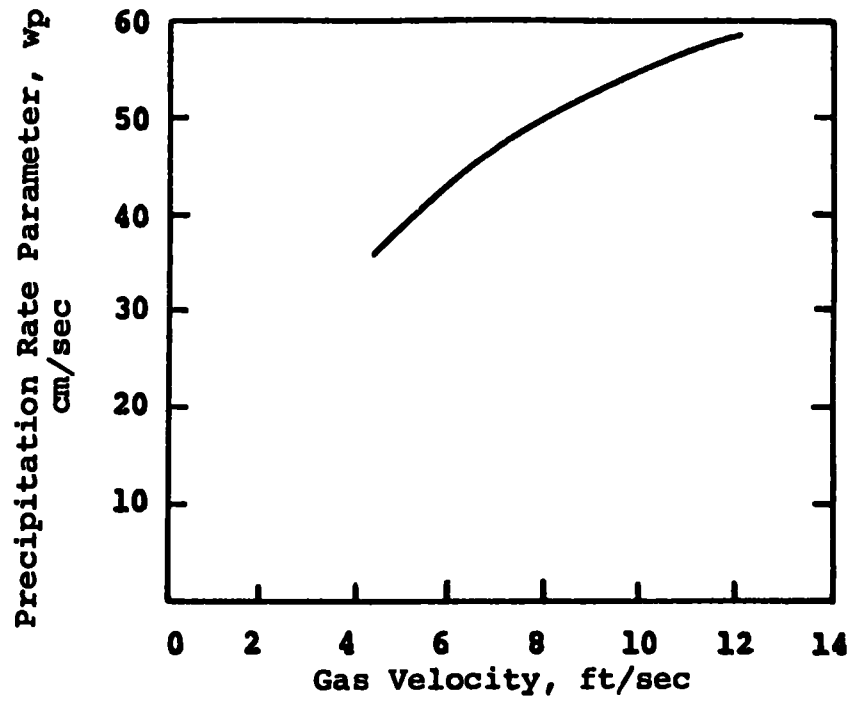
Figure 2.6. Graph of Computed Precipitation Rate
Parameter for Example Showing Increase
in w_p with Increasing Gas Velocity.
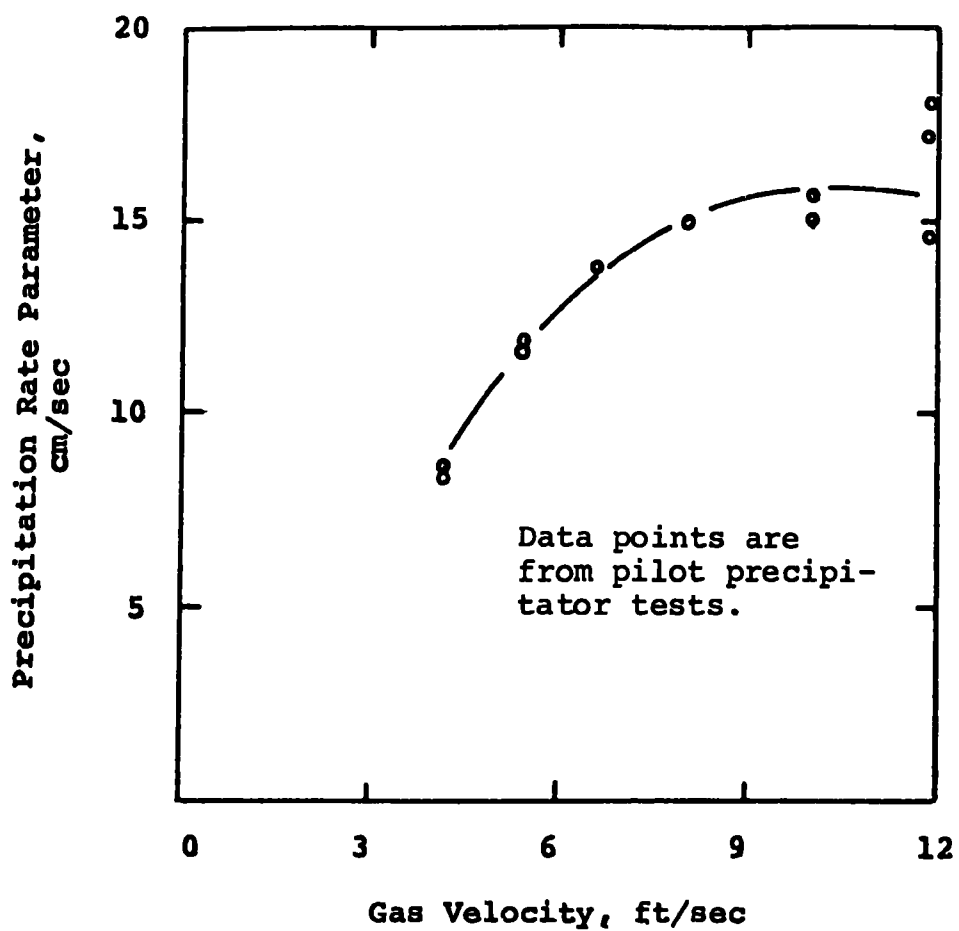
Figure 2.7. Precipitation Rate Parameter vs. Gas
Velocity - Precipitator Model

simulating flue-gas conditions (laboratory). Because of the difficulty in reproducing flue-gas conditions in the laboratory, resistivities measured other than in the flue gas are of questionable value in the temperature region where surface conduction predominates. At elevated temperatures (above around 450°F), laboratory resistivity data are in substantial agreement with those determined in situ.

Measurement of resistivity involves first a collection of a sample of the dust followed by determination of the current and voltage relationships within the dust layer itself. The various methods of measuring resistivity differ primarily in the method of dust collection, the method of applying voltage to the dust layer, and the configuration of the measuring cell.

During the course of this investigation, four types of resistivity measuring apparatus were studied. The first system consisted of a mechanical cyclone collector with a cylindrical cell electrode structure, as shown in Figure 2.8. This apparatus is of the type described by Cohen and Dickinson[7] and consists of a probe that is inserted into the duct to withdraw a sample of the dust-laden flue gas. The cyclone collector removes the dust which falls into the hopper beneath the cyclone. The hopper consists of metallic central and concentric electrodes supported by a Teflon cup which constitute the measuring cell. When the cell is filled with dust, a megohmeter is used to determine the dust resistivity.

Temperature of the cyclone and measuring cell is maintained at flue-gas conditions by means of heaters located inside the enclosure containing the cyclone. A mechanical vibrator is used to compact the dust, thereby giving reproducible packing conditions.

Use of this probe was limited somewhat by the difficulty in maintaining isothermal conditions throughout the system. It was necessary to wrap the sampling probe with heater tape to insure that the gas was not cooled in passing to the cyclone and to measure the temperature of the cyclone and measuring cell with thermocouples rather than depend upon thermometers in the enclosure. With these modifications, the apparatus performs satisfactorily.

To minimize the difficulties associated with maintaining isothermal conditions, a second type of cyclone probe was constructed to be inserted directly into the duct. A thermocouple on the cyclone was used to determine when the cyclone came to the flue gas temperature. When stable temperature was reached, a sample was taken by the cyclone collector. The collector was
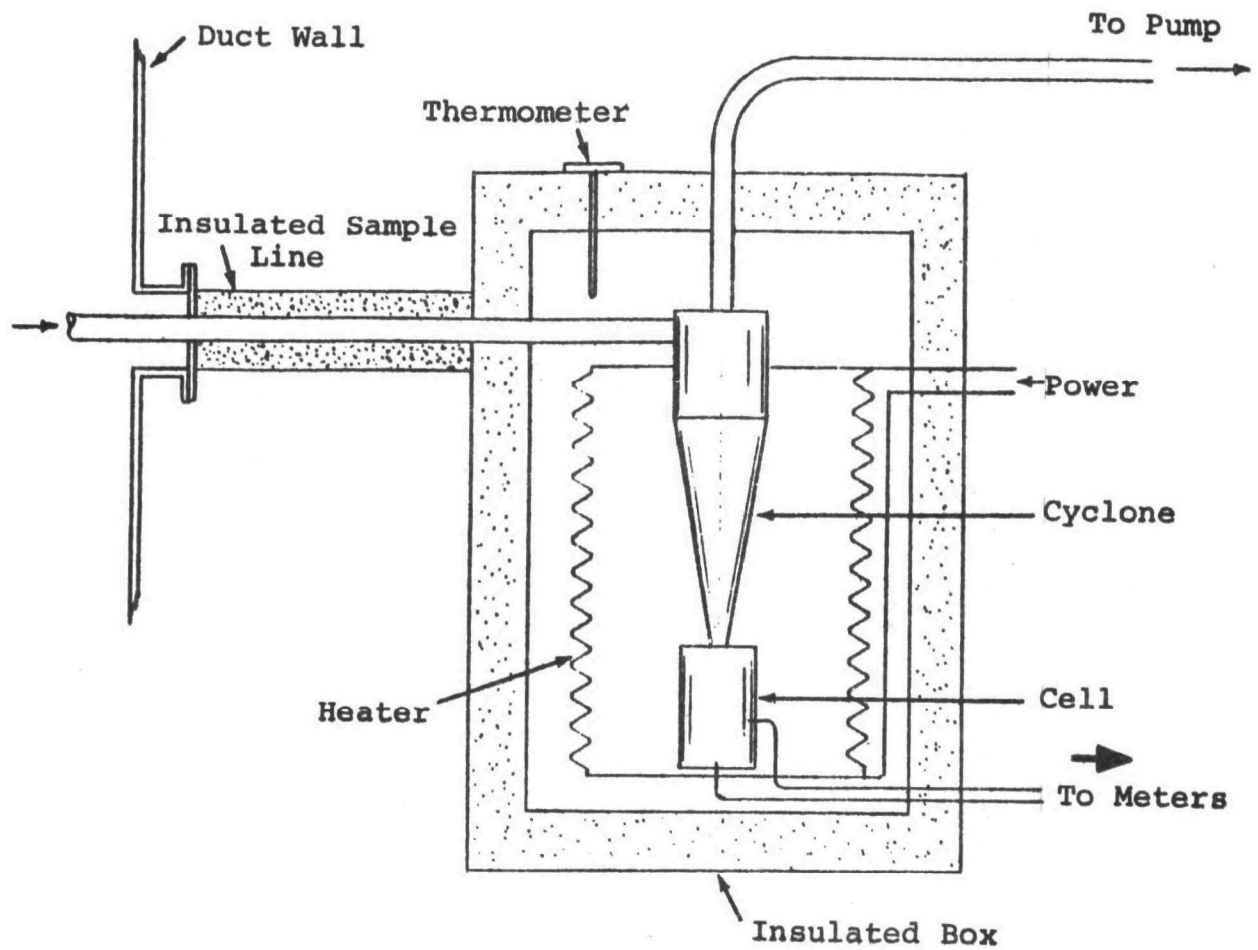
Figure 2.8. Cyclone Collector - Cylindrical Electrode Cell
for Collection External to the Duct

vibrated or rapped to compact the dust sample in the measuring cell. Resistivity was then measured by applying a voltage to the electrodes and measuring the current by means of a picoammeter and current recorder.

Recording of the current through the resistivity cell showed that the current decreased with time (increasing resistance) for a period of around 20 min for fly ash samples. Therefore, the question arose as to which value of resistivity was most representative——the initial value or that obtained when steady-state conditions are reached. This phenomenon of current decay will be discussed later.

The third type of probe used was the point-plane type, shown in Figure 2.9. The apparatus consists of a disc and guard rings as one electrode, and a point electrode located approximately 3.2 cm above the disc. When high voltage is applied across the electrodes, a corona is generated at the point and dust is electrostatically deposited on the disc. When a sufficient layer has been deposited, a second disc, concentric with the point electrode, is lowered onto the dust surface and the resistivity determined from measurements of voltage across the discs and current through the sample. Resistivity was then computed from the sample resistance, cell dimensions, and dust thickness. The apparatus shown in Figure 2.9 was designed so that constant spring pressure was applied to the dust layer and the thickness was measured by means of a dial gauge.

In determining resistivity by the point-plane apparatus, it was observed that the current-voltage relationships were nonlinear. Apparent resistivity decreased as the voltage or electric field increased. The significance of this variation will be discussed later.

The point-plane resistivity apparatus permits an alternative method of measuring resistivity by determining the voltage-current curves with and without a deposited dust layer. This alternative method can serve as a check on the measured resistivity and lends considerable confidence to the resistivity values determined by the point-plane apparatus. However, for very low values of resistivity, the voltage drop across the dust layer is small and the accuracy of this method is not as great as it is for higher resistivities. For high resistivities (10^{11} to 10^{12} Ω-cm), back corona begins at very low values of current. The resistivity must be determined from current-voltage relationships below the onset of back corona. For intermediate values of resistivity, both techniques provide comparable values for resistivity.
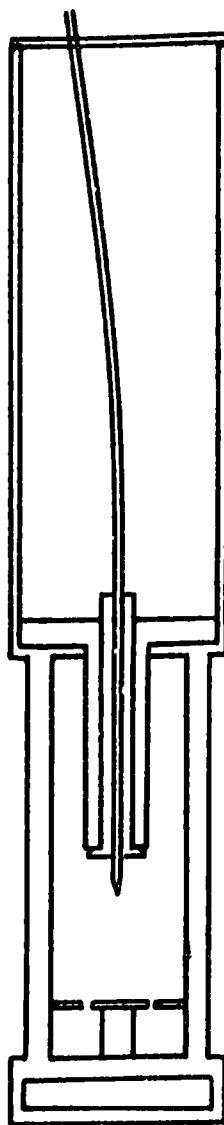
Figure 2.9. Schematic of Point-
Plane Resisvitity Probe

A fourth type of resistivity apparatus utilized was the Electrostatic Precipitator Analyzer (Kevatron) which utilizes a cylindrical wire and tube precipitator for collection of the dust and a cylindrical cell electrode for determining resistivity. Following collection, the dust is rapped from the walls of the collector and falls into the measuring cell where the resistivity is determined from the resistance of a known geometry of the material. Figure 2.10 is a schematic of the system.

A comparison of the various sytems shows that they differ principally in the manner in which the dust is collected and deposited in the cell, in the size and geometry of the measuring cell, and in the manner in which the apparatus is operated.

Since the collection mechanisms are fundamentally different, one question that arises is the particle size distribution of the dust. Cyclone collectors of the type used in the Cohen-Dickinson apparatus, or variations of this apparatus, would not be expected to collect very small particles. This, coupled with the extreme nonisokinetic sampling, would tend to introduce considerable uncertainty as to how representative the collected sample is apt to be.

The point-plane apparatus would tend to suffer from the same difficulties, as would the Kevatron apparatus to some extent. Electrostatic precipitators are in themselves size selective so that larger particles would tend to be preferentially collected, thus preventing the taking of a representative sample.

On the other hand, the dust layer on the precipitator is not of the same particle size distribution as the dust in the gas stream. In terms of particle size distribution, therefore, there is considerable question as to how to extract a sample that would be representative of the dust layer on the precipitator plate, especially since this varies along the precipitator length.

An alternative approach, therefore, is to attempt to get a reproducible sample either by maintaining constant collection conditions on a nonisokinetic system or by attempting to maintain isokinetic conditions and providing a means for collecting all the dust above the minimum size fraction of interest.

Figure 2.11 shows the size distribution of the dusts collected by the cyclone collector, the wire and tube precipitator, and the dust from the precipitator hopper.
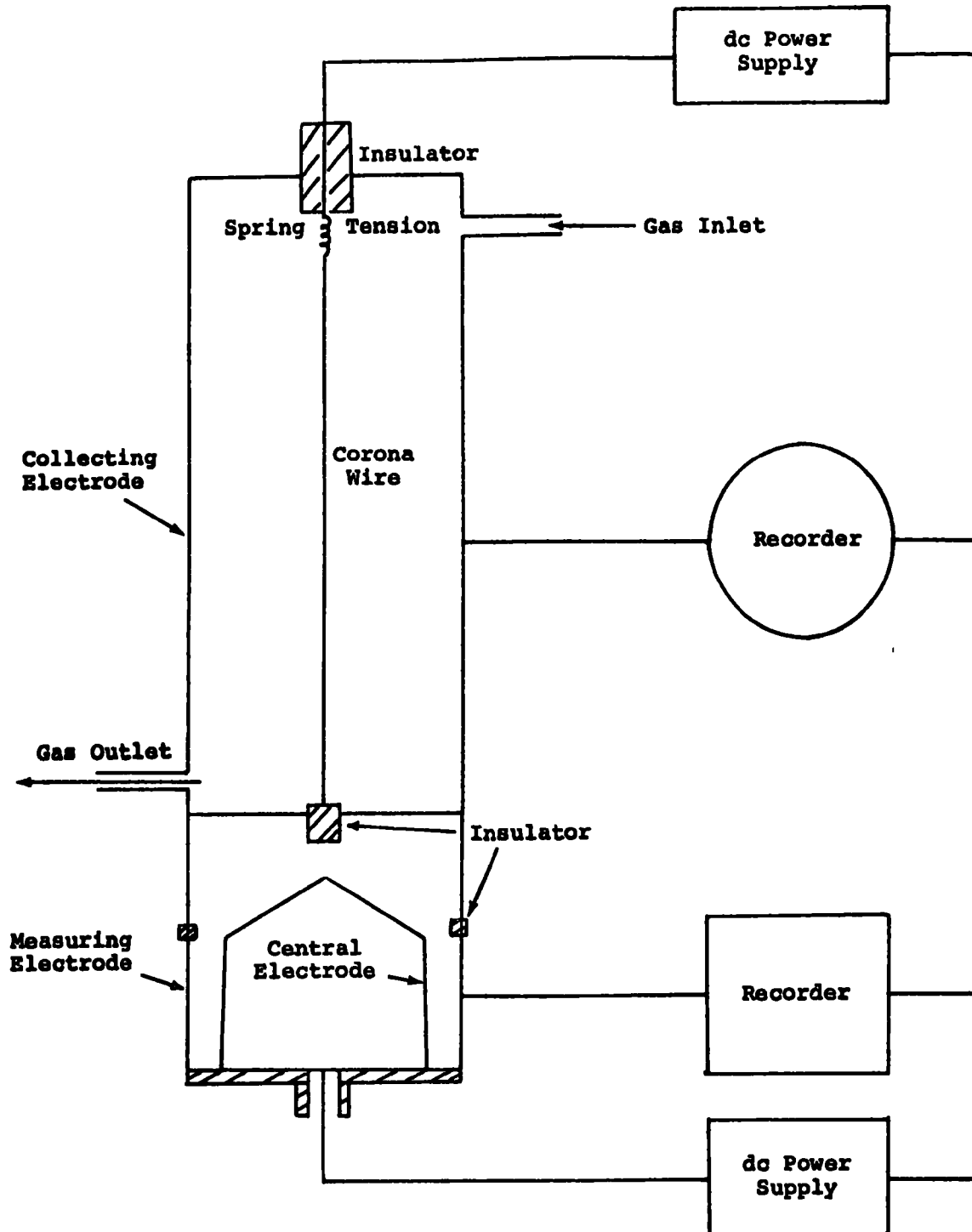
Figure 2.10.   Kevatron Australian Resistivity Probe
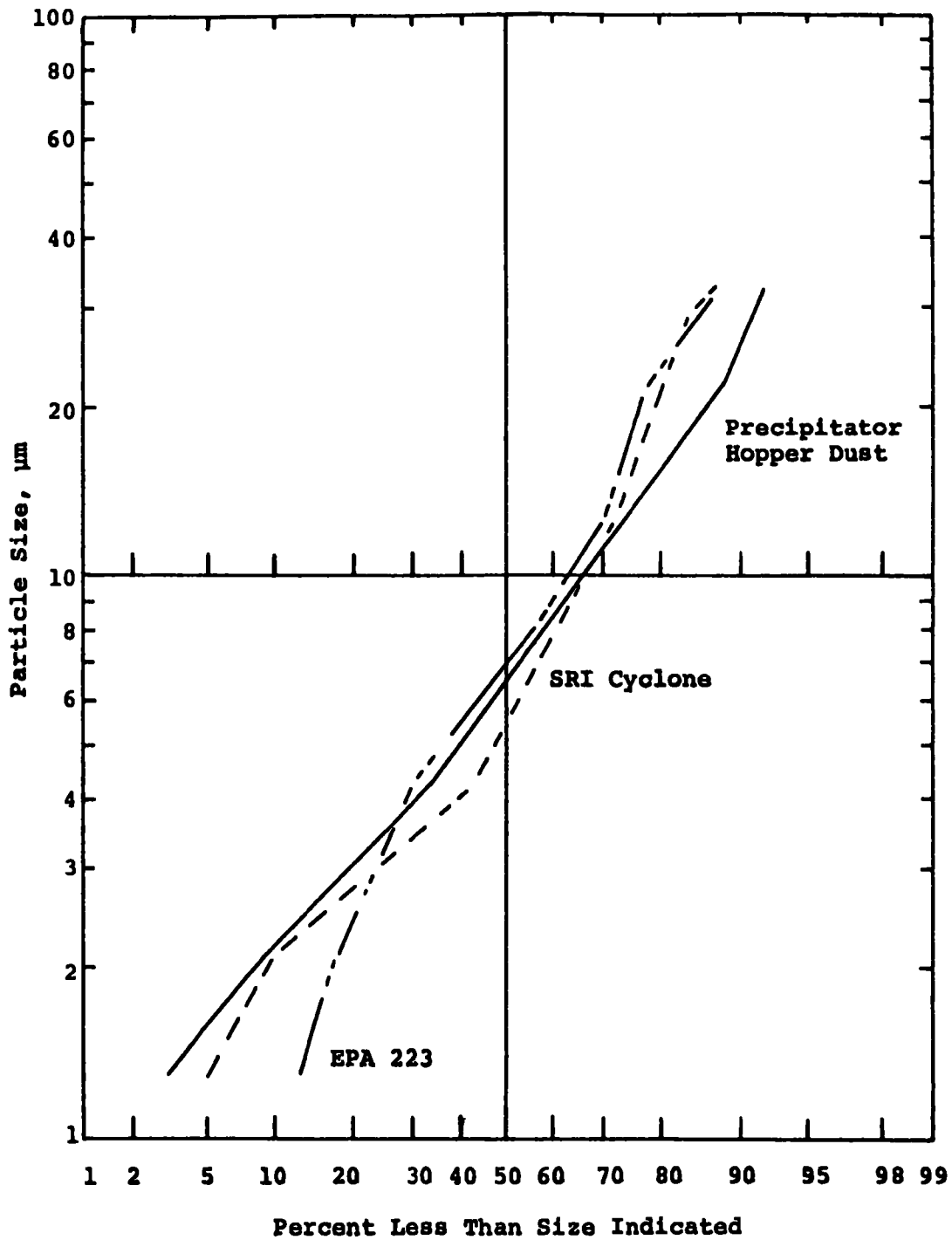
Figure 2.11. Comparison of Particle Size Distributions from Precipitator Hopper and Two Resistivity Probes

The quantitative influence of particle size of the dust on its resistivity was not determined. The effect may vary with the nature of the dust and type of conditioning. In general, we have observed a larger percentage of sulfate on the smaller fraction of fly ash than on the larger. However, size of the dust does not appear to be a major factor. Figure 2.12 shows the variation in resistivity of various size fractions of a fly ash as determined by Bahco as reported by Bucher.[8]

A second difference in the various types of resistivity probes is the degree of compaction or density of the dust in the cell. Cohen and Dickinson[7] report variations in resistivity by an order of magnitude with changes in dust density from around 0.5 to 1.0 gm/cm^3. With fly ash, our experience indicates that variations of the order of 2 may be more realistic. The degree of compaction does vary considerably between the point-plane type apparatus and both the Kevatron and cyclone systems. The dust layer is compacted by the measuring disc in the point-plane probe, whereas the dust is rapped or vibrated into the cells in the Kevatron and cyclone type collectors.

The method of deposition of the dust layer is also different between the point-plane, cyclone, and Kevatron apparatus. In the point-plane apparatus, dust is electrostatically deposited on the surface of the disc and, perhaps, some alignment of the dust particles does occur. Such alignment does not take place in the Kevatron and cyclone type apparatus other than from localized dust electric fields.

All of the effects mentioned above are somewhat secondary to the more pronounced influence of electric field and the variations in resistivity with time as mentioned earlier. Figure 2.13 shows a typical change in resistivity with time for fly ash as determined by the cyclone collector and cylindrical-cell apparatus. Such time dependence of resistivity has been noted by McLean[9] on borosilicate glass and on fly ash at temperatures up to 225°C.

As discussed by White[1] and others, resistivity of most granular materials in the presence of moisture and/or other conditioning materials varies with temperature in a manner indicating two modes of conduction. At temperatures below around 350°F, conduction takes place primarily through an adsorbed layer on the surface of the particles. Above around 400°F, conduction takes place through the material itself. In the intermediate region between 350 and 400°F, both surface and bulk conduction are significant. The equivalent electrical circuit would be a parallel resistance, the value of each being temperature dependent. The mechanisms of current conduction in each of the two modes of conductivity are significant in understanding the observed behavior of resistivity measuring apparatus.
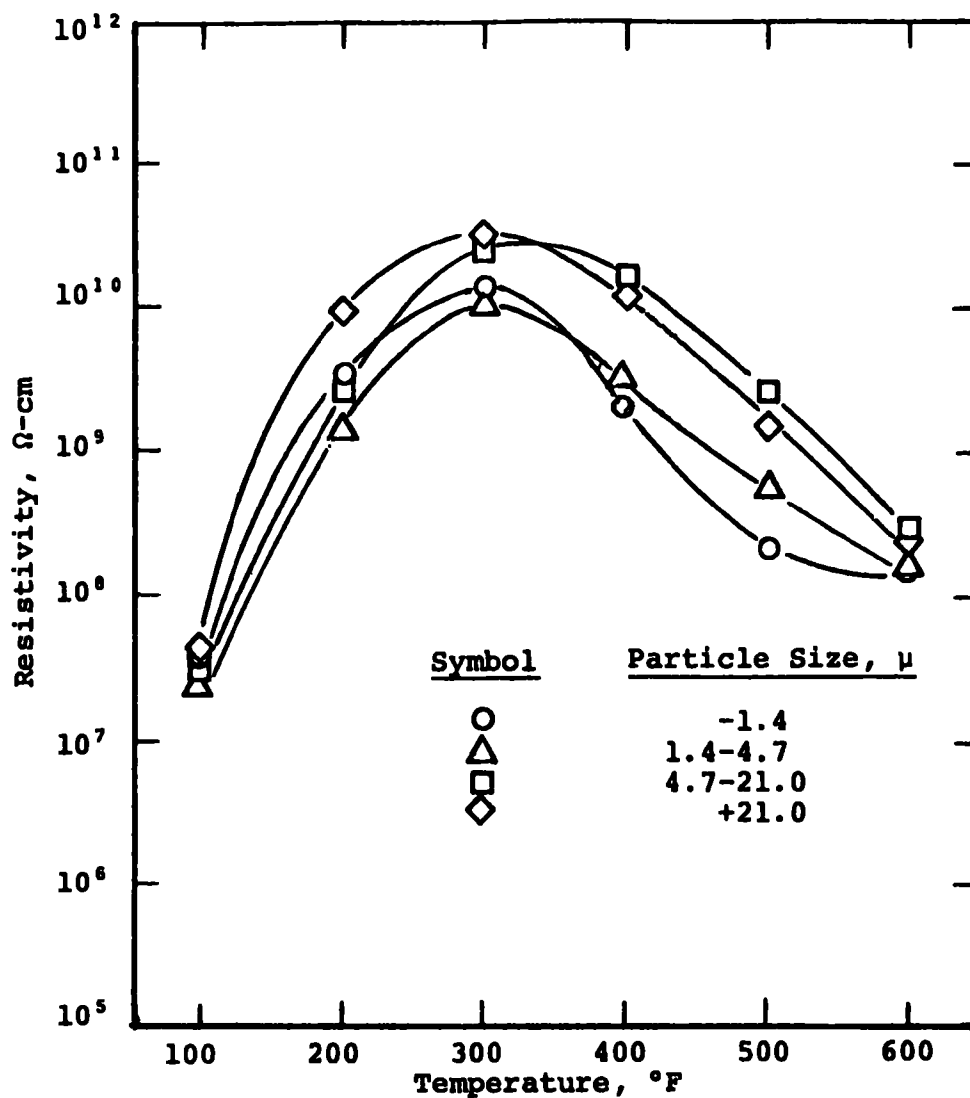
Figure 2.12. Resistivity vs. Temperature for Different
Size Fractions of Beulah Standard Electro-
static Precipitator Ash
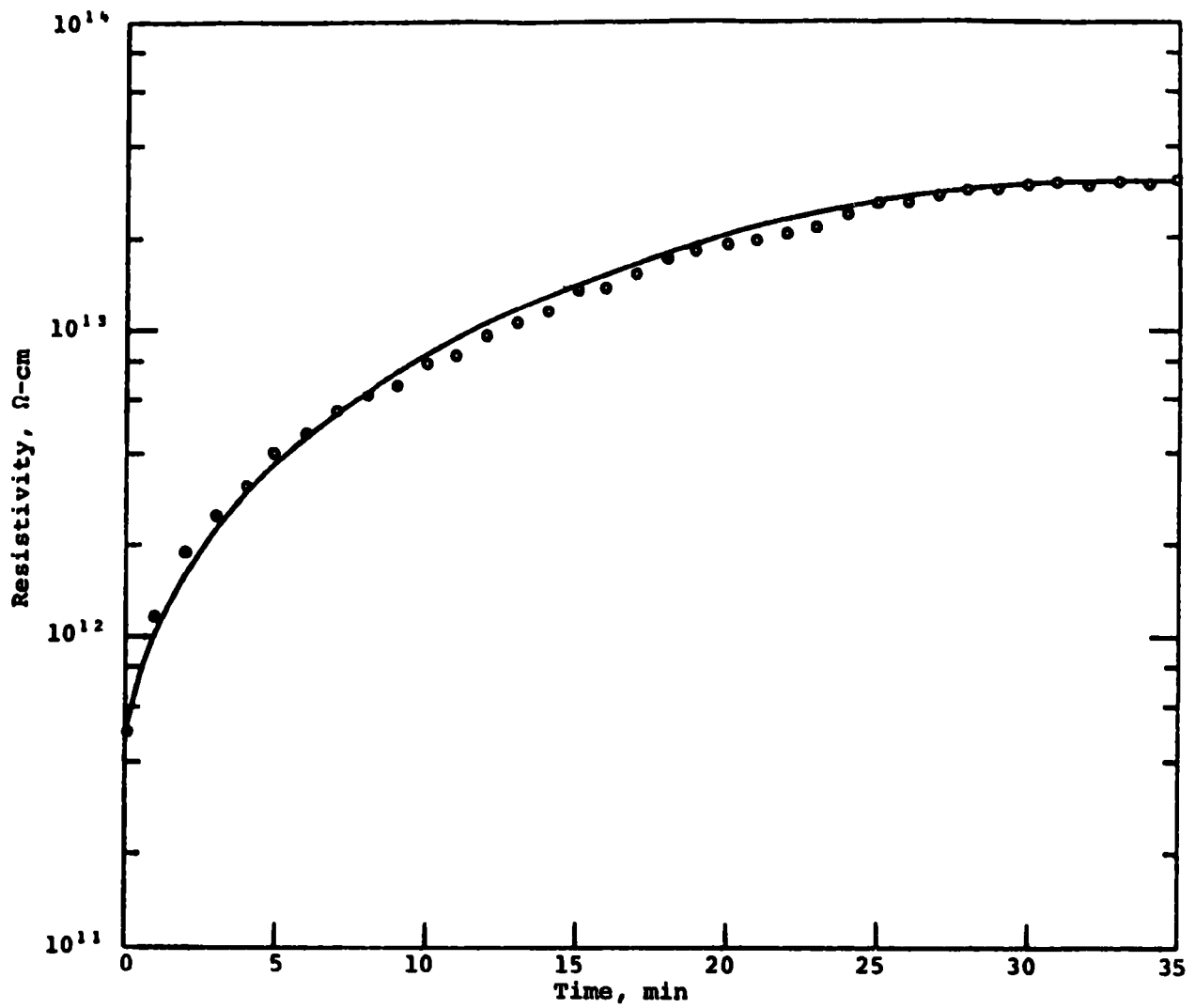
Figure 2.13.   Variation of Fly Ash Resistivity with Time Using the
In-Situ Cyclone Probe at a Temperature of ≈280°F

2. Surface conduction

The results of studies under EPA Contract CPA 70-149 show that conduction on the surface of a fly ash particle is due to an adsorbed layer of water and sulfuric acid. Conduction through this adsorbed layer must be primarily electrolytic, the charge carriers being mainly H^+, OH^-, HSO_4^-, and SO_4^{-2} ions.

In accordance with Faraday's laws, conduction through the layer must be accompanied by charge-transfer processes at interfaces where the fly ash adjoins other materials containing charge carriers of a different type. Such interfaces exist in cells used for resistivity measurements, where the metal electrodes conduct electricity through the migration of electrons. They also exist in deposited layers of fly ash on the electrodes of an electrostatic precipitator, where the electrodes again conduct electricity through the migration of electrons, and the adjacent gas stream conducts primarily through the migration of charged molecules, such as O_2^-. Moreover, in accordance with observations that different ions in solution vary in electric mobility and thus in transference number (the fraction of the current transported), variations in the electric mobilities of different ions in the adsorbed layer on fly ash must be expected. Such variations are to be expected especially as the result of differences in attractive forces between different ions and the surface components of the fly ash.

In an adsorbed layer of only H_2O molecules, the charge carriers in the ash must consist of only H^+ and OH^- ions. If electrodes of electrochemically inert metals are used to determine the resistivity of the ash, the charge-transfer processes at the electrode-fly ash interfaces will lead to the formation of H_2 gas at the negative electrode as the result of the reduction of H^+ ions, and the formation of O_2 gas at the positive electrode as the result of the oxidation of OH^- ions. Alternatively, if the electrodes are not electrochemically inert, another process may occur at either electrode; for example, a metal-oxide coating may be reduced to the metal at the negative electrode, or the metal may be oxidized to produce either metal ions or the metal oxide at the positive electrode. For purposes of illustration, however, it may be hypothesized that only H_2 and O_2 are produced by the electrode reactions, and consideration may then be given to the changes in the composition of the adsorbed layer that occur concurrently as a result of the electric mobilities of the H^+ and OH^- ions.

—41—

If, as in liquid water, the electric mobilities of both H^+ and OH^- ions in an adsorbed layer of H_2O molecules have significant values, the quantity of water on the fly ash near each electrode will gradually decrease, as a result of the fact that neither ion can be supplied at the electrode at the rate that reduction or oxidation occurs. However, if the fly ash has acidic surface components such as SiO_2 that react specifically with the OH^- ion to form an immobile ion such as $SiO_2(OH)^-$, the mobility ratio of H^+ to OH^- ion will be increased and the rate of depletion of the amount of water at the positive electrode will exceed that at the negative electrode. Alternatively, if the fly ash has basic surface components such as Al_2O_3 that have a specific attractive force for H^+ ion, the mobility ratio of H^+ to OH^- ion will be lowered, perhaps to the degree that a depletion of the amount of water will occur only at the negative electrode rather than the positive electrode. In summary, the combination of two phenomena described——gas formation at the electrodes and water depletion on the fly ash at one electrode or both electrodes——will increase the resistance through the ash and lead gradually to an apparent increase in the resistivity of the ash as the time of measurement and the amount of electricity conducted through the ash increase.

If the adsorbed layer contains H_2SO_4, the formation of H_2 and O_2 gas molecules must again be expected on inert metal electrodes. Furthermore, despite the near certainty that H^+ ion will have a much higher mobility than any ion of opposite charge that may be present (HSO_4^- or SO_4^{-2}), the combination of electrode reactions and the transference of the ions must lead to an increase in the concentration of H_2SO_4 at the positive electrode and, more importantly, a decrease in concentration of H_2SO_4 at the negative electrode. The net result of the phenomena described is likely to be a gradual increase in the apparent resistivity of the fly ash during the time of measurement. Gas formation at both electrodes and H_2SO_4 depletion at the positive electrode should overcome the opposing effect of H_2SO_4 enrichment at the negative electrode.

The foregoing discussion represents an effort to explain why the observed resistivity of fly ash may increase substantially with the time of measurement. Now a relatively brief discussion can be devoted to another experimentally observed phenomenon, the decrease in fly ash resistivity with increased electric field. A similar phenomenon, referred to as the Wien effect, occurs in certain liquid electrolytes——aqueous solutions of ionic compounds——that are analogous in composition to the adsorbed layers on fly ash. A decrease in resistivity of aqueous solutions

occurs as increasing electric fields are produced with an ac
power supply (which is typically used in studies of aqueous
solutions, in contrast to the dc power supplies normally used
with fly ash). This decrease is attributed to the reduction
in the effects of inter-ionic attractions that limit the rates
at which individual ions of opposite charge migrate in different
directions. The corresponding decrease in the resistivity of
fly ash can be attributed to a similar reduction in ionic inter-
actions within the adsorbed layer, and perhaps, in addition, a
reduction in ionic interactions with immobile surface components
of the fly ash. (This phenomenon is not associated with a
temperature rise as insufficient electrical energy was supplied
for this to be significant).

3.   Volume conduction

Variations of resistivity with time and electric field
have also been observed in the absence of surface conduction,
where the temperature is above 450°F. Typical current-time
curves show an initial high value of current decreasing with time
at a rate dependent upon many factors, as described by McLean.
The initial current is called absorption current and can be of
short duration in the case of solid borosilicate glass to minutes
in the case of particles of the same material.

Current conduction in siliceous-oxide glass is generally
accepted to be electrolytic. Although the possibility of some
electronic conduction cannot be eliminated, the nature of the
current-time and current-electric field data can be explained on
the basis of rather conventional electrolytic conduction.

In fly ash, conduction by an ionic mechanism is possible
due to the openness of the glass structure in contrast to that of
crystalline oxides possessing long-range order within the crystal
structure. This openness provides a "path" for the migrating charge
carrier and eliminates the need of energy to create structural
imperfections. Conduction is low in this type of system due to
the low ion mobility.

The charge carrier is usually thought to be a monovalent
cation such as Na^+, K^+, or Li^+. However, the carrier may be some
other electrostatically unbalanced species resulting from, for
example, gases or water vapor dissolved in the glass. The charge
carriers, in general, are loosely attracted to the glass structure
and contribute to the openness. When the glass is subjected to an
electric field, mass migration of the carriers occurs toward
their respective electrodes of opposite polarity and a current is
detected.

Below about 300°C, using dc measurements, it is noted that the initial current will decrease with time and eventually reach some "equilibrium" value. The higher the temperature, the shorter the time to equilibrium. This phenomenon is called absorption current. It is believed related to the initial random distribution of the charge carriers and random network glass structure. The glass structure does not provide a uniform energy barrier to the migrating species. Therefore, certain avenues of migration for the carrier are more energetically favorable than others. Ultimately the migration attains an "equilibrium" value when the diffusing species are finally limited in progress by high energy barriers.

If one is concerned with a finite specimen and an electro-lytic conduction mechanism, the direct current will gradually decrease as the concentration of carriers builds up at the elec-trodes, and will ultimately cease when the migrating ions are depleted. The effect is called electrode polarization.

The volume electrolytic conductivity increases with temperature. For conditions under which the current field strength relationship is linear, it can be expressed as an Arrhenius equa-tion, $\log \sigma \sim 1/T$. The conductivity may also be affected by field strength. In this case, the experimental activation energy is altered due to distortion of the energy barriers inhibiting the migration of charge carriers. The net effect is that conduction is enhanced disproportionately at high field strengths.

From the above brief description of ionic conduction, the observed current decay with time and the enhancement of conduc-tivity with increased field strength can be rationalized. It would appear entirely feasible that charge carrier depletion at the points of contact in a particulate or granular material, together with the absorption current phenomena would be adequate to explain the observed behavior. However, in view of the complex nature of the fly ash structure and the presence of many impurities, the possibility of semi-conductor behavior or purely electronic con-duction cannot be competely discounted.

In a precipitator, current is conducted to the dust sur-face by ions either carried on the particulate or unattached. Because of the higher mobility of the gas ions as compared with particulates, approximately 99% of the current is carried by these unattached ions. The method by which the ions arriving at the dust surface are neutralized has not been completely determined and may vary, depending on whether conduction through the dust layer is primarily through the adsorbed layer or through dust par-

ticles themselves. Regardless of the exact nature of the charge-transfer process, the result is that the arriving ions are neutralized at the gas-dust interface and the charge transfer through the dust layer takes place in the same manner that it would in the resistivity cells previously described.

One significant difference, however, is that fresh dust is being precipitated continuously, thus, the dust layer-gas interface is constantly changing. The interface between the dust layer and grounded electrode, however, does not change, and variations in resistivity with time could occur at that interface in much the same manner as in a resistivity probe. However, depletion of the charge carriers occurs primarily at the cathode in the case of a sulfuric acid conditioning system, which would minimize the effect.

The electric field in the dust layer of a precipitator depends upon the current density and the resistivity of the dust $(E = j\rho)$. The limiting field is the breakdown conditions of the interstitial gases, usually around 10 to 20 kV/cm. If dust resistivity is high (around 10^{10} to 10^{11} Ω-cm), the precipitator would normally be operated near the breakdown field of the dust layer. However, if the dust resistivity is low (around 10^7 to 10^8 Ω-cm), the limiting operating condition of the precipitator is not breakdown of the dust layer, but rather sparking across the interelectrode space. Thus, the resistivity seen by the precipitator would be that corresponding to the lower electric field.

The time dependence of resistivity is perhaps a more significant variable. Rapping frequency varies depending upon dust loading and is in the range of 5 to 10 min. If all of the dust were removed from the plate during each rap, the average time that the dust is on the plate would be 2.5 to 5 min. However, in normal rapping, dust moves vertically down the plate during a rap and is either recollected several times prior to finally falling into the hopper or some dust may fall the entire distance in a single rap before being recollected. Thus, the dust may remain in the precipitator during several rapping cycles with current flowing through the dust layer for a period of, say, 10 to 20 min. Thus, the resistivity in a precipitator could vary with time and perhaps be a factor. Again, however, fresh dust being deposited would tend to minimize the effect.

4. Comparison of resistivity measurements by various probes

Since the factors discussed in the previous sections affect the resistivity as measured by the different cells, a comparison was made of resistivities at the same plant utilizing several

resistivity probes. Figures 2.14 and 2.15 are comparison plots
of the resistivity measured by the point-plane probe with that
measured by the cyclone collector, cylindrical cell probe, and
the EPA apparatus which utilizes a wire and pipe precipitator
for collection and a cylindrical cell electrode for resistivity
measurements. Figure 2.16 shows the comparative resistivities
between the steady-state values of the cylone probe and those
measured by the point-plane apparatus at maximum field strength.
In addition to the scatter, the steady-state values from the
cyclone probe are at least one order of magnitude higher than
those measured by the point-plane probe.

Figure 2.14 shows the settled out cyclone data plotted
against the point-plane data using the point-plane data at 2.5
kV/cm, which corresponds to the field in the cyclone apparatus.
A somewhat better agreement between the two methods is apparent
with compensation for the influence of electric field.

Figure 2.15 shows the peak values of resistivity from the
Kevatron and cyclone probes plotted against point-plane data for
the same (2.5 kV/cm) field. In this case, much better agreement is
obtained between the cyclone and point-plane data. The EPA data
are still higher than the average of the cyclone or point-plane
data, although there is statistically insufficient data to draw
firm conclusions regarding the Kevatron values.

The logic of comparing the peak current values of resistivity
from the cyclone with the point-plane data can be rationalized
to some extent by the fact that fresh dust is being deposited on
the surface during the precipitation process. Thus, even though
corona current is flowing during the collection interval, the dust
surface in contact with the upper disc has not been subjected to
a current flow for an appreciable time. The interface between
the dust and lower electrode has had current flowing during the
collection period. However, polarization effects are not likely
at the anode surface.

The agreement between resistivities as measured by the
methods compared is not extremely bad when one considers the
scatter of the data when using a single apparatus. However, some
basis on which to compare the data in a rational manner needs to
be resolved.

In further consideration of the factors that might cause
differences in resistivity values as measured by the various
methods, several observations were made in the laboratory and in
the field regarding the differences in time variation between the

Figure 2.14. Comparison of Kevatron and Cyclone Resistivities
with Point-Plane Resistivities at an Electric
Field of 2.5 kV/cm. Settled Values for Cyclone,
Peak Values for Kevatron.
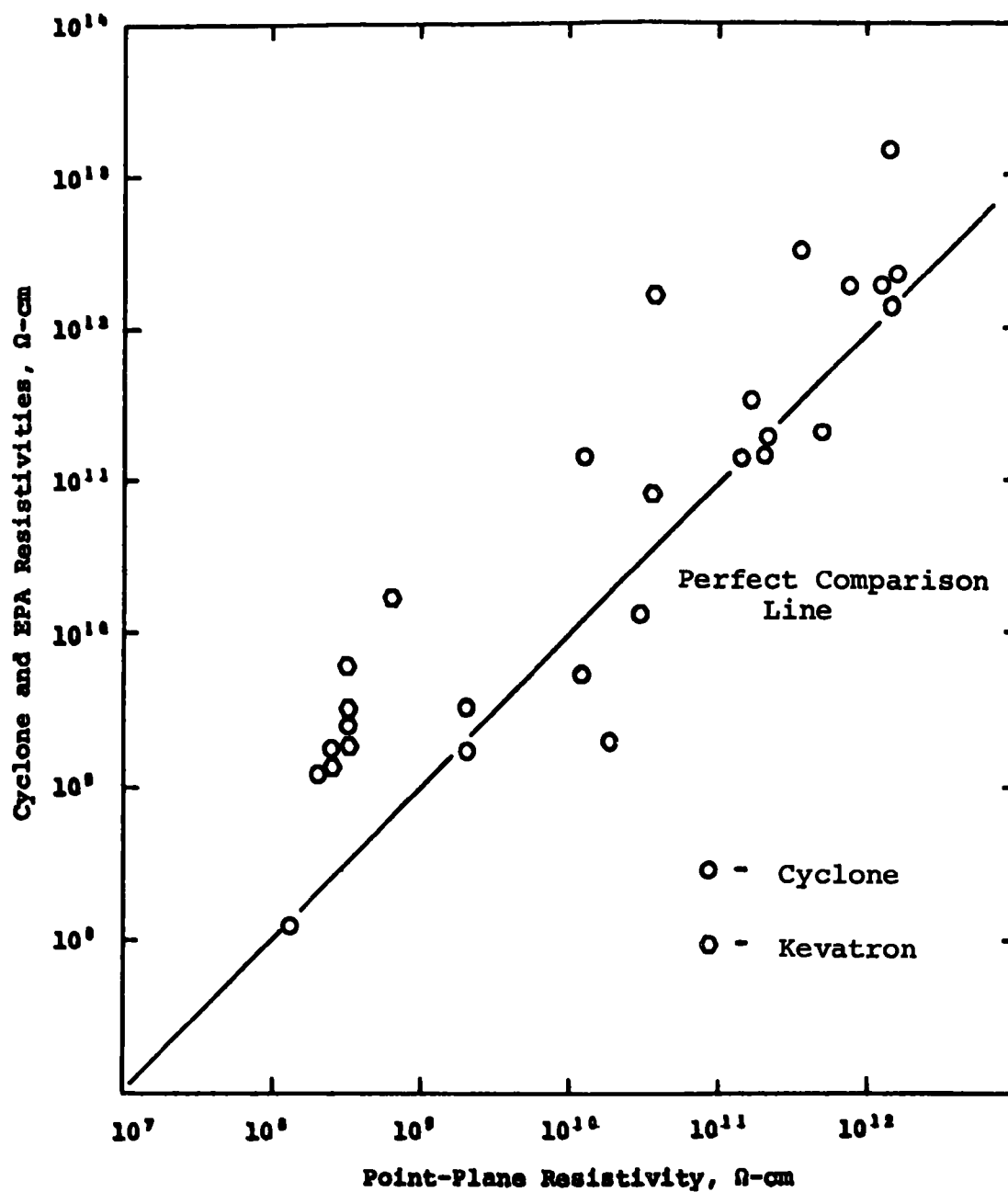
Figure 2.15. Comparison of Kevatron and Cyclone Resistivities
with Point-Plane Resistivities at an Electric
Field of 2.5 kV/cm. Peak Current Values Used
for Cyclone and Kevatron.
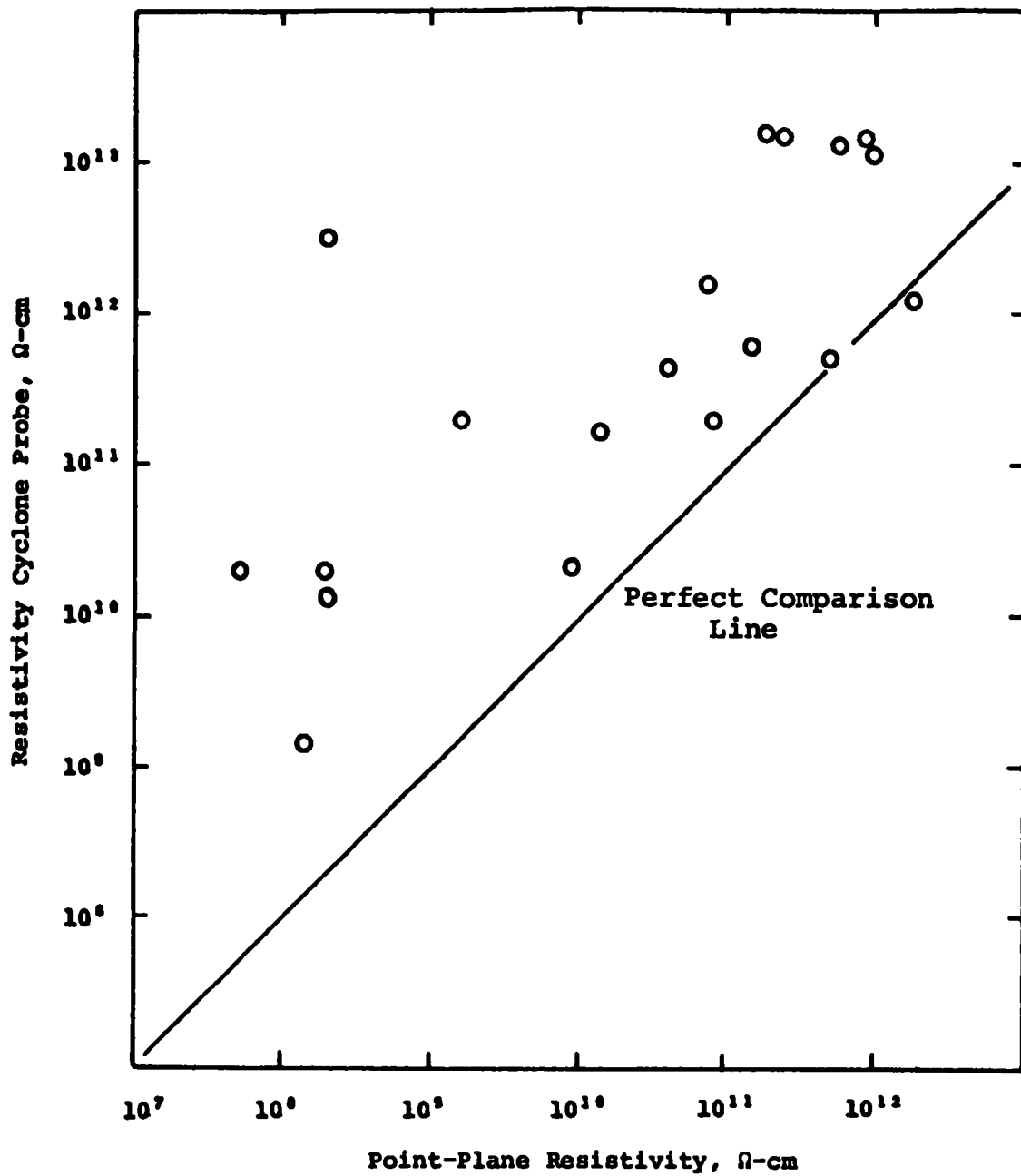
Figure 2.16. Comparison of Cyclone Resistivities with Point-Plane Resistivites. Maximum Electric Field on Point Plane. Settled Values for Cyclone.

two types of cells; parallel disc and cylindrical. In general, a greater variation in resistivity with time was observed with the cylindrical cell than with the point-plane apparatus.

A difference in the electrochemical properties of the electrode materials is one possible explanation for the difference in the effects of the two electrolytic phenomena in the cells with cylindrical and disc electrodes. In the cylindrical cell constructed in this laboratory the electrodes are made from stainless steel, whereas in the parallel disc cell, the electrodes are made from copper. Gas formation may occur less extensively at copper electrodes than at stainless steel; if so, the overall effect from electrolytic processes in the parallel disc cell will be less than that in the cylindrical cell.

A difference in current densities at the electrodes is still another possible explanation for the difference in the effects of the electrolytic phenomena in the two cells. At least superficially, the difference in current densities may appear to be small. For fly ash with a resistivity of 1×10^{10} Ω-cm in the cylindrical cell fabricated in this laboratory——with electrode diameters of 0.47 and 1.27 cm and a height of 4.44 cm——current densities of 0.54 and 0.20 $\mu A/cm^2$ will be produced at the two electrodes with a typical value of 2.5 kV/cm as the average electric field in the sample. For the same ash in the parallel disc cell——with an area of 5 cm^2 on each of the disc electrodes and a typical sample thickness of 0.05 cm——a current density of 0.25 $\mu A/cm^2$ will be produced at the two electrodes with a typical value of 2.5 kV/cm as the average electric field in the sample. In view of differences in sampling packing densities, however, the actual current densities at the cylindrical electrodes may be substantially different from those at the disc electrodes. Sample packing between the cylindrical electrodes occurs only as the result of rapping or vibration; sample packing between the disc electrodes, on the other hand, occurs under an applied pressure. The number of contact points per unit of surface area between the fly ash particles and the cylindrical electrodes is, therefore, likely to be much smaller than the number of contact points between the particles and the disc electrodes. Consequently, even with approximately equal current densities computed for the two types of electrodes on a superficial basis, the actual current densities and the intensities of electrolytic effects may be much greater at the cylindrical electrodes than at the disc electrodes.

A difference in the degree of isolation of fly ash from the flue gases following collection in the two types of resistivity cells may also lead to a difference in the effects of the electrolytic phenomena in the two types of cells. Samples collected with cyclone probes and deposited between cylindrical electrodes must be more completely isolated from the flue gas than the samples collected with the point-plane apparatus and located between parallel disc electrodes. If the ash is collected with a reactive material such as H_2SO_4 on its surface and then isolated from the flue gases, changes in surface composition should occur as a result of chemical reactions, accentuating the changes associated with electrolytic processes. We have encountered evidence that fly ash collected in the cyclone apparatus will contain more SO_4^{-2} than ash collected simultaneously in the point-plane apparatus. It is reasonable to expect that any H_2SO_4 reacting with fly ash after collection can be less easily replenished by further adsorption of H_2SO_4 vapor from the gas stream in the cyclone apparatus than in the point-plane apparatus.

These factors need to be resolved in attempting to arrive at comparable methods of measuring resistivity.

5. Factors influencing fly ash resistivity

The factors previously discussed point out the considerations in making meaningful fly ash resistivity measurements and comparing the values determined by the various types of apparatus. In addition to this, resistivity can change drastically between fly ash from different types of coals. The factors responsible for these variations are those that influence both surface and volume conduction.

In the temperature region where surface conduction predominates, resistivity changes with temperature and the amount of conditioning material present in the gas. In the case of fly ash, the conditioning agent is H_2SO_4 formed by the water and SO_3 in the flue gas. The sulfur content of the coal determines the sulfur dioxide content of the flue gas. Under most conditions, around 1% of the SO_2 in the flue gas is converted to SO_3, and hence for normal circumstances, the sulfur content is a reasonably good estimate of the SO_3 present in the flue gas and therefore is a good measure of the resistivity that can be expected at any given temperature within the range where surface conduction predominates.

However, several factors can alter these normal relations. First, the percentage of SO_2 converted to SO_3 can change depending upon the temperature-time conditions, amount of excess air, and perhaps upon the surface composition of the ash. Since a large quantity of SO_2 is present in the flue gas, even a small increase in the percentage converted can alter resistivity of the ash considerably.

The second factor that can alter the normal resistivity-sulfur relationship is the basicity of the ash. A highly basic ash surface will react with the available SO_3 to form a sulfate that in itself has high resistivity. Once the sulfate is formed, a layer of H_2SO_4 can be adsorbed on the surface and this is responsible for the change in resistivity.

In addition to uncertainties in fly ash resistivity in the temperature region where surface conduction predominates, variations also occur in the high temperature range where volume conduction is primarily responsible for the resistivity. Composition of fly ash can vary widely between various types of coal. These variations can influence the resistivity of the ash as a result of day-to-day variations in composition from the same coal seam.

Table 2.2 lists average, maximum, and minimum values of the various compounds in coal ash samples taken from the Colstrip mine. Out of 21 samples, the CaO content varied from a minimum of 13% to a maximum of around 30%. Figure 2.17 shows the variation in resistivity with temperature for two samples of this ash over a range of temperatures. It is apparent that resistivity of the ash was above 2×10^{10} Ω-cm, even at 600°F for this particular sample.

Table 2.2 Variation in Chemical Analysis
of Fly Ash from Western Coal

Compound	Average	High	Low
SiO_2	36.3	40.6	32.2
Al_2O_3	19.6	22.2	15.6
Fe_2O_3	4.74	8.5	3.5
TiO_2	0.69	0.9	0.3
P_2O_5	0.36	0.8	0.20
CaO	19.1	29.7	13.3
MgO	4.31	6.6	1.40
Na_2O	0.27	0.4	0.20
K_2O	0.11	0.2	0.10
SO_3	12.85	14.6	11.0
	98.33	124.5	77.8
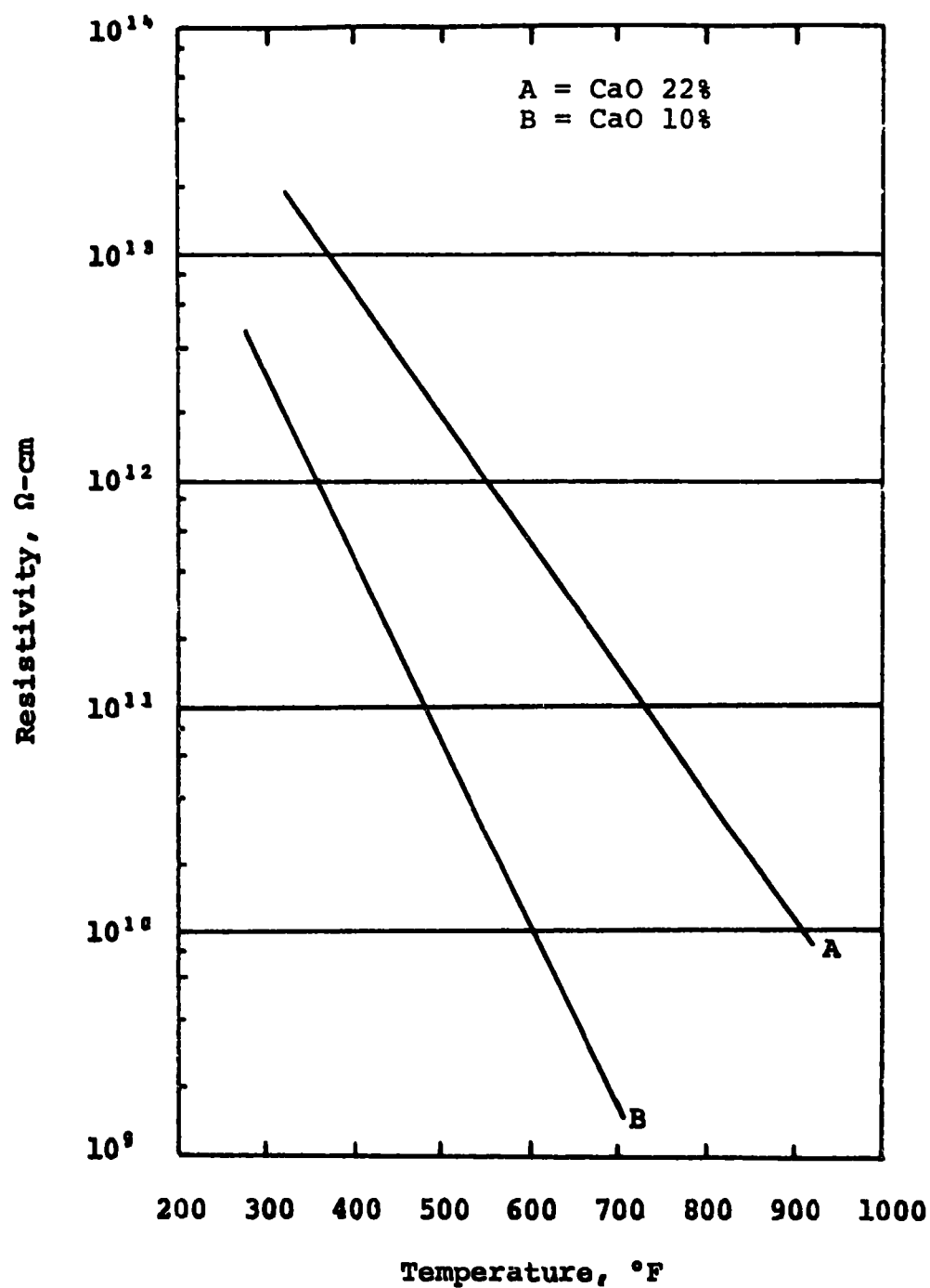
Figure 2.17. Laboratory Resistivity Measurements
for Two Fly Ash Samples from Western
Coal (Pre-Dried Ash Samples).

Figure 2.18 shows the variation in resistivity for various oxides as a function of the parameter 1/kT as reported by White.[1] It is apparent from these data that rather wide changes in resistivity can occur between different oxides, and hence it is not surprising that variations in bulk resistivity of fly ash occur. However, for the majority of fly ash, resistivity values at 600°F are sufficiently low so as not to consitute a problem.

Figure 2.19 is a composite plot of the resistivity data taken on several fly ash samples utilizing a point-plane probe.

D.   Sparkover and Back Corona

The phenomena of sparkover and back corona constitute practical limits on the operation of an electrostatic precipitator since they determine the maximum current and voltage at which the precipitator will operate. From the standpoint of modeling or predicting precipitator performance, it is necessary to establish the maximum current and voltage conditions as related to measurable properties of the dust and precipitator electrode geometry. Studies of sparking and back corona under this contract were directed toward review of the theory of sparkover and experimental verification of the influence of dust resistivity on sparkover and back corona conditions.

Electrical properties of a precipitator are defined by the curves relating secondary voltage and current. Under clean collection electrode conditions, the secondary voltage can be increased with a corresponding increase in secondary current until the electric field in the interelectrode space breaks down and a spark propagates from the anode to the cathode. In the case of negative corona, the anode is the collection electrode, which is at ground potential.

The shape of the voltage-current curve as well as the sparkover voltage is determined by the electrode geometry and spacing. For a wire and plate or cylinder precipitator, the primary variables are the diameter of the wire and the separation between wire and plate or cylinder. Except for very small wires, smaller diameter wire results in higher current for a given voltage if the pipe diameter is held constant. Both the wire diameter and spacing alter the electric field and hence determine the conditions for spark initiation and propagation.
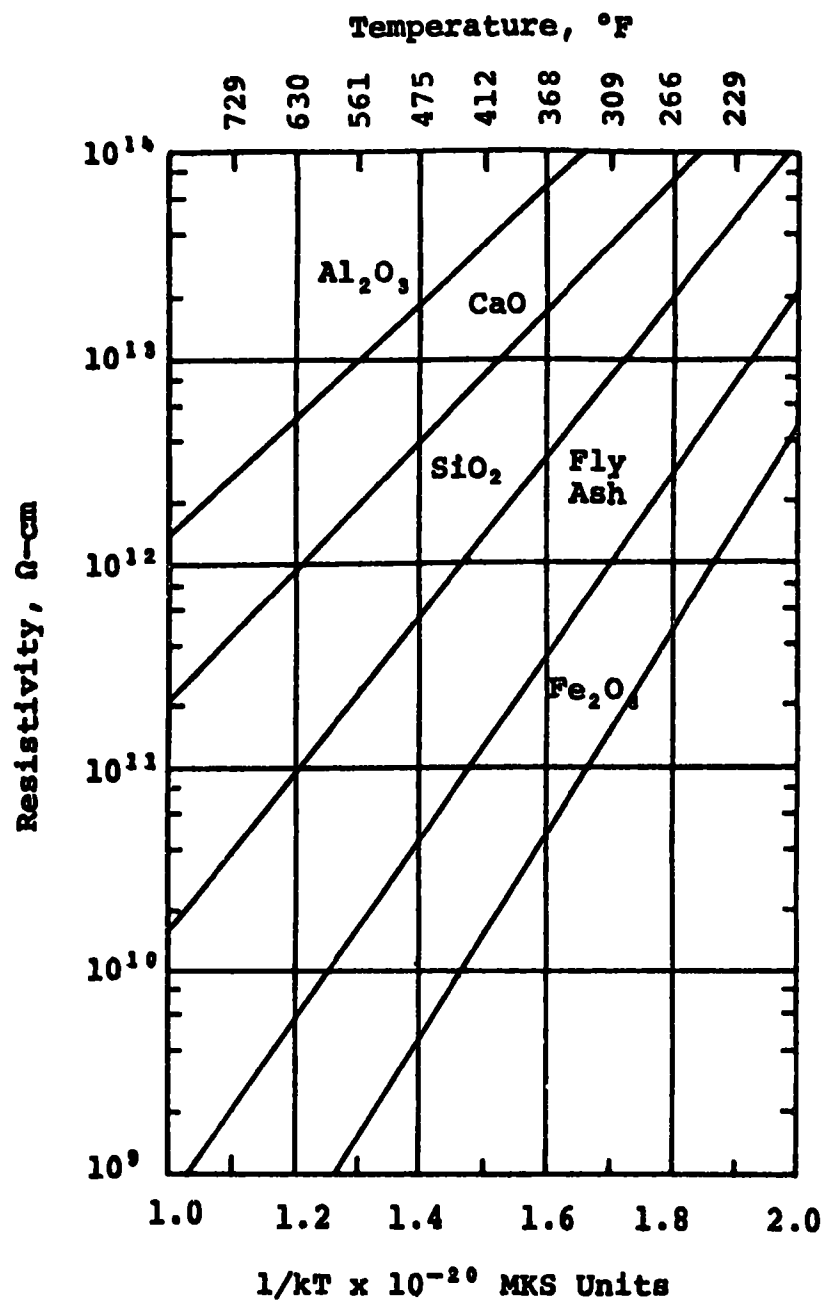
Figure 2.18. Variation in Resistivity for Various Oxides as a Function of the Parameter 1/kT
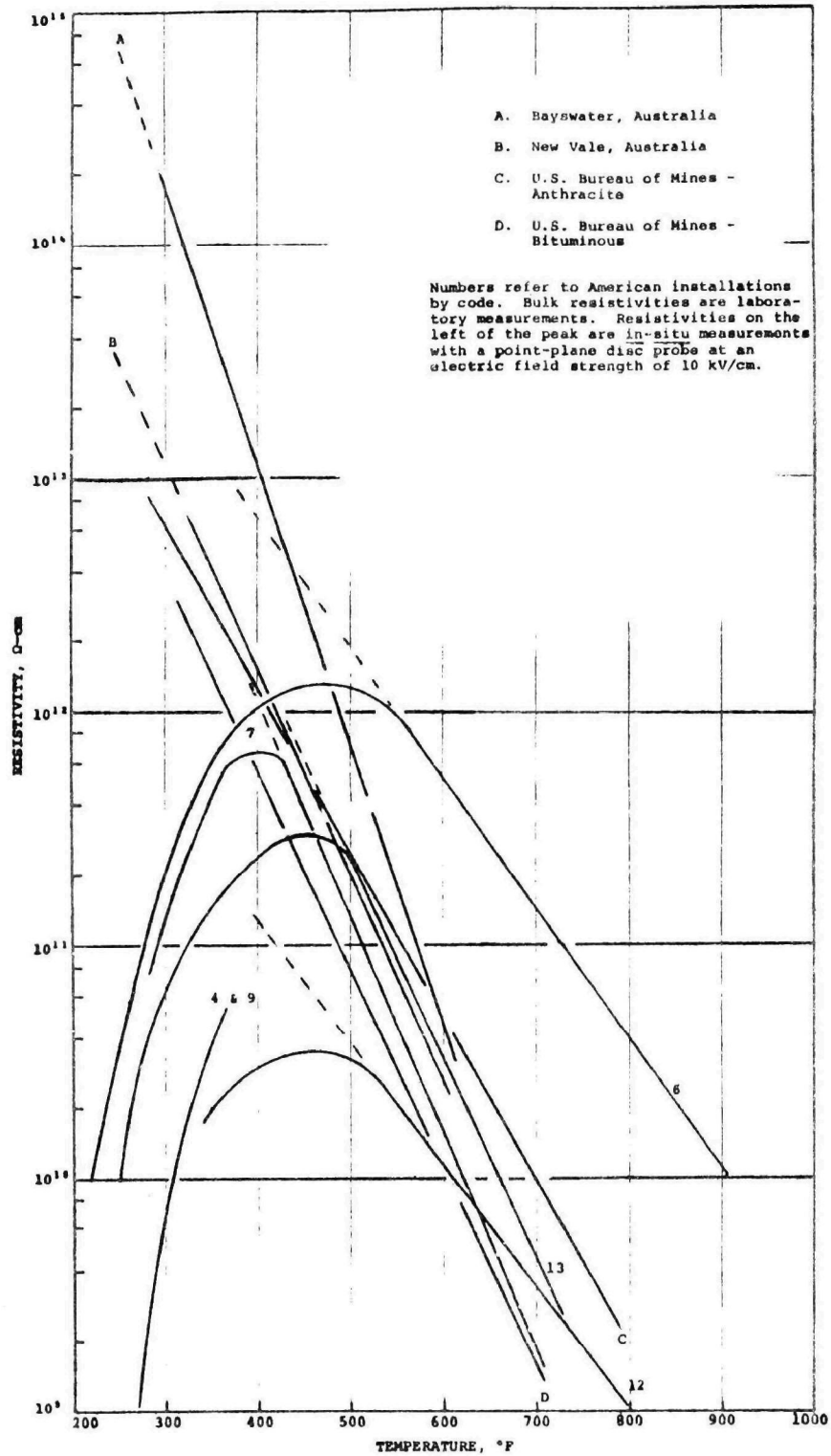
Figure 2.19. Composite Plot of Resistivity Data for
Several Fly Ash Samples

Fundamental studies of the mechanism of spark initiation and propagation have been made by Penney[10,11], Loeb[12], and others. These studies indicate that sparking originates from streamers or flares at the anode and propagates across the interelectrode space provided there is sufficient voltage across the electrodes.

In the case of clean electrodes, the conditions for sparking are simply that localized breakdown occurs, usually at a small region of high field strength near the collection electrode. The conditions necessary to cause the localized breakdown are generally sufficient to propagate the spark across the interelectrode space.

If dust is present on the collection electrode surface, the voltage-current curves will be altered by the voltage drop in the dust layer, which is given by

$$V_d = j\rho t \qquad\qquad . \quad 2.5$$

If the dust layer resistivity is low (around 10^7 Ω-cm), the voltage drop across it will be low and the voltage-current curve will be shifted as though the electrode spacing were decreased. High dust resistivity, on the other hand, can result in large voltage drops and high electric fields within the dust layer itself. The field in the deposit can be computed as $E = j\rho$. For reasonably high dust resistivities, electric fields in the deposit can be rather large for currents normally encountered in precipitator practice. As the field is increased, a point is reached where it exceeds the breakdown strength of the interstitial gases. The breakdown strength can vary depending on the size and composition of the dust, as well as the gases; however, for the majority of industrial dusts, breakdown generally occurs in the range of from 10 to 20 kV/cm.

Breakdown of the dust layer can cause one of two events to take place. If the dust resistivity is in the intermediate range, breakdown of the dust layer can cause a sudden increase in the interelectrode voltage since the voltage drop that was previously across the dust layer is now added to the voltage that previously was established between the discharge electrode and dust layer surface. If this voltage is sufficiently high, a spark will propagate across the interelectrode space. Localized breakdown of the dust can act in much the same fashion as a point, thus reducing the voltage required for spark propagation.

If the resistivity of the dust layer is increased further, the voltage drop across the dust layer can be exceptionally high even at low current densities, and breakdown can occur at voltages lower than those required to propagate a spark across the interelectrode space. If this occurs, a condition of back corona develops and the voltage-current curves of the precipitator depart from the normal curves characteristic of a pure resistive effect.

The condition of back corona can be observed in the laboratory as a diffuse glow over the dust layer surface. A continued increase in voltage and current will result in sparking, provided the power supply has sufficient capacity.

The significance of a back corona condition is that the breakdown releases positive ions (for the negative corona precipitator), and these ions are propelled by the electric field into the interelectrode region. If they impinge on negatively charged particles, they serve to reduce the normal charge or charge the particles with the opposite polarity.

When a back corona condition develops, the character of the current-voltage curve changes. Increases in voltage beyond the onset of back corona result in an abnormally rapid increase in current as compared with the normal case.

From theoretical considerations, the conditions limiting precipitator operation are summarized graphically in Figure 2.20. Curve 1 in this figure is a clean plate, voltage-current curve for a point-plane precipitator with a point-to-plane spacing of 1.12 cm. Curve 2 is calculated on the basis of a dust layer thickness of 0.20 cm and a resistivity of 10^8 Ω-cm. Curve 3 is for a resistivity of 10^9 Ω-cm, and Curve 4 corresponds to a dust resistivity of 10^{10} Ω-cm. The dotted line 5 represent the voltage drop in the dust layer corresponding to the breakdown field strength for dust layers of 0.2 cm.

In the case of Curve 2, it is apparent that breakdown in the dust layer would occur only at very high current densities. Before this point is reached, the voltage across the interelectrode space is sufficient to cause a spark to propagate. This would theoretically occur when the voltage from the dust layer to the discharge electrode equals the clean plate sparking condition. Because of the voltage drop across the dust layer, sparking would theoretically occur at a voltage corresponding

1. Clean Plate - Point-to-Plane Spacing, 1.12 cm

2. 2 mm layer dust - 10^8 Ω-cm resistivity

3. 2 mm layer dust - 10^9 Ω-cm resistivity

4. 2 mm layer dust - 10^{10} Ω-cm resistivity

5. Line designating electric field in deposit reaches 20 kV/cm for 2 mm layer

NOTE: Arrow designates sparking
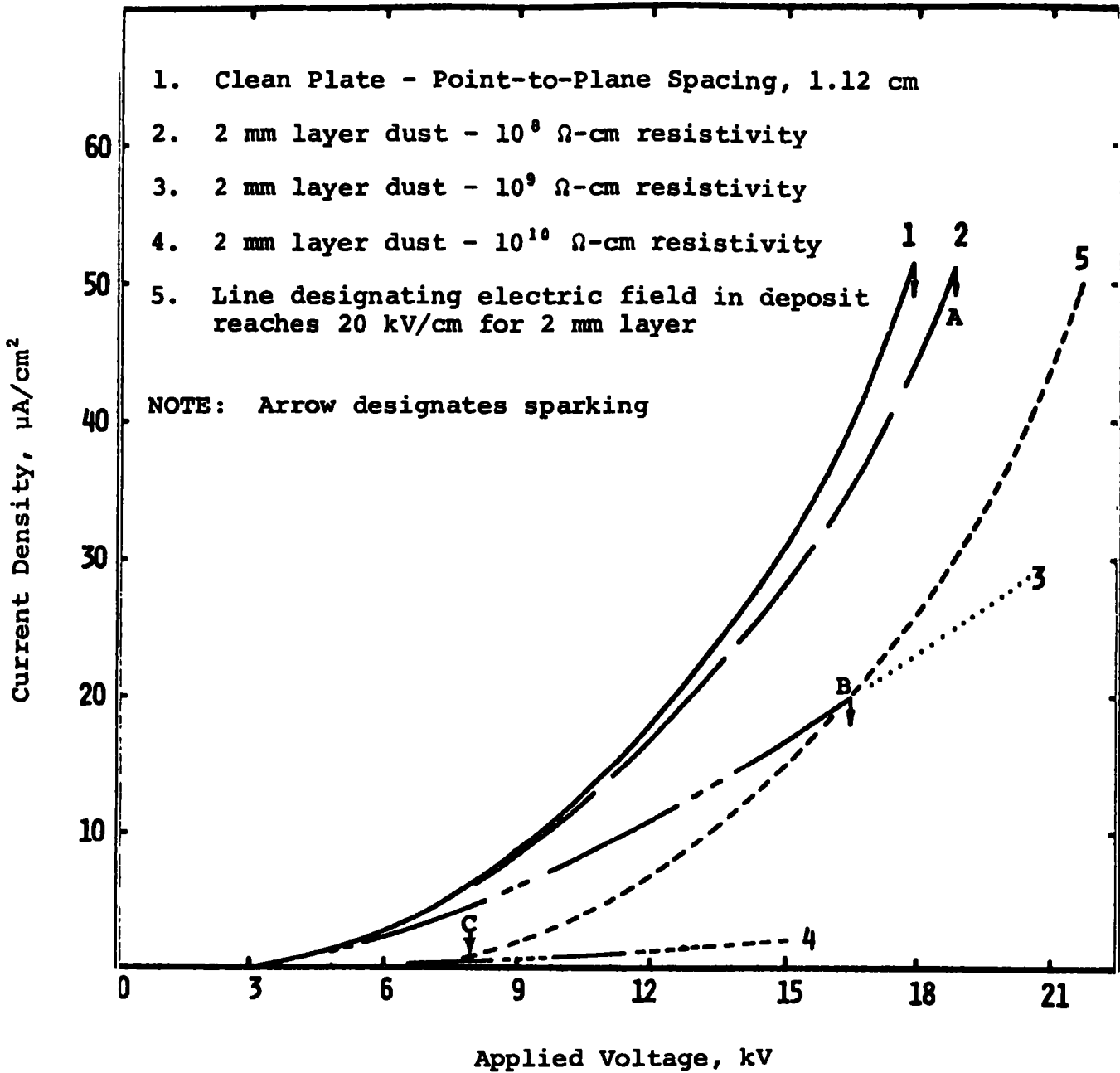
Figure 2.20. Behavior of a Point-to-Plane Electrostatic Precipitator Based on Theoretical Considerations of Sparking and Back Corona. Clean Plate Curve is Measured Curve, Remaining Curves Computed.

to Point A. This condition, therefore, represents one criterion for sparking in which there is no breakdown in the dust layer.

In the case of the dust with a resistivity of 10^9 Ω-cm, the voltage drop across the dust layer would exceed the breakdown field for a 0.2 cm dust layer at a current corresponding to Point B. At this point, localized breakdown would result in a voltage developing across the interelectrode space (dust layer surface to discharge electrode) equal to the voltage required for spark propagation on a clean plate electrode. When this condition is reached, sparking will occur. This consitutes the second criterion for sparking; that is, when breakdown of the interstitial gases occurs at a voltage sufficient for the combined electrode-to-dust-surface voltage and the voltage drop across the dust layer to equal the clean plate sparkover voltage.

Point C represents the third condition which corresponds to a high dust resistivity. Here breakdown occurs at a voltage sufficiently low so that the combined electrode-to-dust-surface voltage and the voltage drop across the dust layer is less than that required for propagation of a spark. Under these conditions, a back corona develops without sparking. However, if the voltage is increased, the current will increase somewhat along the curve for constant breakdown voltage until a voltage sufficient to cause a spark to propagate is reached. This consitutes the third criterion for sparking; that is, a back corona condition precedes the sparkover voltage.

Several factors can modify sparkover conditions. If the dust layer thickness is increased, the voltage drop across the dust layer will increase proportionately. The breakdown voltage is thus greater so that this voltage drop added to the electrode-to-dust-surface voltage is sufficient for a spark to propagate. Thus, the increased thickness can cause a change from a back corona to a sparking condition for the same dust.

The waveform of the applied voltage is also thought to influence the sparkover characteristics. The sharp rise rates on the leading edges of the waveform results in a higher peak to average voltage and consequently field on the device.

Changes in the character of the dust can also alter sparkover and back corona conditions. The presence of conductive particles in the dust (such as unburned carbon) can alter the localized field strength and cause breakdown to occur at lower voltages than would be predicted.

Also, very fine dust of high resistivity material can act in somewhat the same fashion as a solid insulator to increase breakdown strength. These factors can alter the specific conditions; however, the generalized theory of sparkover and back corona can be used to predict behavior if the specific conditions are known.

1.   Experimental verification

Studies of sparking and back corona conditions were made in the laboratory utilizing dust of varying resistivities to determine how closely the limiting conditions of sparkover and back corona could be predicted. The apparatus utilized in these studies was a point-plane precipitator with dimensions as shown in Figure 2.21. The procedure followed was to obtain a voltage-current curve for a given spacing from the point to the grounded plate. A dust layer was then placed on the grounded electrode and screeded to give the desired thickness. The plate spacing was then adjusted so that the distance from the point to the dust surface was equal to the previous point-to-plate spacing. The V-I curve with the dust layer was then obtained. In each case, the voltage was increased until sparkover occurred. Dusts used in the experimental work were fly ash from two sources, aluminum oxide (activated alumina, 80 to 325 mesh chromatographic grade) and sulfur. All data were taken in air at ambient temperature (70°F) utilizing an X-Y recorder to obtain the voltage-current curves. In the case of the high resistivity dust, the current scale was expanded in the low range to detect the initial rapid current increase indicative of the onset of back corona. Resistivity of the dust was measured with two parallel discs following each test.

Table 2.3 shows a comparison of the resistivity as determined from the V-I curve and that measured by the parallel disc method. The values agree reasonably well when compared at equivalent field strengths and current densities.

Figure 2.22 shows the V-I curves for the dusts with various resistivities. The data are for a dust layer thickness of 0.23 cm.

The data shown illustrate the conditions for spark propagation reasonably well. Point A of Curve 2 indicates sparking at a voltage reasonably close to the clean plate sparking voltage plus the voltage drop in the dust layer. Points B and C show sparking occurring at near the predicted breakdown field strength; however, the voltage at which sparking occurs is less than that required to propagate a spark under clean plate conditions.

A - High Voltage Supply

B - Current Measurement

C - Ground
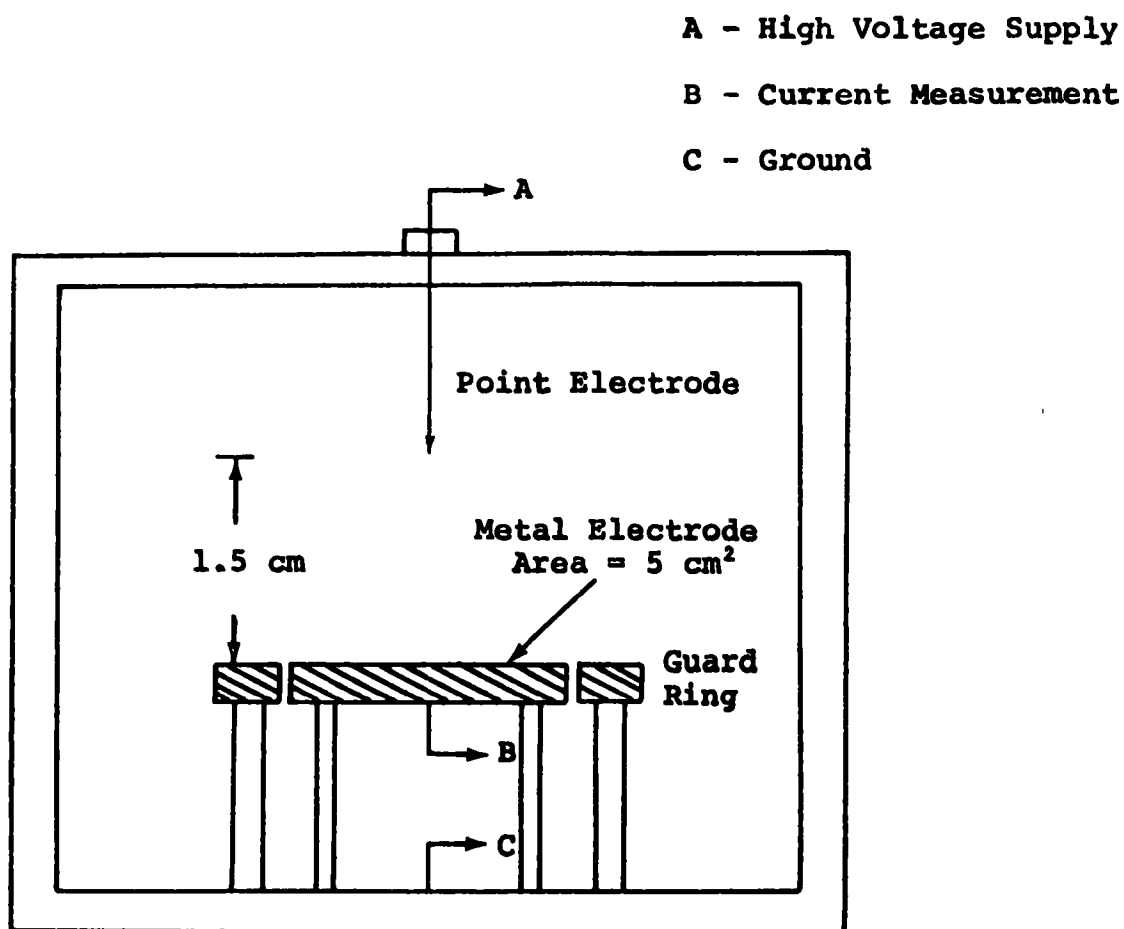
Figure 2.21. Dimensions of Point-Plane Precipitator Used in Laboratory Studies of Sparking and Back Corona Conditions

Table 2.3. Comparison of Resistivity Determined by
the Parallel Disc Method and the V-I Curve Method
(Direct Current Tests)

Parallel disc	V-I curve
6×10^7	4×10^7
7×10^8	3.1×10^8
1×10^{10}	5.7×10^9
8×10^{12}	1.4×10^{11}*

*Back corona noted.

In reviewing the probable causes for spark propagation
occurring at lower than clean plate voltage, it was concluded
that two factors could contribute to this condition. First,
breakdown in the dust layer is accompanied by visible light
emission. Acker[11] states that one mechanism of spark propa-
gation is by photoionization since the current rise is more rapid
than would be possible by electron flow. If so, the emissions
accompanying breakdown could account for the lower spark propaga-
tion voltage. A second factor in the lower breakdown voltage is
the probability that the breakdown in the dust layer acts as a point.
Since point-to-point breakdown occurs at much lower voltage, this
could account for the behavior noted.

2.   Relation to precipitator operation

The theory of sparkover and back corona applies to full-size
precipitators. Since a precipitator is normally operated with a
time-varying voltage, the peak current and waveform would determine
sparkover conditions. Also, variations in spacings from wire to
plate, as well as areas of localized high fields, can alter the
sparkover conditions.
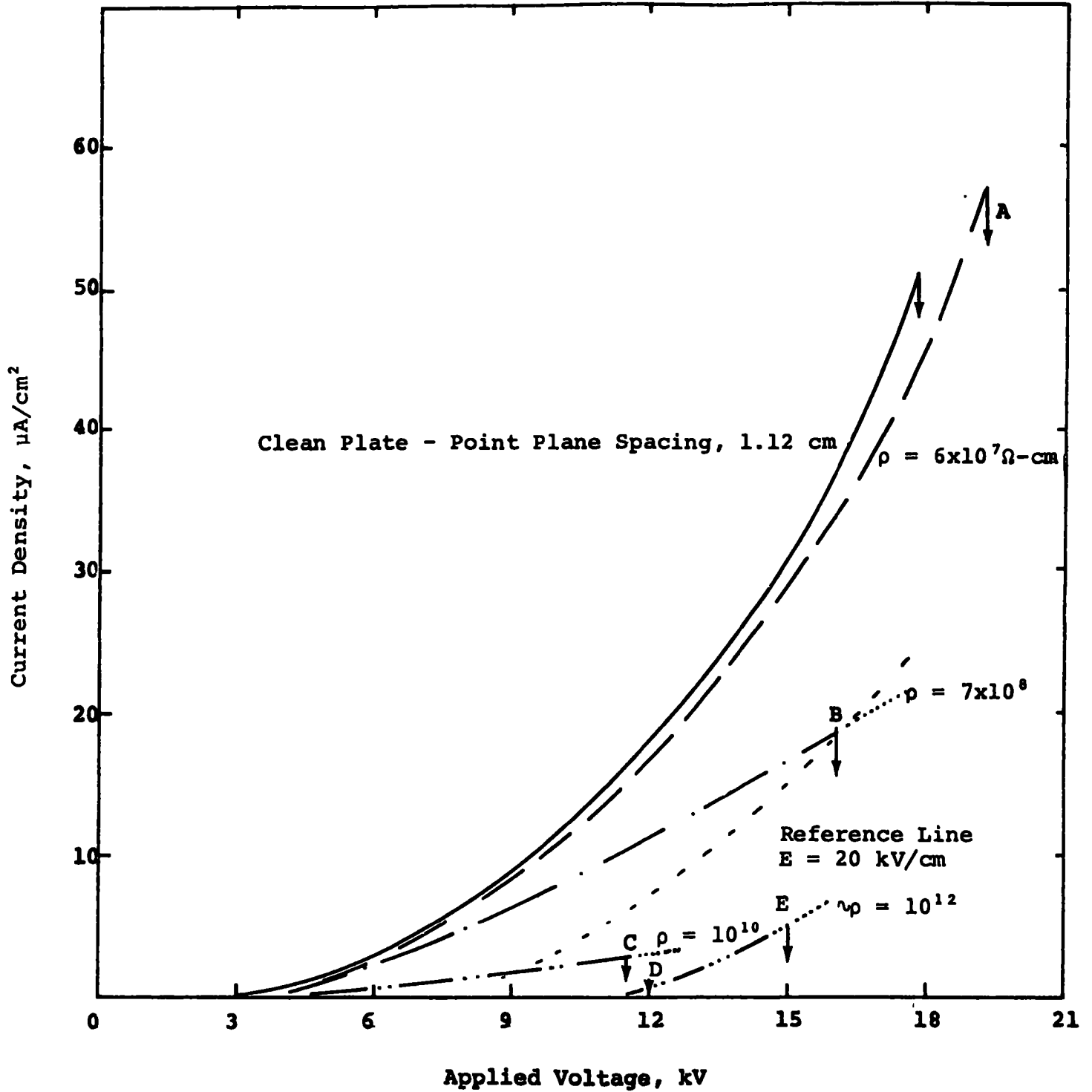
Figure 2.22. Experimental Volt-Current Curves for Point-Plane Device with a Variety of Dust Resistivities. Dust layer thickness is 2.3 mm.

Figure 2.23 shows the voltage-current curves for a precipitator section. Curve 1 was taken when the precipitator was operating at 260°F with a 3% sulfur coal. Dust resistivity under these conditions is low and the curve should approximate a clean plate curve very closely.

Curve 2 corresponds to conditions of around 1% sulfur coal with a correspondingly higher resistivity. Also plotted on the same figure are the theoretical voltage-current curves corresponding to resistivities of 1×10^{12} to 1×10^{13} Ω-cm. From the appearance of the curves, a back corona condition would be predicted around Point A. The V-I curves would indicate the dust resistivity to be high (1×10^{13} Ω-cm). Once back corona is established, the voltage drop across the dust layer would tend to be constant and the V-I curve would depart from the typical purely resistive behavior. The gaseous breakdown would cause the curve to act more like a gaseous discharge tube with a constant voltage drop which is equivalent to the breakdown field strength.

Figure 2.24 is a similar curve for a second precipitator operating on fluorspar dust with very high resistivity. Again, the behavior suggests that breakdown of the dust layer occurs at very low current and that the shape of the curve parallel to the clean plate curve suggests that the back corona condition causes a constant voltage drop across the dust layer. In the case of very high resistivity dusts, the shape of the V-I curve can be further altered as a result of more complete breakdown of the dust layer.

Results of the studies so far have not correlated measured resistivities with the apparent resistivity as indicated by the V-I curves, the latter suggesting higher resistivities in most cases than is indicated by resistivity measurements on the particular dust. Additional studies to correlate measured resistivities with V-I curves are indicated.

The optimum operating point for a precipitator in a back corona condition also needs study. Many precipitators with high resistivity dusts are set to operate under spark-limiting conditions. Since, for high resistivity dust, back corona precedes sparkover, studies of optimum operating conditions need to be made.
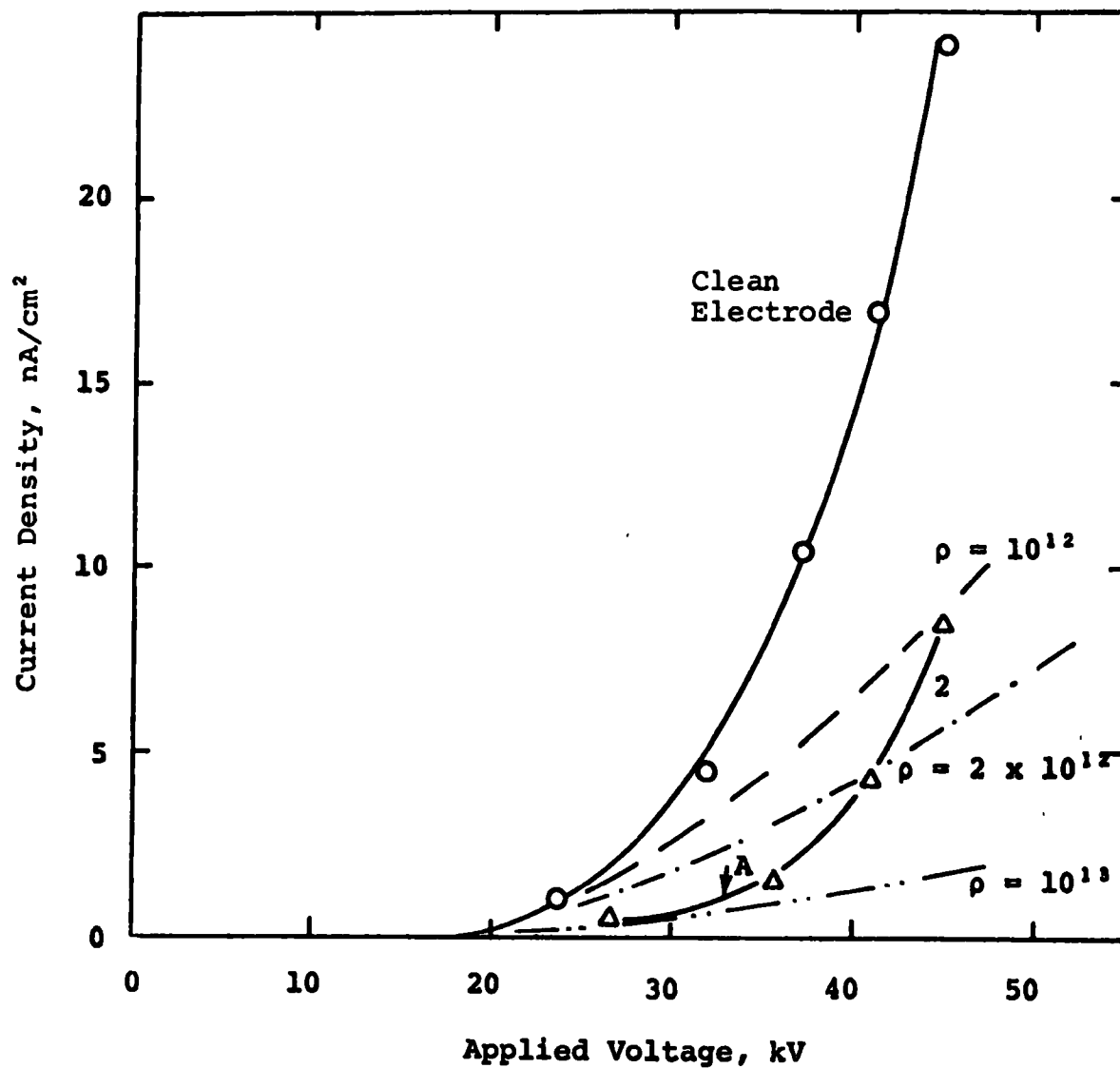
Figure 2.23.   Voltage-Current Curves for a Precipitator
               Section
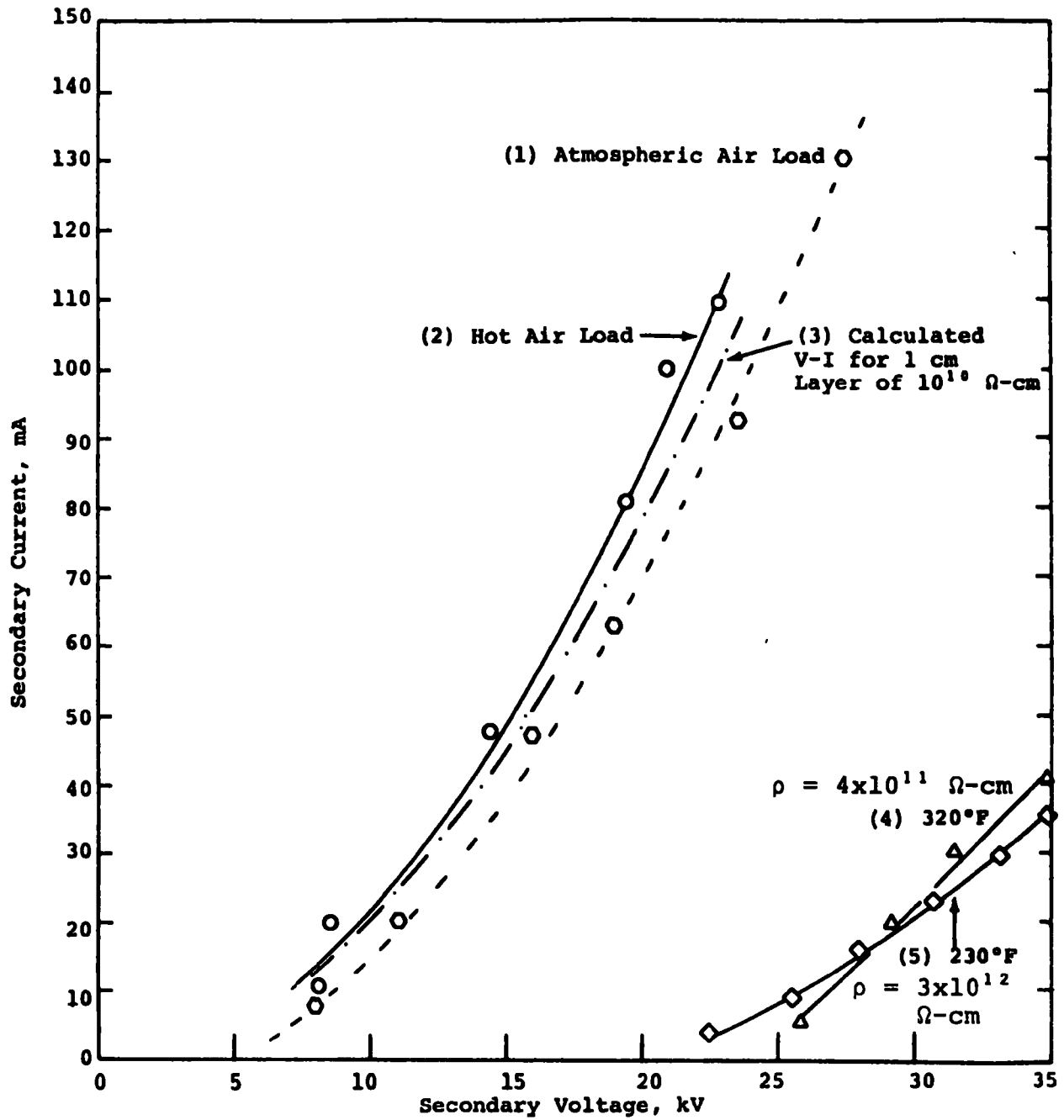
Figure 2.24. Voltage-Current Curve for a Precipitator Operating on Fluorspar Dust with Very High Resistivity

E.   Optimization of Precipitator Design
      for High Resistivity Dusts

The theory of precipitator operation states that the migration velocity of a dust particle is proportional to both the charge on the dust particle and to the value of the electric field in the vicinity of the collection electrode as shown by

$$w = qE_p/6\pi a\eta \qquad\qquad 2.6$$

Thus, the two electrical quantities of interest are the charge and the field.

The operating point for electrostatic precipitators used to collect high resistivity materials is limited by the sparking rate of the power supply or by the current limit in the absence of sparking. The spark rate of the power supply is determined by the electrical conditions at the surface of the dust layer as discussed in Section D. With a reasonably high resistivity dust layer on the plates, sparking occurs when the electric field in the dust layer reaches that value that causes an electrical breakdown of the interstitial gas.

The electric field in the dust layer is related to the current density and resistivity as shown by

$$E = j\rho \qquad\qquad 2.7$$

When E approaches the breakdown strength of air, about 20 kV/cm, a sparkover in the dust layer leads to a spark between the electrodes of the electrostatic precipitator. Equation 2.7 suggests that either the resistivity or the current density may be modified to improve the operating characteristics of a precipitator collecting high resistivity dusts.

In such an installation, two requirements must be met. In one case, it is necessary to experimentally verify Equation 2.6 to be sure that the migration velocity, and hence collection efficiency, is really dependent on the collection electric field rather than on power density or current density, as is sometimes assumed. In the second case, the significance of particle charging time must be known. These two pieces of evidence will be sufficient

to determine the desirability of pursuing a low current density precipitator with a precharging section.

Equation 2.6 was evaluated by operating the model precipitator at conditions which would provide an electric field at the collection plate that was essentially constant for the values of current density that differed by a factor of 10. The two sets of electrical conditions are shown in Table 2.4.

Table 2.4. Model Precipitator Operating Conditions for Comparative Efficiency Tests

Item	Standard conditions	Reduced current
Voltage, kV	37	45
Current, μA	300	30
Electric field, kV/cm	1.85	1.95
Current density, A/cm	17.0×10^{-9}	1.7×10^{-9}
Electrical power, watts	11.1	1.35
Corona wire diameter, in.	0.109	0.250

The precipitator model was operated with the inlet section functioning as a charging section and with the collection plates replaced by a rod curtain arrangement as shown in Figure 2.25. This charging section was installed to assure that the particles were uniformly charged for both test conditions.

The evaluation of Equation 2.6 was made by determining the percentage collection efficiency as a function of position for the two conditions as shown in Figure 2.26. This figure indicates that for the low current density, the collection efficiency is actually improved over that for the standard current density. The actual electrical power expended in the standard condition is about a factor of 8 greater than that for the condition with reduced current density. These tests show that if the particulate material is charged, then the collection efficiency is determined by the collection electric field at the surface of the dust.

Charging Section   Collection Section

0.109 in. wire

Standard Configuration

0.250 in. wire

Low Current Density Configuration
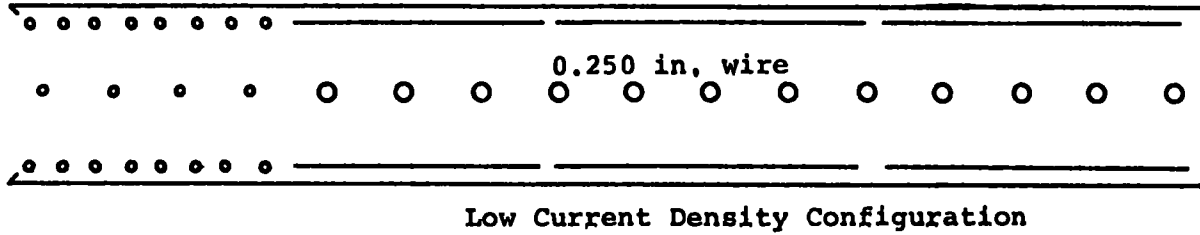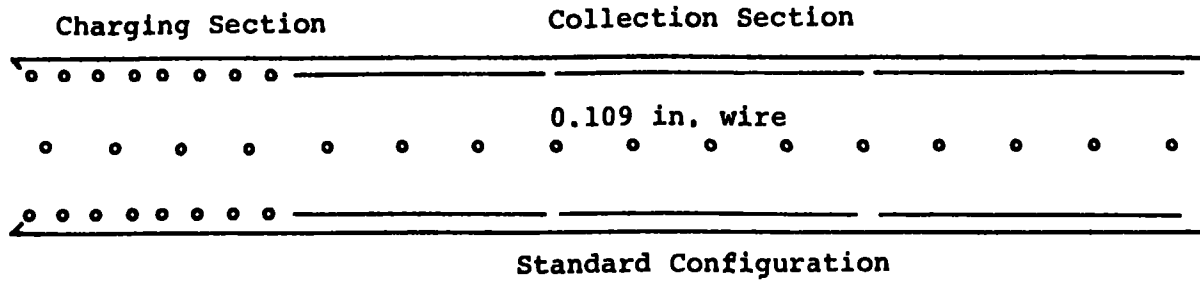
Figure 2.25.   Schematic of Standard and Reduced Current Density
Test Conditions for Southern Research Institute
Model Precharging Tests
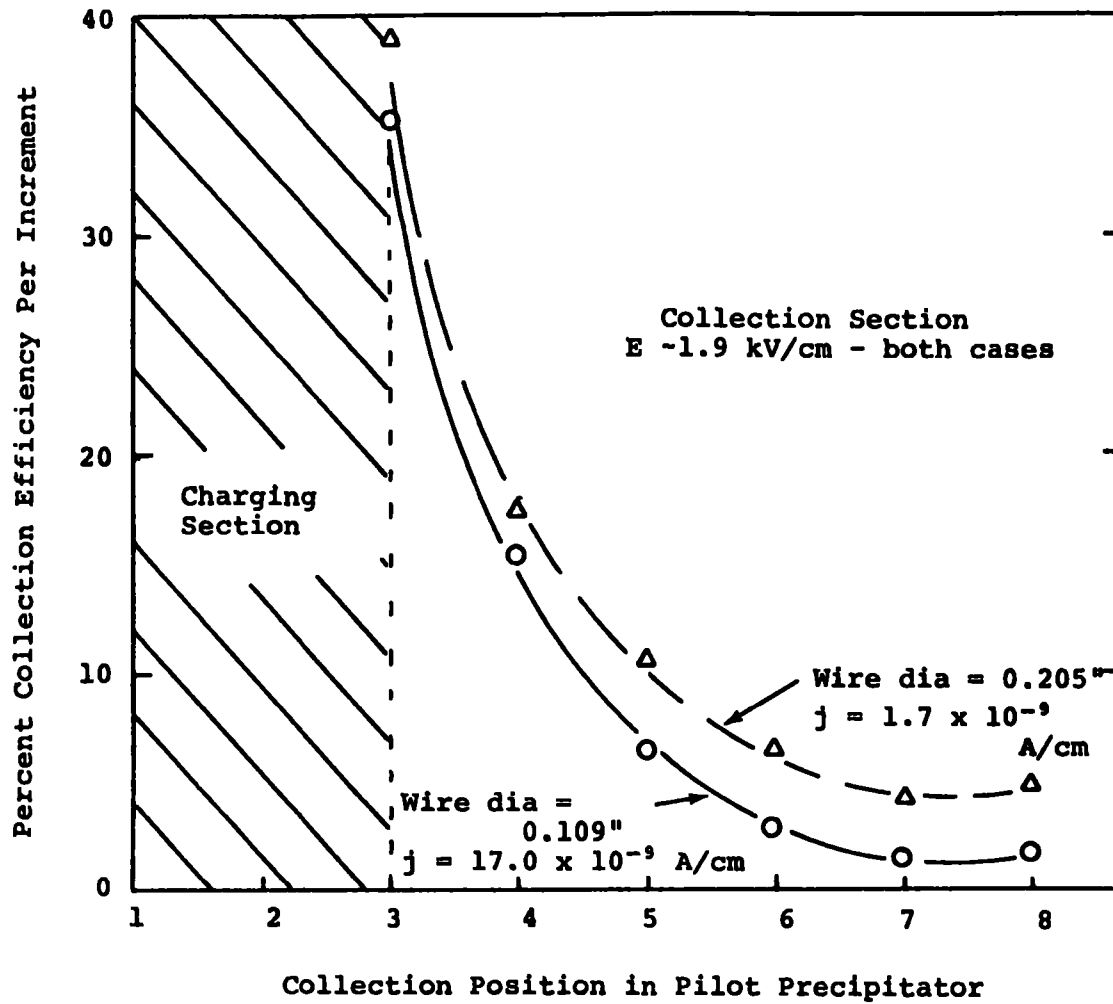
Figure 2.26. Comparison Between the Collection Efficiency for Standard Conditions and Reduced Current Density Conditions for Constant Electric Field

The significance of particle charging considerations was also verified experimentally. (If contemplated to develop a precipitator with a reduced current density in the collection zone, it is necessary to determine if a high current density charging section ahead of this collection zone is also required.) If the precipitator could be operated at reduced currents throughout the entire precipitation zone, then the solution to the high resistivity problem would be simplified. However, since theory states that the particle charging time constant is also increased for reduced currents, a reduced collection efficiency would result.

The significance of particle charging was evaluated by operating the pilot precipitator at normal current densities and with current densities reduced by a factor of 5. The percentage of material collected as a function of position through the precipitator model is shown in Figure 2.27. If the material were instantaneously charged to saturation, the collection as a function of position as predicted by the Deutsch-Anderson equation would be a decreasing exponential function. As the charging time increases, the collection vs position curve should be shifted to the right. The high current density curve in Figure 2.27 shows the dust to be charged to near saturation at Position 2, while for the reduced current density case, the near-saturation charge occurs at Position 3. Thus, particle charging time is seen to be significant.

The requirements for a precipitator that is optimized for collecting high resistivity dust particles can be summarized. The current density in the collection zone must be reduced below a value that will cause the electric field in the deposit to exceed the breakdown strength of the gas in the interstitial regions of the deposit; and some means must be provided to apply a near-saturation charge to the dust prior to introduction into the collection zone. The ability to apply this charge to the dust is also limited by the electrical resistivity of the dust. Some preliminary work has been done utilizing a small corona wire in conjunction with a rod curtain type of grounded electrode system to provide a high current density charging section. The rods were heated to reduce the resistivity of the thin deposit that collected on the rods. It seems that this may be one technique for providing a high current charging section for dusts with high resistivity, but insufficient experimental evidence was available to prove this point conclusively. The evidence does point to the possibility of collecting high resistivity materials by tailoring the current density and electric field combinations to provide an optimized design.
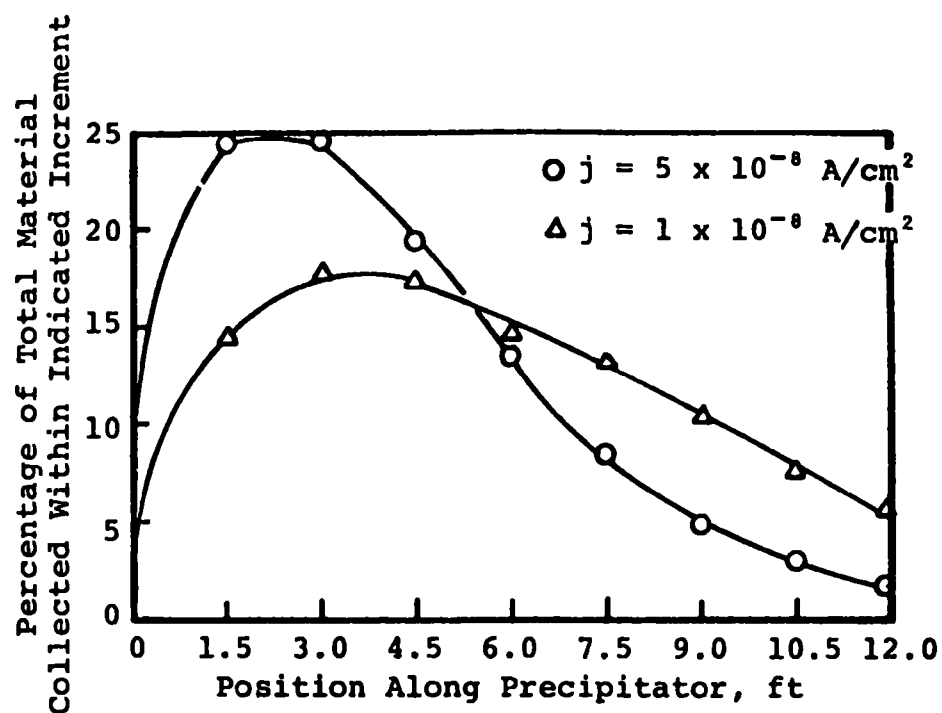
Figure 2.27. Comparison Between the Percentage of
Material Removed within Each Increment
of Length for Two Values of Current
Density

F.   Bibliography - Section 2

1.   White, H. J., *Industrial Electrostatic Precipitation*, Addison-Wesley Publishing Co., Inc., Reading, Mass. (1963).

2.   Cooperman, P., "A New Theory of Precipitator Efficiency," Paper No. 69-4, APCA (1969).

3.   Robinson, M., *Atmos. Environ.* 1, 193 (1967).

4.   Heinrich, D. O., *Staub*, 23, 83 (1963).

5.   Williams, J. C. and Jackson, R., *Proc. Symp. Interaction Fluids Particles*, Inst. Chem. Engrs. (London) pp 282-288, discussion pp 291-293, 297-298 (1962).

6.   Penney, G. and Hewitt, J. G., "Some Measurements of Abnormal Corona," *Communication and Electronics*, published by AIEE (July 1958).

7.   Cohen, L. and Dickinson, R. W., "The Measurement of the Resistivity of Power Station Flue Dust," *J. Sci. Instrum.* 40 (1963).

8.   Bucher, W. E., "A Study of the Bulk Electrical Resistivity Characteristics of Fly Ash from Lignite and Other Western Coals," a Thesis submitted to the faculty of the University of North Dakota, Grand Forks, North Dakota (December 1970).

9.   McLean, K. J., "Electrical Conduction in High Resistivity Particulate Solids," a Thesis submitted to Wollongong University College, University of New South Wales (December 1969).

10.   Penney, G. and Craig, S., "Pulse Discharges Preceding Sparkover at Low Voltage Gradients," Amer. Inst. Elec. Engrs. Meeting, New York City, Paper No. 61-91 (1961).

11.   Acker, F. E. and Penney, G., "Influence of Previous Positive Streamers on Streamer Propagation and Breakdown in a Positive Point-to-Plane Gap," *J of Appl. Physics* 39, No. 5, pp 2363-2369 (April 1968).

12.   Loeb, Leonard B., *Electrical Coronas, Their Basic Physical Mechanisms.* Uni. of Cal. Press, Berkeley and Los Angeles, 1965.

SECTION 3. REENTRAINMENT STUDIES

In dry-type precipitators, efficiency is determined by the loss of dust due to reentrainment in addition to those factors that determine collectability. Reentrainment losses can be quite serious for some types of dust, causing substantial degradation of precipitator performance.

The study of reentrainment under the current contract was undertaken to review the present technology relative to reentrainment losses and to provide a basis for determining those losses quantitatively.

The effect of reentrainment on overall precipitator efficiency depends upon the length of the precipitator, the plate area rapped at one time, and the percentage of material lost from each section and the number of sections. Figure 3.1 shows the influence on precipitator efficiency of loss of various percentages of the collected dust from a precipitator composed of four sections. Assuming that a constant percentage of the dust collected is subsequently reentrained by any mechanism, the degradation in efficiency can be computed on the basis of the Deutsch-Anderson equation. That is, the material reentrained from the first section will add to the dust burden entering the second section, etc. The amount of dust removed by the second section will be greater than it would if no reentrainment occurred, thus, the degradation of efficiency is not as great as would perhaps be expected.

Reentrainment of dust in a precipitator can result from:

- direct scouring of the dust by aerodynamic drag of high velocity gases,

- carry through of some dust during rapping or falling of its own weight,

- release of collected dust when sparking occurs,

- saltation due to impaction of a large particle on the dust layer,

- repulsion of dust due to electrical forces

- hopper losses caused by aerodynamic penetration, air inleakage, and full hoppers.

Resultant Collection Efficiency, %

100

90

80

70

60

50

40

30

20

10

0

99.9%

99%

90%

80%

$$\eta = 1 - \frac{(1 - r\eta_s)^4}{100}$$

% Reentrainment Per Section (1-r)

90 80 70 60 50 40 30 20 10

0 10 20 30 40 50 60 70 80 90 100

% of Collected Dust Reaching Hopper
Vertical Transport Efficiency (r)
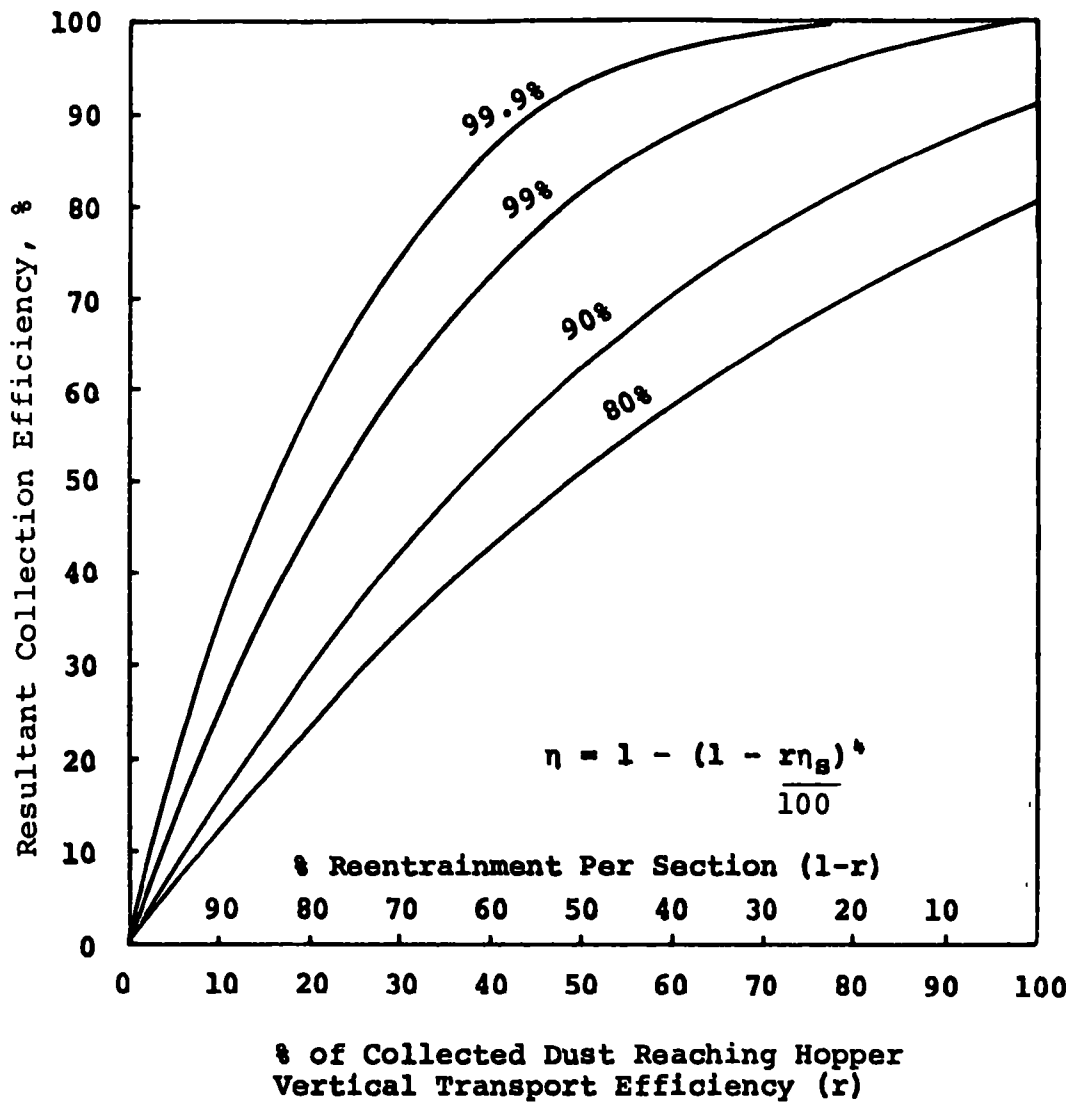
Figure 3.1. Effect of Reentrainment on the Efficiency of
a Four-Section Precipitator Designed for a
No Reentrainment Efficiency as Indicated

Qualitative and quantitative studies were made during this program to determine the magnitude of the reentrainment due to these various effects.

A.   <u>Scouring</u>

One potential mechanism of reentrainment loss is direct scouring of the dust by a high velocity gas stream. In terms of precipitator performance, scouring could be significant since loss of collected dust would take place more or less continuously and seriously reduce precipitation efficiency.

Scouring in a precipitator can take place if the aerodynamic drag force exceeds the adhesive and cohesive forces acting on an individual particle or on an agglomeration of particles.

In a practical precipitator, these forces are dependent upon the type of dust being collected, the electrical properties of the dust, and the gas velocity, turbulence, and uniformity.

Studies of reentrainment due to scouring were made with the small-scale precipitator by precipitating a dust layer of about 2.0 mm thickness, cutting off the dust feed, and running the precipitator at various gas velocities for a period of 30 minutes. If scouring were present, a greater percentage of the dust would be collected in the downstream sections and less in the upstream sections.

Since scouring is related to the electrical holding force, the test series was repeated at various voltages ranging from 0 to 30 kV. Figure 3.2 shows the percentage of the zero overrun collection efficiency for the range of voltages used. This shows that some scouring takes place at voltages below around 15 kV, which is around the corona onset voltage.

The air temperature for these tests was around 125°F so that the fly ash resistivity was in the vicinity of 1×10^9 Ω-cm, which is moderately low for fly ash precipitators.

The lack of scouring under these conditions was somewhat unexpected, especially since there is evidence that some scouring might take place in a full-size precipitator at lower velocities than the maximum used in these tests. It was suspected that the uniformity of gas flow in the small-scale precipitator with the smooth plate might not give the same conditions for scouring as in a full-size precipitator with baffle plates. To explore this effect, 1½ in. baffles spaced 9 in. apart were added to the
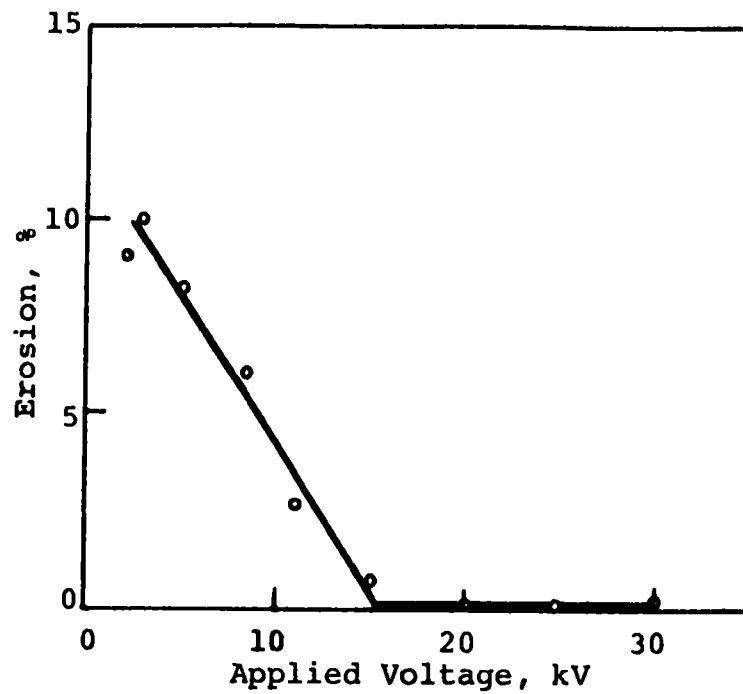
Figure 3.2.   Relationship Between Scouring
               for Various Applied Voltages
               Defined as Excess Loss Over No
               Overrun Collection Efficiency

plates and the tests repeated. Again, no evidence of direct scouring was found at gas velocities up to 12 ft/sec.

The conclusion to be drawn from these tests is that scouring of the collected dust does not appear to take place at gas velocities up to 12 ft/sec with a rather typical fly ash (10 μm mmd). Larger particle size or higher gas velocities would perhaps show scouring effects.

In full-size precipitators, the same general conclusion may be reached, that is, that no scouring as defined here is likely to take place at gas velocities below 12 ft/sec. When extremely poor gas flow or a dust with rather poor cohesive properties is encountered, some scouring may occur. However, the influence appears to be considerably smaller than might be expected.

B.   Rapping Reentrainment

Loss of dust during rapping constitutes one of the major sources of reentrainment losses in a precipitator. Under some conditions, these losses can be visually observed as puffs of dust that escape during and immediately following a rapping cycle. These rapping losses can be minimized by proper adjustment of the rapping intensity and frequency.

Studies were made with the small-scale precipitator of the conditions required to give minimum rapping losses. Some problems peculiar to the plate height as compared with a full-scale precipitator were encountered, particularly with regard to the influence of the dust layer falling into the hopper and causing breakup and reentrainment. However, by installing a plexiglas window on one side of a precipitator section and observing the nature of the dust breakup and fall, qualitative observations were made regarding optimum conditions for rapping.

The condition required for optimum dust removal is that the dust fall as a sheet layer into the hopper. This requires that a sufficient thickness be built up so that a rap will dislodge it as a unit. Otherwise, if the dust layer is thin, a more severe rap will be required to remove it and, in addition, the dust will powder and be propelled into the gas stream where it will be carried out of the precipitator. At the other extreme, the dust layer can be allowed to build up until the weight of the dust is sufficient to overcome the adhesive or cohesive forces and falls of its own accord. When this occurs, the dust layer falls free with a velocity sufficient to cause self-reentrainment and extensive loss of dust. On free-fall from tall plates,

velocities in the vicinity of 50 ft/sec can be reached causing excessive localized scouring. Thus, rapping frequencies should be adjusted between these two extreme conditions.

Rapping intensity can also be adjusted to give minimum loss of dust. If rapping is too light dust will not be released from the plate at the time of rap, and on the succeeding rap the thickness will be sufficient to cause an avalanche effect. On the other hand, too severe a rap will cause the dust to be propelled from the plate a sufficient distance to fall freely. In addition, too severe a rap causes powdering of the dust with subsequent reentrainment loss.

Under ideal rapping conditions, the dust layer is dislodged from the plate and slides down the plate until it is recaptured by the precipitation process.

The factors that influence dust loss due to reentrainment are the gas velocity, resistivity, particle size, and adhesive and cohesive properties of the dust.

The influence of resistivity of the dust on reentrainment has not been sufficiently recognized. In the case of a high resistivity dust, the electrical forces holding the dust to the plate are large and rapping intensities required to dislodge the dust are high. Under these conditions, considerable powdering of the dust can occur with accompanying high losses. In some instances, dust resistivity is so high that it is impractical to remove it by conventional rapping. In such cases, power-off rapping is required and rapping puffs are visible during the rap and the losses are excessive as compared with more conventional rapping.

At the other extreme, low resistivity can also result in excessive reentrainment losses. In the case of fly ash precipitators operated at low temperature (260°F) with high sulfur coal, reentrainment losses can be as high as 20 to 30%.

The effect of low dust resistivity on performance is manifested by excessive rapping puffs when viewed visually or with optical obscuration instruments.

Qualitatively, the effect of low resistivity would appear to be that the dislodged dust is not re-precipitated following rapping and falls freely into the hopper. It would, therefore, act in much the same manner as permitting too thick a dust layer to form. Adjustments to the rapping intensity and rapping frequency can minimize the effect of these losses. Use of impact absorbing

materials as well as minimizing the rapping impact have been attempted in an effort to control rapping intensity and minimize losses. However, when very low dust resistivity is encountered, such as results from high sulfur coal at low gas temperatures, it has not been practical to control rapping sufficiently to overcome the higher rapping losses.

C.   Electrical Forces

The electrical field in the dust layer is determined by the current density and dust resistivity. If the resistivity of the dust is lower than around 10^{10} Ω-cm, the field in the dust layer will be lower than in the space immediately adjacent to it. This abrupt change in electric field can occur only if there is an accompanying positive surface charge. The magnitude of this charge is dependent upon the difference between the electric field in the dust layer and in the adjacent gas stream. For dust resistivities in the range of 10^6 to 10^7 Ω-cm, this positive surface charge may propel the collected dust back into the gas stream and contribute to reentrainment.

Tests made on the small-scale precipitator demonstrated this effect when a layer of low resistivity dust (10^8 Ω-cm) was precipitated onto the plates. The voltage was then increased, which increased the electric field in the gas more than in the dust deposit. The result was that with an increase in voltage, dust particles were removed from the plates, dropping into the hopper. No measure of this type of reentrainment was attempted.

D.   Sparking

Sparking can influence reentrainment in two ways. The spark itself can cause disruption of the current in a localized section of the precipitator. This interruption of the corona current causes loss of electrical holding force in the affected area and dust can be reentrained during this period. A second influence of sparking is that energy dissipated in the spark causes the dust in the vicinity of the spark to be expelled into the gas stream.

The conditions contributing to reentrainment due to sparking can vary depending upon the precipitator design. If the spark is rapidly quenched, the effect is minimized. However, with poorly designed electrical energization equipment a spark or power arc can persist for a reasonably long period of time, and the effect can become quite serious in terms of reentrainment as well as other factors influencing performance.

E.   Saltation

   The impact of a large particle on a precipitated dust layer can dislodge previously collected dust and constitutes another potential source of reentrainment.

   The saltation effect has been studied by Penney,[1] Robinson,[2] and others. However, it is difficult to distinguish this type of reentrainment loss from others in a precipitator since it occurs during the precipitation process. It may be regarded as a type of scouring loss since the dislodged particles will be picked up by the gas stream and probably is dependent upon gas velocity. No attempts were made during this program to identify this type of reentrainment loss independently.

   The effects of saltation, sparking, and electric field differences are difficult to separate quantitatively. Sparking and electric field effects are perhaps aggravated during rapping and are manifested by increased rapping losses.

F.   Hopper Losses

   In addition to losses of the dust from the collection electrodes, losses also occur in the vicinity of the hopper. Vertical dust concentration profiles can show dust levels at the bottom of the precipitator considerably higher than at the top. This can be due to gas sweeping into the hoppers and reentraining dust or to rebounding of the dust as it falls into the hoppers. These effects can be minimized by proper baffling.

   In the small-scale precipitator, studies of reentrainment were clouded by the magnitude of the losses associated with dust falling into the hopper. Visual observation with the plexiglas window showed that dust falling into the hopper following a rap was powdered by the impact and rebounded approximately one-third of the height of the collection plate. Similar effects occur in full-size precipitators, resulting in a smaller percentage of the total reentrainment for the tall plates.

G.   Full-Scale Precipitator Tests

   Detection of reentrainment losses in a precipitator can be made by several methods as discussed by White.[3] These include: (1) plotting precipitator losses as a function of gas velocity

---

[1]Refer to the Bibliography at the end of this section.

on semi-log paper and observing the point of departure from
linearity, (2) measuring the particle size distribution of the
inlet and outlet dust and observing the presence of larger parti-
cles in the outlet, and (3) measuring the electrical charge on
particles and observing the increase in the number of positively
charged particles.

In view of the previous discussions of reentrainment
factors, it is reasonable to assume that each of the methods of
detecting reentrainment might be more sensitive to particular
reentrainment mechanisms. If reentrainment is due to powdering
of the dust as a result of intense rapping, large particles may
not be present. If dust resistivity is very high, reentrained
particles may still have a negative charge. On the other hand,
if reentrainment is due to erosion occurring either during rapping
or as direct scouring, one would expect to find a preponderance
of large particles. Low dust resistivity would also tend to
produce positively charged particles regardless of the mechanism
by which reentrainment occurred.

In general, each of these methods is primarily useful in
detecting the point at which reentrainment becomes severe.
Reentrainment losses obviously occur over the entire range of
conditions. Detection by the above techniques, therefore,
primarily indicates an abnormal condition of operation.

A number of field tests were made and data examined to
indicate conditions of excessive reentrainment losses. One of
the primary objectives of these studies was to identify the cause
of poor performance associated with the use of low gas tempera-
tures on precipitators used with boilers burning high sulfur coal.

Figure 3.3 shows the precipitator penetration as a function of
gas velocity for two full-size precipitators. These curves show
the excess penetration over that predicted from the Deutsch equation.
Curves 1A and 1B are for a precipitator used on a boiler burning
3 to 4% sulfur coal at temperatures of 275 to 300°F and hence
widely varying resistivities. In the case of the low resistivity
ash (275°F), the departure from the Deutsch equation penetration
occurred at around 5.5 ft/sec, whereas the precipitator would
follow the Deutsch efficiency prediction to around 7.5 ft/sec when
collecting the higher resistivity ash corresponding to the 300°F
flue gas temperature. Curves 2 and 3 show similar effects for
two different plants.

The significance of these data is that excessive losses
can occur within the range of gas velocities normally encountered
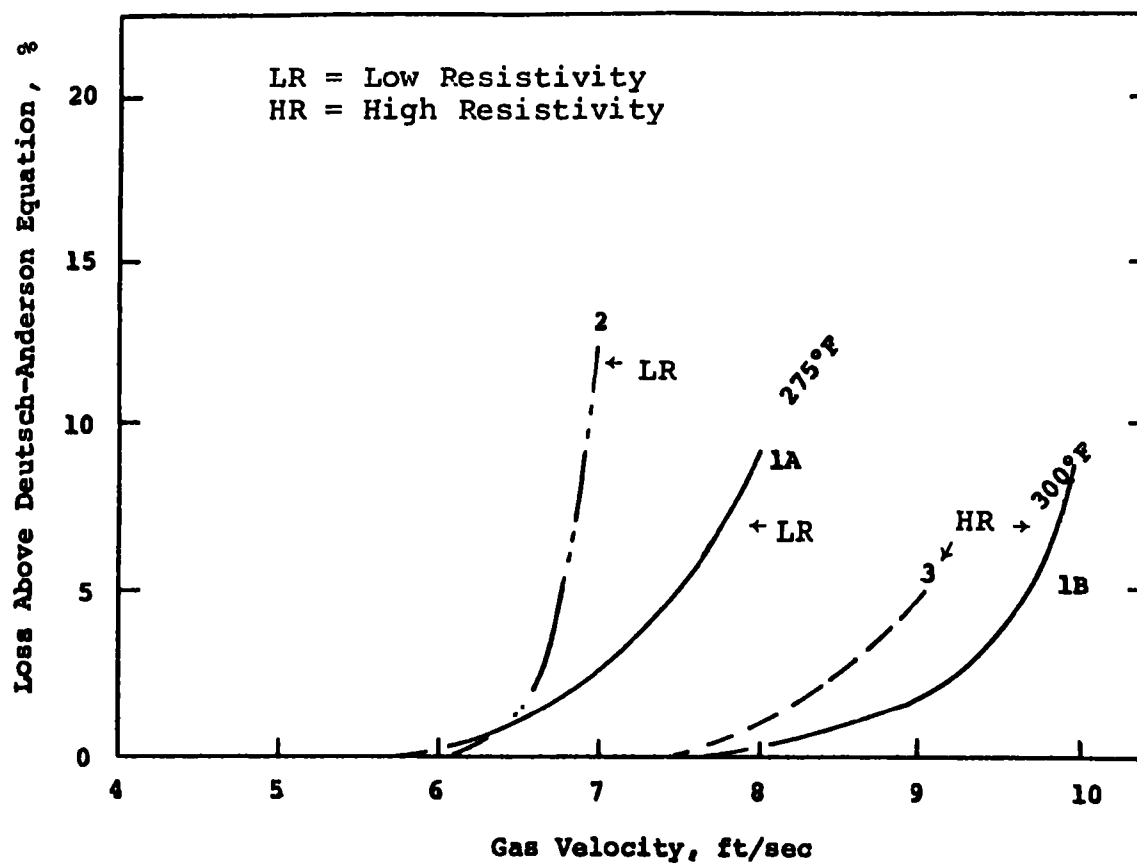
Figure 3.3. Precipitator Losses as a Function of Gas Velocity for Two Full-Size Precipitators

in fly ash precipitators and that these losses are dependent on dust resistivity. Thus in many instances where high gas velocities are encountered along with high dust resistivities, attempts to improve performance by reducing dust resistivity can result in little or no improvement due to excessive reentrainment. When changes are made in dust resistivity, for example, by addition of conditioning agents or reduction of gas temperature, rapping should be optimized. Even so, when gas velocities are high and perhaps nonuniform, reentrainment losses can prevent substantial improvement in performance by reducing dust resistivity.

H.   Conclusions

The individual factors related to particulate reentrainment have been discussed. However, at this point, the theoretical relationships between the variation in these factors and the reentrainment conditions in a precipitator cannot be definitively given. The measurements made with the pilot-scale precipitator, while yielding insight into the phenomenon of reentrainment, do not provide data that can be applied in an engineering manner to full-scale units. At this time, it is necessary to approach the problem of reducing reentrainment losses in any particular installation on an individual basis. The descriptions given above will provide guidance, but the particular solution to a given reentrainment problem must be determined individually.

I.   Bibliography - Section 3

1.   Penney, G. W., "Adhesion and Cohesion in Dust Collection," progress report, Carnegie Institute of Technology, Pittsburgh, Pennsylvania, Grant #RG-6402(C2) (January 1961).

2.   Robinson, M., "Collection and Erosion Mechanisms in Electrostatic Precipitation," precipitator evaluation in terms of dimensionless parameters, Research-Cottrell, Inc., Bound Brook, New Jersey.

3.   White, H. J., Industrial Electrostatic Precipitation, Addison-Wesley Publishing Co., Inc., Reading, Mass. (1963).

SECTION 4. REFINEMENT OF PRECIPITATOR
MATHEMATICAL MODEL

A simplified computerized model of an electrostatic pre-
cipitator model was developed under a previous contract. This
model was developed using several simplifying assumptions for the
purpose of illustrating the utility of a theoretically based
mathematical approach to the problem of predicting precipitator
performance.

One purpose of the current contract was to further develop
and refine this simplified model to more closely predict the
behavior of actual precipitator installations. The first step
in this development process was to upgrade the model by incor-
poration of factors covered by present theory. The next step was
to modify the system of equations from the electrostatic system
of units to the more popular MKS units. And finally, factors
were added to include those functions that were omitted because
of the simplifying assumption in the initial model.

A. Collection Efficiency

The Deutsch-Anderson equation is a mathematical expression
that is used to relate the collection efficiency of electrostatic
precipitators to the physical parameters of collection electrode
area and volume flow rate of a precipitator system, together with
a term that is associated with the collectability of the dust
particles, designated precipitation rate parameter. This
expression is repeated from a previous section below

$$\eta = 1 - \exp{-\left(\frac{A}{V_g}\right)} w, \qquad\qquad 4.1$$

and is used both for empirical and theoretical considerations and
forms the basic equation for the precipitator mathematical model.

The Deutsch-Anderson equation has been used as an empirical
equation to develop proprietary data that serves as a measure
of the electrostatic collectability of various material. When
used in this sense, for an installation with a known volume flow
rate, collection plate area, and collection efficiency, a value
for w can be determined for that installation. In reality this
w is a measure of the performance for that installation utilizing
that particular dust, and is termed a precipitation rate
parameter.

B. Migration Velocity

The Deutsch-Anderson equation is also useful for theoretical analyses. In this case, the term, w, applies specifically to the electrical migration velocity that results from the charged dust driven by the force resulting from the applied electric field, which yields a velocity where the viscous drag force from the gas balances the electrical force. The relationship that is used for describing this electrical migration velocity given previously as equation 2.3 is

$$w = \frac{qE_p}{6\pi\eta a}$$

which becomes for field charging

$$w = 2\frac{\varepsilon}{\varepsilon+2}\frac{\varepsilon_0 E_0 Epa}{\eta}\frac{1}{1+\frac{\tau}{t}} \qquad 4.2$$

Thus, the theoretical migration velocity for field charging is seen to be a function of the dielectric constants, $\varepsilon, \varepsilon_0$; collection electric field, $E_0 Ep$; the gas viscosity, η; the particle radius, a; and the charging time constant expression. These factors are utilized in the computer model to predict a particle migration velocity and a collection efficiency for each particle size.

1. Particle charging

There are two charging mechanisms active in electrostatic precipitation; field and diffusion charging. Even though both mechanisms are active in charging, field charging is the dominant charge mechanism for large particles while diffusion charging is dominant for small ones. The computer model can be programed to compute the charge for each mechanism and select the one that yields the greater value. This technique will lead to some error in the value of charge for those particle sizes where both mechaisms can provide significant charge. The equations relating charge to the various system parameters are given in Equations 4.3 and 4.4 for field and diffusion charging, respectively.

$$q(t) = 12 \frac{\varepsilon \, \varepsilon_0}{\varepsilon + 2} \pi a^2 E_0 \frac{1}{1 + \frac{\tau}{t}} \qquad\qquad 4.3$$

$$q(t) = \frac{4 \pi E_0 \, akT}{e} \ln \left(1 + \frac{a v N_0 \, e^2 t}{4 E_0 \, kT} \right) \qquad\qquad 4.4$$

2. Electric fields

The two electric fields used in Equation 4.2b refer to the charging and collection electric fields in the precipitator. The charging electric field used is the space and time averaged field in the interelectrode space. Thus, a single value is determined for the charging field that results from the applied voltage and resultant current that is present in the precipitators. This electric field is averaged over the interelectrode space and is utilized for computing the charge for each particle size. The expression for the electric field as a function of position is given in Equation 4.5.

$$E(r) = \left[\left(\frac{E_0 \, r_0}{r} \right)^2 - \left(\frac{r_0^{\,2} - r^2}{r^2} \right) \cdot \frac{i}{2 \pi \varepsilon_0 \, \mu_i} \cdot \frac{\rho}{\rho_i} \right]^{\frac{1}{2}} \qquad\qquad 4.5$$

The collection electric field used in the computer model is the time averaged value of the electric field adjacent to the collection electrode surface. This field is described by the same equation as the charging field. However, the numerical value is different because the collection field is determined by evaluating Equation 4.5 at a radius that corresponds to the collection electrode spacing, while the charging field results from a spatial average of Equation 4.5.

C. Particle Size Consideration

The Deutsch-Anderson equation specifically applies to the collection efficiency for particles with a given migration velocity. Since the migration velocity is a function of particle size, a single value of migration applies to a single particle size.

Thus, for a particle size distribution that occurs in practice, a range of migration velocities will be required. To approximate this continuum of migration velocities, the inlet particle size distribution is approximated by a first-order approximation such as is shown in Figure 4.1. Within each increment, the total material is considered to be effectively represented by a number of particles with the same particle size that represents the total mass of particles within that size increment. This solution for discrete particles represents an approximation to the solution for a continuous size distribution.

D.   Particle Charging Time

The particle charging rate is related to the free ion density in the vicinity of the particle being charged. The free ion density is related to current flow at the point of charge. As the particles acquire an electrical charge, this rather immobile charge carrier causes a reduction in current, with the resultant decrease in the free ion density. These factors are included in the particle charge time expression in the computer program.

E.   Particle Reentrainment

At the beginning of this contract period, particle reentrainment was considered to be associated with several variables from the precipitator. Specifically, reentrainment was thought to occur by:

- scouring of the dust from the plates,

- scouring of the dust from the hopper,

- erosion from the dust layer falling after rapping,

- erosion from dust clumps falling voluntarily, and

- erosion by impaction from particles being collected (saltation).

The above effects were included in the computer equations as terms that reintroduced collected material into the subsequent sections of the precipitator. Thus, the concentration of material in the jth increment of the precipitator is expressed as the
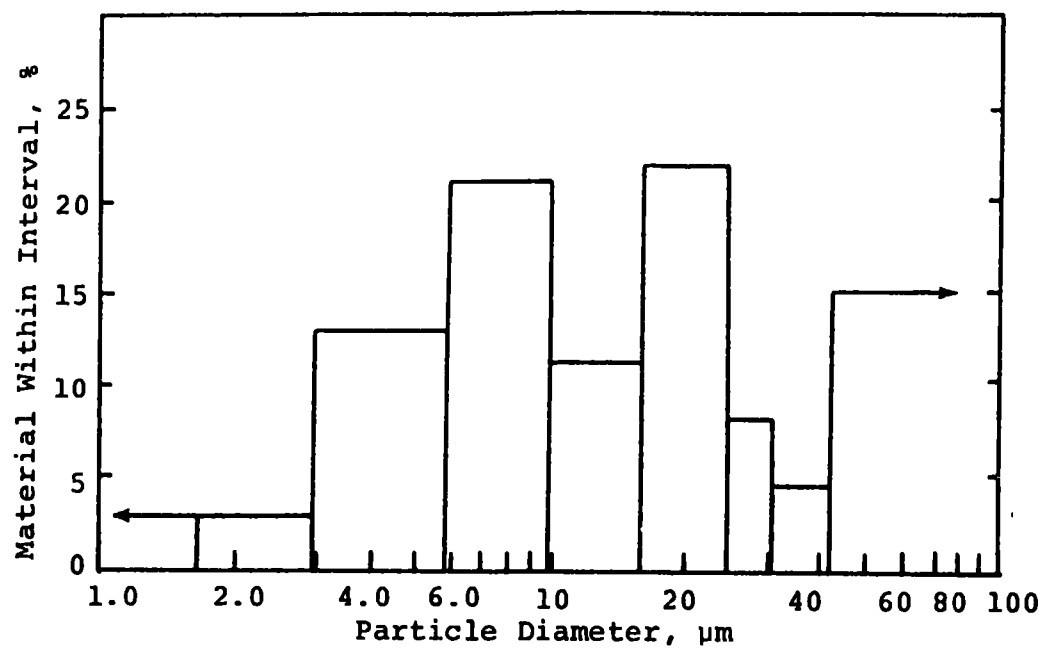
Figure 4.1. Approximation of Inlet Particle Size Distribution

concentration in the j-1 increment, less that collected in the j-1 increment plus that reentrained in the j-1 increment due to the various causes expressed in the equation shown below:

$$XNO(j) = XNO(j-1)-DXNO + K(V - V_c) DXO + R(j-1) DXNO \qquad 4.6$$

where

$XNO(j)$ = the number density of particles of size increment j in the inlet of a section,

$DXNO(j-1)$ = the number of particles in size range j collected,

$K(V - V_c)$ = the percentage of particles collected in size range j that were reentrained by velocity erosion, and

$R(j-1)$ = the percentage of particles collected in size range j that were reentrained due to rapping.

These factors were included in the computer program prior to the experimental investigations conducted with the pilot model. The model work with reentrainment studies suggests that these terms will require modification (see Section 3 - Reentrainment).

A system flow diagram with the pertinent equations is shown in Figure 4.2. A computer program is included in Appendix 2.

F.   Verification of the Precipitator
      Mathematical Model

The mathematical model of an electrostatic precipitator system, described in Section 2, was developed fundamentally for use as a design and analysis tool. In order for this systems model to be useful, the behavior of physical models must be reasonably predictable. The operating data from a variety of tests with the SRI pilot-scale precipitator were used as input data for the model. A list of these data is shown in Table 4.1. The computer model predicted a collection efficiency for each test condition. The results of these computations are compared with the measured efficiencies for each of these tests in Figure 4.3. The data taken from the pilot precipitator were without rapping. Since erosion only occurs for gas velocities in excess of about 30 ft/sec, the reentrainment factors were set to zero. Thus, the model was set to neglect reentrainment.

$$E(r) = -\left[\left(\frac{r_a\, E_0}{r}\right)^2 - \left(\frac{r_a^2}{r^2} - 1\right)\frac{1}{2\pi\varepsilon_0\mu_i}\frac{\rho}{\rho_i}\right]$$

E(r) → **Average Value** → $\frac{a}{b}$

I_1

$\dfrac{I}{Lw}$

I

$\dfrac{I}{A_p}$ → j

A_p

$\dfrac{1}{1 + \dfrac{E_c}{j\pi t}}$

μ / a / r

E_c

$A_i \quad N_i \times A_i$

Material Left

$\dfrac{3\varepsilon}{\varepsilon + 2}\, r_i^2\, E_c$

$\dfrac{r_i}{\varepsilon}$

$N_i + \Sigma(R-1)N_i$

Reentrainment Factor, R

q(t)

E_c

$\dfrac{q(t)\, E_c}{6\pi\eta r_i}$

$\dfrac{r_i}{\eta}$

N_i → $\Sigma\Sigma\eta/ft\ N_i$

L_p → $\dfrac{L_p}{v}$ → v

L_p

w_i

$\dfrac{A_p}{v_g}$ → $\dfrac{A}{v_g}$ → $1 - \exp\left(-\dfrac{A}{v_g}\dfrac{w_i}{L_p}\right)$

N_i → $\dfrac{\Delta N}{N}$ → η (efficiency)

a = Wire Radius
b = Collector Radius
f = Roughness Factor
d = Relative Air Density
E_0 = Breakdown Field Strength
V_0 = Breakdown Voltage
I = Total Current
Lw = Corona Wire Length
i = Current/Length
μ = Ion Mobility
S = Surface Area of Dust per cm^3 of Gas
A_p = Area of Plate
j = Current Density of Plate
E_c = Average Electric Field
$q_s q_i$ = Saturation and Present Charge
ε = Dielectric Strength Relative
r_i = Radius of Particulate
v_g = Volume Flow Rate
t = Time Lapsed in Collector
w_i = Migration Velocity
N_i = Number of Particles
L_p = Precipitator Length
v = Gas Velocity
η = Efficiency, viscosity
Δ = Increment
Σ = Summation
R = Reentrainment Factor

Note: Expressions for diffusion charging have been added to the program, but since we do not have sufficiently valid size distribution data for particles smaller than 1.3 μm, diffusion charging as yet contributes no significant charge.

Figure 4.2 Computer System Flow Diagram

-91-

Table 4.1. Operating Data for the Pilot-Scale Precipitator

Test No.	Collection area ft²	Gas flow rate ft³/min	Applied voltage volts	Total current amps	Dust load gr/ft³	Wire radius in.	Wire-to-Plate spacing in.	Efficiency, %	
								Measured	Computed
1	72	1500	36,000	0.0012	0.50	0.049	5	77.1	80.2
2	72	1800	36,000	0.0012	0.54	0.049	5	76.4	76.9
3	72	654	37,000	0.0012	1.2	0.049	5	84.0	92.1
4	72	804	36,000	0.0012	1.03	0.049	5	87.3	89.8
5	72	654	36,000	0.0012	1.05	0.049	5	83.5	92.0
6	72	1800	36,000	0.0012	0.99	0.049	5	68.7	77.5
7	72	1800	35,000	0.0012	0.35	0.049	5	74.5	76.5
8	72	1500	34,000	0.0012	0.56	0.049	5	75.6	80.3
9	72	1200	35,000	0.0012	0.71	0.049	5	83.0	84.2
10	72	1000	36,000	0.0012	0.83	0.049	5	86.0	86.9
11	72	804	36,000	0.0012	0.90	0.049	5	87.3	89.7
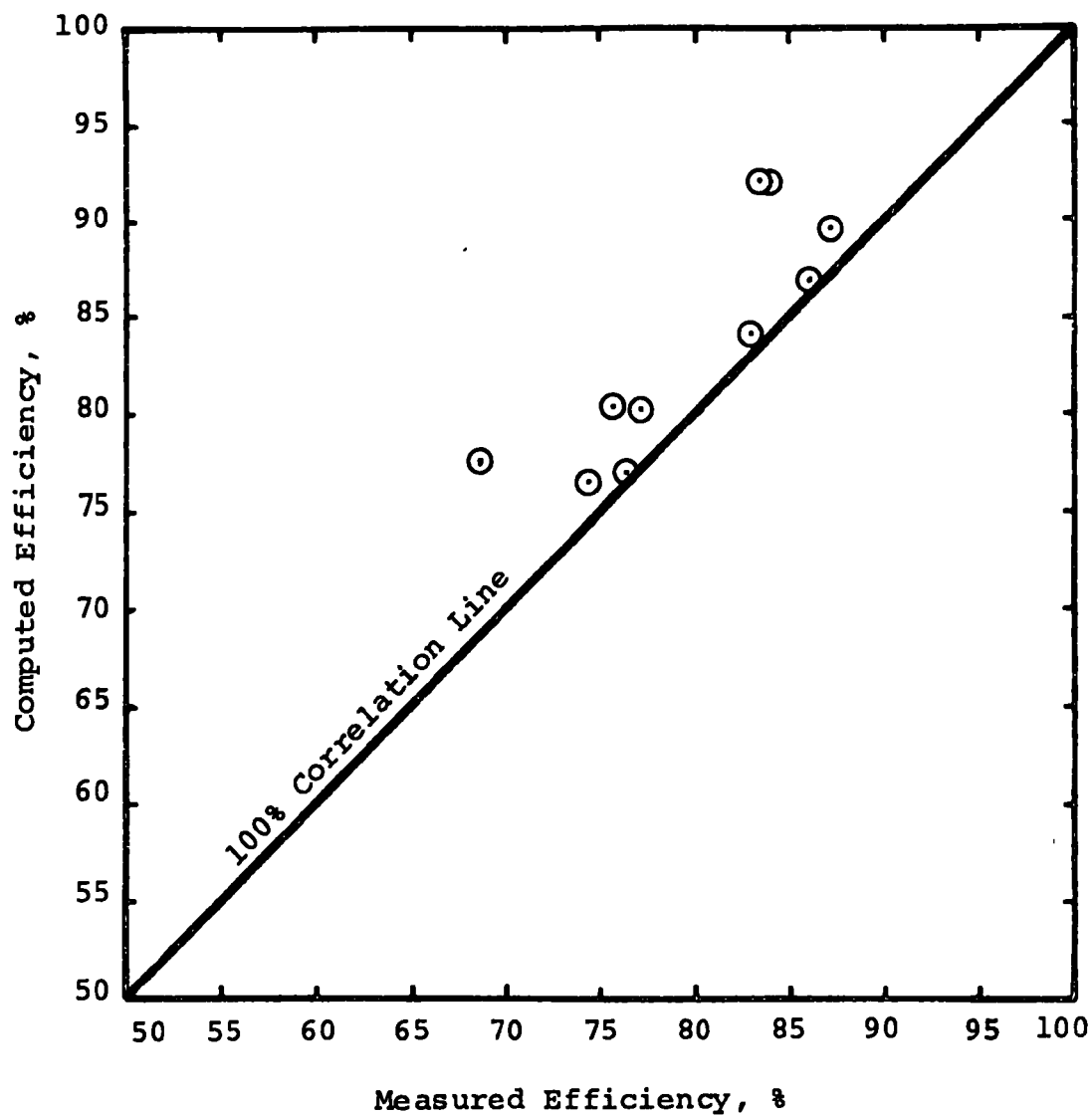
Figure 4.3.   Comparison of Computed and Measured
             Collection Efficiency for Various
             Test Conditions Utilizing the Model

The laboratory data for the model precipitator show good correlation with the mathematically predicted values. Thus, the model is concluded to be fairly representative of the pilot model precipitator. As a means of determining how closely the computer model approximates the behavior of full-scale field installations, data from selected field tests where reentrainment was considered to be minimal were used for comparison. The results of these computations are shown in Figure 4.4, with the input data for operating characteristics shown in Table 4.2.

G.   Conclusions

The precipitator performance model requires additional refinement before it can be used to reliably predict the behavior of field installations. The areas considered to be important are gas velocity, temperature and resistivity variations across the face of the precipitator, as well as a better definition of reentrainment losses.
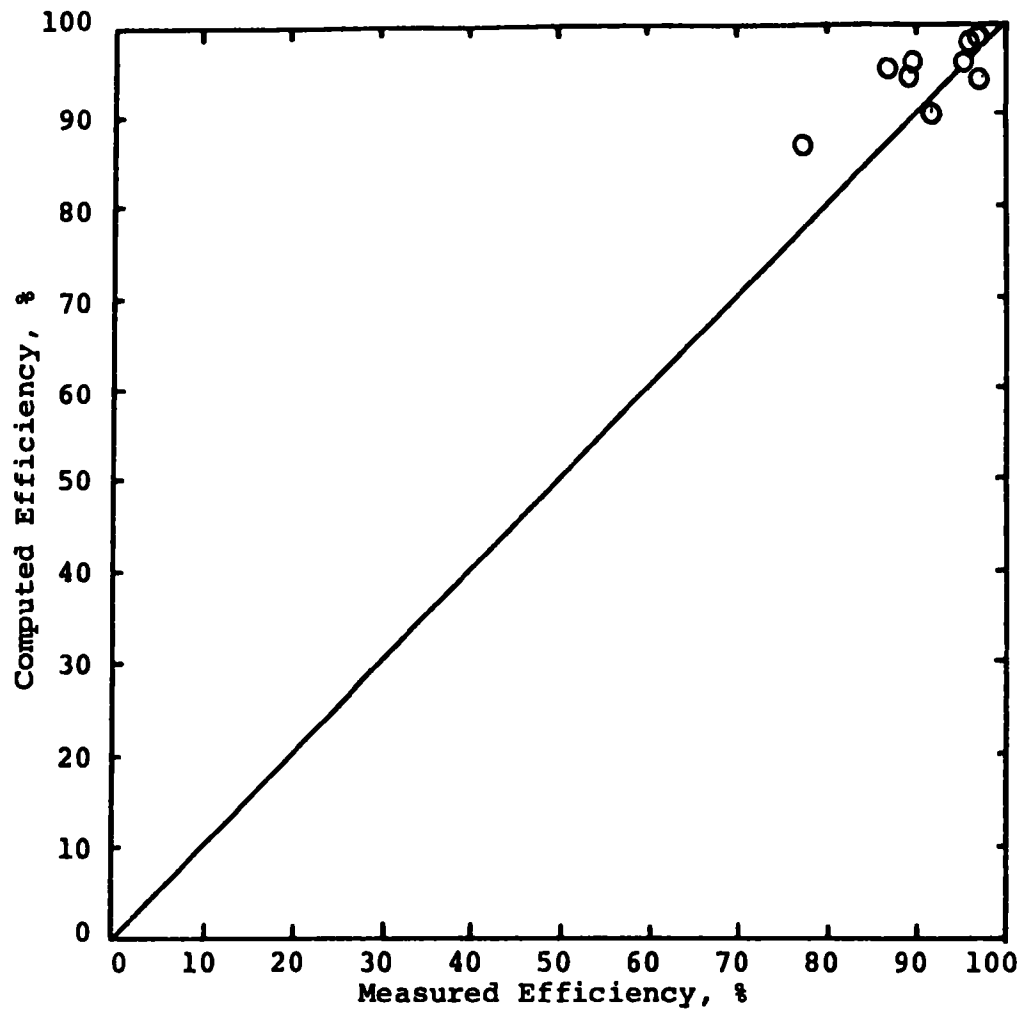
Figure 4.4. Comparison of Computed and Measured
Collection Efficiency Under Field
Test Conditions

Table 4.2. Operating Data for Selected Field Installations

Test No.	Collection area M	Gas flow rate M³/sec	Applied voltage volts	Total current amps	Dust load kg/M	Wire radius M	Wire-to-Plate spacing M	Efficiency, % Measured	Efficiency, % Computed
1	2300	119.7	44,300	0.83	0.0014	0.0014	0.114	95.6	95.2
2	2300	123.5	40,600	0.76	0.0018	0.0014	0.114	96.7	93.6
3	3310	162.2	33,700	0.37	0.0014	0.0014	0.114	92.2	90.4
4	3310	156.7	37,800	0.92	0.0012	0.0014	0.114	95.6	95.7
5	3374	191.5	32,300	0.14	0.005	0.0014	0.114	89.9	96.9
6	3374	185.8	34,000	0.14	0.006	0.0014	0.114	89.2	96.4
7	8623	295.6	34,200	1.605	0.007	0.0014	0.114	98.3	99.8
8	3374	184.3	33,900	0.14	0.005	0.0014	0.114	88.8	97.2
9	3310	155.3	32,500	0.29	0.0012	0.0014	0.114	78.4	87.0

SECTION 5. ECONOMIC COMPARISONS FOR COLLECTION OF HIGH RESISTIVITY DUST

It is well known that a dust resistivity above a value of about 2×10^{10} Ω-cm is detrimental to precipitator performance. The electric field in a dust layer of excessive resistivity will, at normal current densities, exceed the breakdown strength in localized regions, resulting in excessive sparking and back corona. When high efficiency collection of high resistivity dust is desired, it is necessary to effect changes in design or operating conditions of precipitators collecting such material. The options available are as follows:

- enlargement at normal operating temperature,
- conditioning at normal operating temperature,
- high temperature operation, and
- low temperature operation.

Each of these options requires an appreciable expenditure above that required for electrostatic precipitation of a dust with acceptable resistivity values at normal operating temperature. This section presents a comparison of the economic and engineering considerations pertaining to each method of overcoming the problem of high dust resistivity. Factors not associated with resistivity, such as design of mechanical and electrical components, are not considered in this discussion.

A.   Basis for Comparison

In order to establish a basis for comparison of the various solutions to a high resistivity problem, a precipitator designed for a 250 MW power plant with an acceptable resistivity at 270°F will be used as a base point. It will be assumed that the precipitation rate parameter used for design of the base unit is 13 cm/sec, or 25.8 ft/min. This particular value was selected because it was reported by Oglesby and Nichols[1] to represent an average design precipitation rate parameter for the electrostatic precipitation of fly ash produced from coal-fired utility boilers.

---

1. Refer to Bibliography at the end of this section.

From the Deutsch-Anderson equation, the plate area required for a given collection efficiency and gas flow is obtained by

$$A = \frac{V}{w} \ln \left(\frac{100}{100-\eta}\right) \qquad\qquad 5.1$$

The gas flow from a 250 MW plant at 270°F will be approximately 800,000 acfm. Thus, for a 99% collection efficiency

$$A = \frac{800,000 \text{ acfm}}{25.8 \text{ ft/min}} \ln 100 = 143,000 \text{ ft}^2 \text{ or } 179 \text{ ft}^2/1000 \text{ acfm.}$$

The cost of such a precipitator can be estimated from a recent compilation of precipitator costs.[1] The average cost per acfm of gas treated, for precipitators treating 500,000 to one million acfm at a collection efficiency of 99% or greater, was reported as about $0.827 per acfm in the period 1965 through 1969. This cost includes foundation, erection, and electrical work. If the mid-point of this period, 1967, is used as a basis, the cost of the precipitator, corrected to the first quarter of 1971 by means of the Marshall and Stevens Equipment Cost Index, may be estimated by

$$\text{Cost} = 8.0 \times 10^5 \text{ acfm} \times \$0.827/\text{acfm} \times \frac{315}{263}$$

$$= \$793,000 \text{ or } \$3.20/\text{kW.}$$

B. Enlarged Precipitator at Normal Temperature

It is theoretically possible to obtain desirable collection efficiencies in precipitators whose efficiencies are limited by high resistivity dusts simply by increasing the plate area. This approach has been employed in Australia, with specific collecting areas as high as 550 ft^2/1000 acfm in use.[2] For a dust with very high resistivity, however, the increase in plate area required can be excessive to the point of impracticality.

Consider as an example a fly ash at 270°F with a resistivity in excess of 10^{12} Ω-cm, which results in a precipitation rate parameter of 3 cm/sec. The increase in plate area required over the previously described base unit is proportional to the decrease in precipitation rate parameter. Thus, to obtain 99% collection efficiency

$$\text{Area} = \frac{13.1}{3.0} \times 143,000 = 625,000 \text{ ft}^2 \text{ or } 780 \text{ ft}^2/1000 \text{ acfm.}$$

The cost of such a unit may be estimated from data given by Oglesby and Nichols[1] in which erected costs of precipitators with collection efficiencies greater than 99% are given as a function of the volume of gas treated. Since the plate area required at a given effective migration velocity and efficiency is directly proportional to the volume of gas treated, it may be assumed that the functional relationship between plate area and cost is the same as that between gas flow and cost if the precipitation rate parameter and efficiency have no bias with respect to volume flow. Such an assumption should be sufficiently accurate for cost estimation purposes.

The slope of erected precipitator cost on log-log-coordinates as a function of volume flow was found to be 0.75. Thus, using the reasoning indicated above, the cost of the enlarged unit is given by

$$\text{Cost} = \$793,000 \ \left(\frac{625,000 \ \text{ft}^2}{143,000 \ \text{ft}^2}\right)^{0.75} = \$793,000 \ (4.38)^{0.75} =$$

$$\$2,400,000 \text{ or } \$9.60/\text{kW}.$$

This cost estimate does not include a penalty for the additional space requirements resulting from the installation of a precipitator with a plate area 4.38 times larger than would be required under normal circumstances. These space requirements would, in many cases, make such an enlargement at an existing installation completely impractical.

C. Fly Ash Conditioning with Sulfuric Acid Vapor

Data obtained by Southern Research Institute under EPA Contract CPA 70-149[3] have established that a high dust resistivity problem can be solved by injecting sulfuric acid vapor into the flue gas ahead of the precipitator. Successful conditioning was obtained with fly ashes of widely different compositions, and with systems employing both anhydrous SO_3 and 66° Bé H_2SO_4 as sulfuric acid vapor sources. The details and method of operation of different types of conditioning systems are described in the final report on the above contract.

In order to compare fly ash conditioning with other approaches to solving a high resistivity problem, it is necessary to consider both capital and operating costs of the conditioning system. A cost comparison of existing conditioning facilities has indicated that an anhydrous SO_3 system requires less capital cost than does a system utilizing sulfuric acid. Therefore, conditioning cost estimates presented here are based on such an installation.

For a 250 MW plant, the capital expenditure required for installing an anhydrous SO_3 conditioning system is estimated as $169,000. Total estimated operating costs, including capital charges at 14.5%/year, labor and maintenance, and energy and raw materials range from $57,100/year at an injection level of 10 ppm sulfuric acid vapor to $79,200/year at 20 ppm. For these two injection levels, energy and raw material costs comprise $24,100/year and $46,200/year of the respective total costs. The calculations were based on 7000 operating hr/year at full load.

An improvement in the precipitation rate parameter of 467% has been reported as a result of conditioning for a unit which was operating with a very high resistivity dust. It is therefore reasonable to assume that the installation of a conditioning unit would increase the effective w value from 3-5 cm/sec to 13 cm/sec, which is the w assumed for the "normal" precipitator used as a basis for comparison. Thus, the total capital expenditure would be $793,000 for the precipitator plus $169,000 for the conditioning plant, or $962,000.

D.   High Temperature Operation

There is a growing trend in recent fly ash precipitator installations to locate the precipitator ahead of the air heater at temperatures in the neighborhood of 700°F. At this temperature, the controlling conduction mechanism in the precipitated dust layer is intrinsic or volume conduction, instead of the surface conduction mechanism which predominates downstream from the air heater at lower temperatures. Thus, the fly ash resistivity at high temperature is not sensitive to the SO_3 or moisture content of the flue gas. Most published resistivity data indicate that resistivities below the critical 2×10^{10} Ω-cm will occur above 600°F; therefore, high temperature operation offers an alternative solution to high dust resistivities resulting from combustion of low sulfur coals.

Another advantage of high temperature operation is that fouling of the air heater by fly ash is reduced. However, in installations burning high sulfur coal with a basic fly ash, it is probable that removal of this ash ahead of the air heater would result in increased corrosion rates of air heater cold end elements. For installations in which coal and oil firing are employed, high temperature operation minimizes oil ash handling problems.

The principal motivation for installing a hot precipitator is to overcome the excessive size requirements brought about by high dust resistivity at lower temperatures. There are, however, two

factors which partially offset the reduced size as a result of lowered resistivity: (1) a higher gas volume must be treated due to the higher temperature, and (2) the decreased gas density results in lower corona voltages and electric fields.

Design precipitation rate parameters, w, for hot precipitators reported to Southern Research Institute range from 8.8 to 10.5 cm/sec. For the 250 MW unit discussed previously, the gas flow at 700°F is given by

$$800,000 \times (\frac{460 + 700}{460 + 270}) = 1,270,000 \text{ acfm.}$$

To obtain a 99% collection efficiency, the plate area required using 8.8 cm/sec (17.3 ft/min) as w

$$A = \frac{V}{w} \ln 100 = \frac{1,270,000}{17.3} \ln 100 = 338,000 \text{ ft}^2 \text{ or}$$

$$266 \text{ ft}^2/1000 \text{ cfm at } 700°F, \text{ or } 423 \text{ ft}^2/1000 \text{ cfm}$$

$$\text{at } 270°F.$$

It can be seen that, in spite of the partially offsetting factors of increased gas flow and lowered electric fields, high temperature operation results in design migration velocities sufficiently high to allow a reasonable plate area. Recalling the earlier discussion of precipitator enlargement at 270°F for a high resistivity dust with a w of 3 cm/sec, a plate area of 625,000 ft^2 was required for the same efficiency.

Cost data relating to hot precipitators are rather limited because of the small number of installations in operation. Table 5.1 summarizes the costs of hot precipitators reported by various utilities to Southern Research Institute. The high total cost for Plant F may be due to the fact that this installation was the first of its type. As would be expected, the precipitators installed on existing units are more expensive than those installed on new installations. Plant D provides a basis for comparing the use of a hot precipitator with the other options. It is a new installation in the same size range as the 250 MW unit employed as a basis for comparison, and the total installed costs are given. The costs of ductwork should be included in comparing hot precipitators with other options because of the additional ducting cost associated with such an installation.

Table 5.1. Cost of Hot Precipitators Reported
to Southern Research Institute

Plant	No. of units and capacity	Basis for cost	Cost $/kW
A	2 units, 285 MW total	Precipitator, installation & ductwork-retrofit, 99% eff.	14.60
B	2 units, 360 MW total	Precipitator, installation & ductwork-retrofit, 99% eff.	9.07
C	1 unit, 920 MW	Precipitator, delivered & erected, no ductwork-new unit, 99% eff.	5.15
D	1 unit, 350 MW	Total installed cost, including ductwork, new unit, 99% eff.	7.2-8.6
E	1 unit, 110 MW	FOB cost only	6.80
F	1 unit, 1000 MW	Precipitator (followed by mechanical collector), and erection	4.70
		Complete installation, including ductwork, ash handling and foundations.	10-12

Plant D has a plate area of 564,000 ft^2 and a median cost of $7.90/kW, or $2,770,000. The cost of a 250 MW unit can be estimated by again assuming that precipitator costs show a power rule variation with area, using an exponent of 0.75. Thus, for a 250 MW unit with 8.8 cm/sec migration velocity at 700°F,

$$\$2,770,000 \ \left(\frac{338,000}{564,000}\right)^{0.75} = \$1,890,000, \text{ or about } \$7.55/kW.$$

Similarly, if a migration velocity of 10.5 cm/sec is used as a design basis, the cost estimate would be

$$\$2,770,000 \ \left(\frac{284,000}{564,000}\right)^{0.75} = \$1,660,000, \text{ or about } \$6.65/kW.$$

E.   Low Temperature Operation

The shape of the resistivity-temperature relationship in
stack gases indicates that low temperature operation can be used
as a solution to the problem of high dust resistivity. The dis-
cussion of low temperature corrosion and fouling in Section 6
has shown that most plants with high fly ash resistivity will not
be prevented from operating in the 220-240°F range as a result of
corrosion and fouling in the cold end elements of the air preheater.
Thus, the principal economic considerations are the limits of the
temperature range required for proper resistivity and the feasi-
bility of obtaining and controlling such temperatures at the pre-
cipitator inlet.

Figure 5.1 shows resistivity as a function of temperature
at Plant 6.[4] The in-situ resistivity data indicate that accept-
able resistivity values are obtained in the 220-240°F range.
This plant was originally designed for a precipitator inlet
temperature of 300°F, and changes in the boiler were made to
lower stack temperature. The economizer surface in the boiler
was increased and provisions were made, using excess fan capacity,
to dump excess air blown through the air heater. The use of a
steam coil heater, which preheats combustion air prior to the
air heater, was also reduced. Another modification was the in-
stallation of a mixing baffle to overcome gas velocity and
temperature distribution problems at the precipitator inlet.
Figure 5.2 gives the flue gas flow plan.[4]

It should be noted that in-situ resistivity measurements
are needed to determine the required range of precipitator inlet
temperatures. For a new installation, such data could be obtained
from combustion of the projected fuel in a similar full-size unit,
or from measurements at the plant under consideration in a
temporary duct prior to installation of the precipitator. Selec-
tion of a design temperature and precipitation rate parameter in
the absence of such data would be hazardous.

The effect of low temperature operation on boiler economics
varies considerably with local conditions. The selection of an
optimum stack gas temperature in the absence of secondary con-
straints, such as space limitations and corrosion hazards, is a
trade-off between the savings resulting from high heat recovery
and the expense involved in installing and maintaining additional
heat exchanger surface. Some utilities operating stations with
low-cost, low sulfur lignite and sub-bituminous coals have de-
signed units with stack temperatures in the neighborhood of 300°F,
apparently concluding that the addition of more heat recovery
surface is not justified. Thus, the procedure of lowering stack
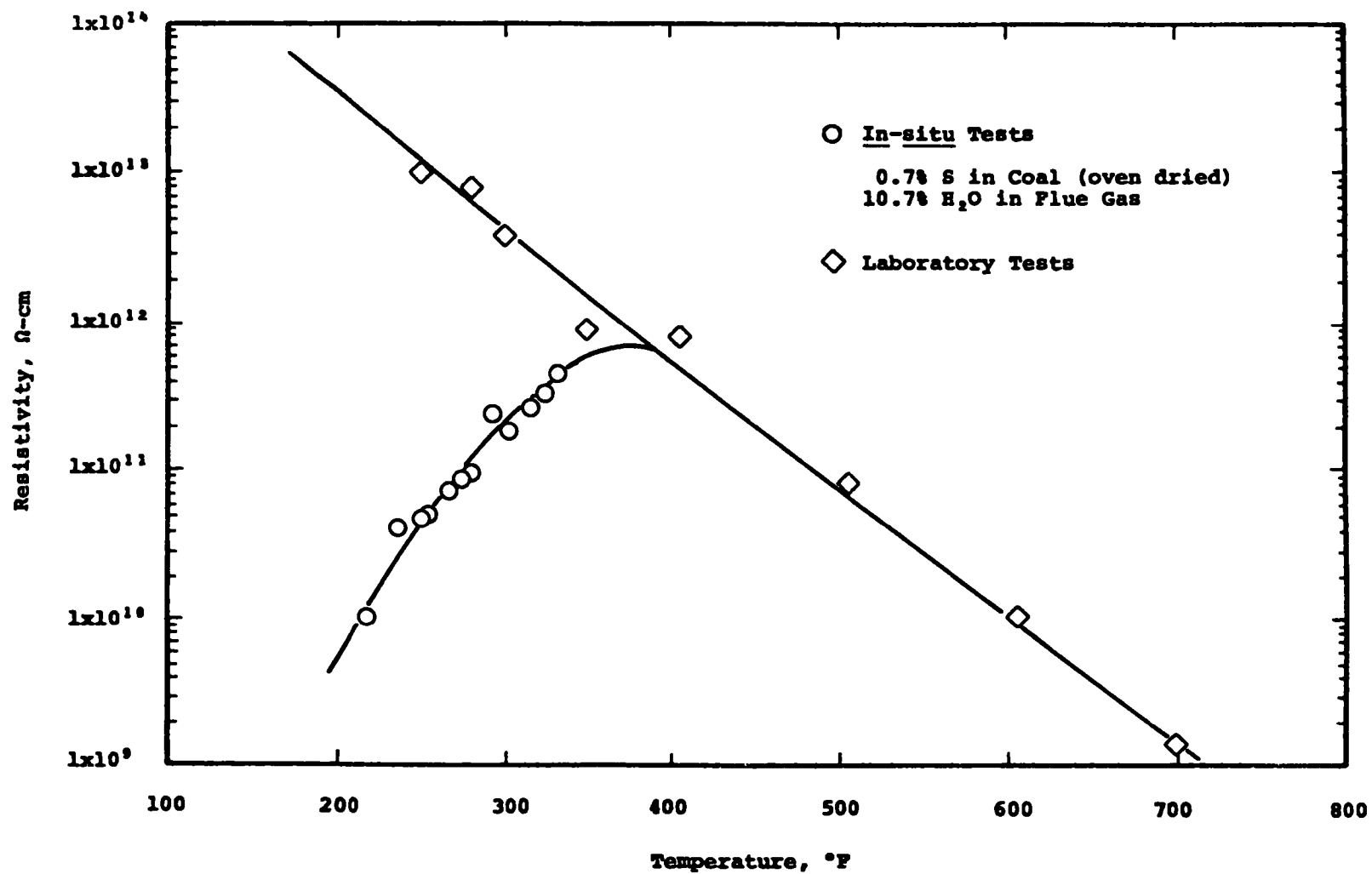
Figure 5.1. Resistivity as a Function of Temperature at Plant 6
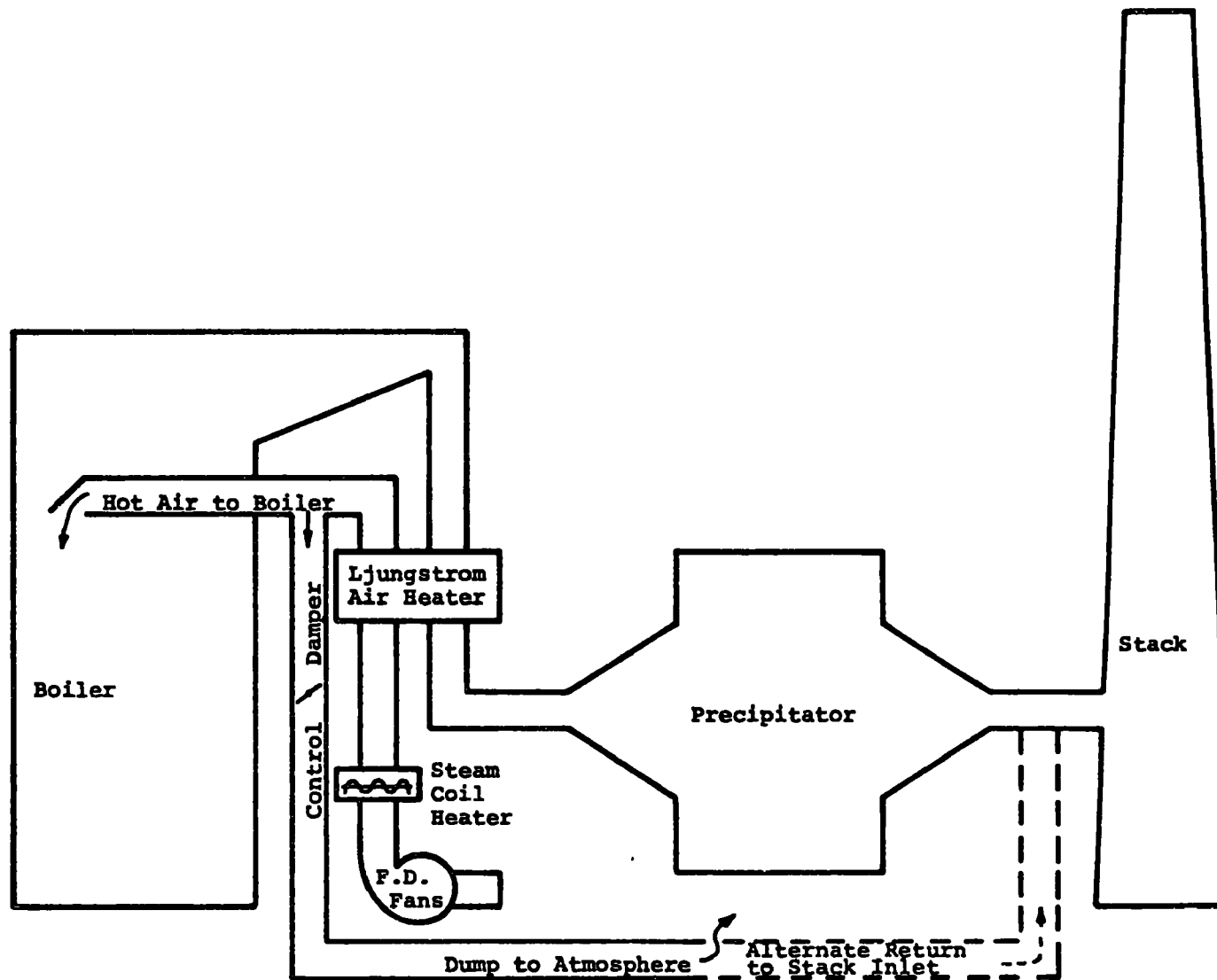
Figure 5.2. Schematic of Flue Gas Flow Plan

temperature by dumping excess combustion air is not an unreasonable concept, particularly with low fuel cost. The fuel cost at Plant 6, for example, is about $0.18/10^6 BTU. At higher fuel costs, the theoretical economic optimum stack temperature decreases. If an optimum design temperature is assumed for higher fuel costs, a smaller relative amount of excess combustion air needs to be dumped to lower stack gas temperature to the degree dictated by resistivity considerations.

Although it is recognized that the procedure illustrated in Figure 5.2 is not practical with some boiler designs, it can be used to illustrate the comparative costs of the low temperature solution to high resistivity. A precipitation rate parameter of 10.1 cm/sec, which is based on the experience of Plant 6, was used as a basis of calculation.

For a 250 MW plant, the cost of a precipitator designed for 99% collection efficiency with a w of 10.1 cm/sec at 220 to 240°F is estimated as $920,000. It is assumed that sufficient heat exchanger surface is included in the boiler to lower stack gas temperature from 300°F to 270°F, and that a mixing baffle and provision for dumping excess air are added to allow a uniform temperature of 220°F to be obtained. The cost of these additions is estimated at about $164,000. If a permanent by-pass is added to the system to reheat the stack gas, the total cost of the alterations is estimated as $332,000. Thus, the total estimated cost associated with the low temperature precipitator is $1,250,000 with stack gas reheating provisions, and $1,080,000 without these provisions. Stack gas reheating using dumped excess air may be desirable because of plume bouyancy problems.

No provisions have been made in the estimate for the incremental costs associated with purchasing excess fan capacity. However, the amount of excess air dumped relative to net combustion air at Plant 6 was about 13%, with 80°F ambient air, to achieve a 50°F reduction in stack temperature. The incremental costs associated with the purchase of this amount of additional capacity for a new installation are not likely to be significant when compared with the other items.

The fuel loss and fan energy consumption cost estimates for low temperature operation are given in Table 5.3. A 0.8% degradation in boiler efficiency with 13% excess air dumped was assumed for 7000 operating hours/year in the calculations. Electric power costs were assumed at $0.005/kWh. These estimates are rather conservative in that it is unlikely to be necessary to dump 13% excess air for 7000 hours. Figure 5.3 gives the cost of losses in boiler efficiency for various fuel costs.
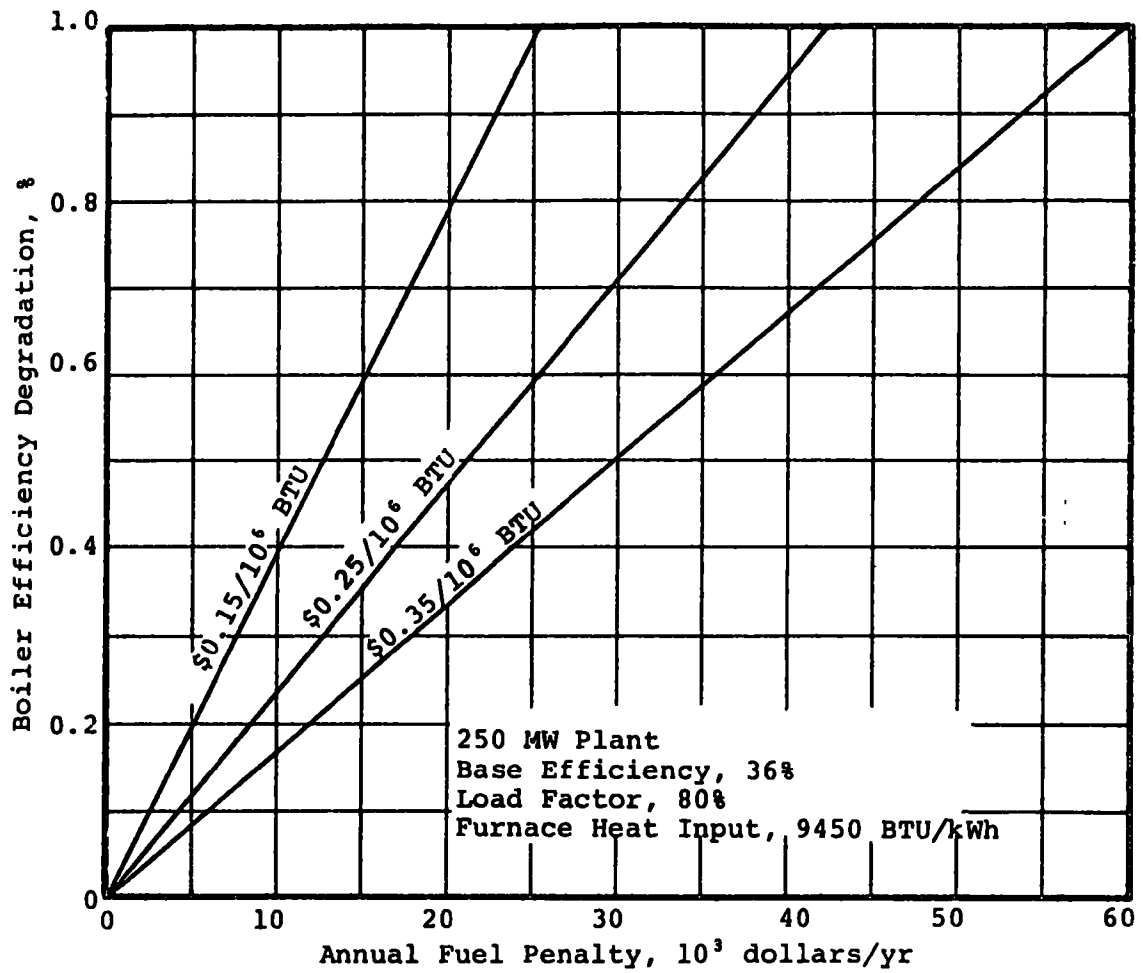
Figure 5.3. Cost of Boiler Efficiency Loss

F.   Overall Comparison

The estimated total capital investment required for the
various precipitator configurations is given in Table 5.2.
Annual incremental capital charges given in Table 5.3 were
computed by taking 14.5% of the difference between the total
capital costs of the various options and the base precipitator
cost of $793,000. Thus, the totals in Table 5.3 represent the
estimated additional annual expenditures required for collection
of high resistivity dusts. It is assumed that no appreciable
differences exist between the operating and maintenance costs
of the precipitators employed in the different configurations.

This comparison indicates that the least desirable option
for very high resistivity dusts is a large precipitator at
normal temperatures. Even though such an arrangement can be
less expensive than a hot precipitator, considerably more area
is required, and the probability of meeting design collection
efficiencies is less due to the fact that the enlarged precipi-
tator must operate with resistivities outside the desirable
range.

The use of a hot precipitator, based on presently available
cost data, is likely to be more expensive due to higher capital
cost than either conditioning or low temperature operation.
There are certain advantages associated with this extra cost,
such as operational simplicity and relative insensitivity of dust
resistivity to changes in coal sulfur content.

The relative desirability of low temperature operation as
compared to conditioning obviously depends on such factors as
boiler and air heater design, fuel costs, and concentration of
conditioning agent required. The estimates in Table 5.3 indicate
that low temperature operation, even when air dumping is required,
can be an economically competitive solution to high resistivity.
The air dumping procedure is costly, but it allows for flexibility
in that increasing cold end temperatures is possible by dumping
less excess air. This may be desirable if it becomes necessary
to burn a fuel of higher than planned sulfur content, which could
lower resistivity excessively and cause low temperature corrosion
and fouling. The principal drawback with low temperature opera-
tion, for a new installation, is that rather comprehensive
in-situ resistivity-temperature data are required to establish a
firm basis for design. Also, if a plant is designed for operation
at 220-240°F exit temperatures with no provision for temperature
variation via air dumping, changes in fuel composition could cause
problems with both air heater and precipitator operation.

Table 5.2. Estimated Total Capital Investment
99% Efficient Precipitator
250 MW Unit

Configuration	Base	Enlarged		Condi-tioned	Hot		Cold via air dump	
Temperature, °F	270	270		270	600-700		220-240	
Precipitation rate parameter, cm/sec	13	3.0	4.5	13	8.8	10.5	10.1	
							With stack reheat	Without stack reheat
Capital investment, $	793,000	2,400,000	1,770,000	962,000	1,890,000	1,660,000	1,250,000	1,080,000

Table 5.3. Estimated Incremental Annual Cost in Dollars - High Resistivity Dust

99.0% Efficiency - 250 MW

Load Factor = 0.8

Configuration:	Enlargement		Conditioning		Hot		Cold via air dump			
w, cm/sec:	4.5	3.0	13		8.8	10.5	10.1			
Precipitator area, ft^2:	417,000	625,000	143,000		338,000	284,000	175,000			
Injected SO$_3$ concentration:			10 ppm	20 ppm						
							With stack reheat		Without stack reheat	
Fuel cost/10^6 BTU:							15¢	25¢	15¢	25¢
Incremental capital charge @ 14.5%/yr:	142,000	233,000	24,500	24,500	159,000	126,000	66,000	66,000	42,000	42,000
SO$_3$ plant:										
Maintenance			8,500	8,500						
Operations			24,100	46,200						
Air dump:										
Fuel loss							19,900	33,200	19,900	33,200
Fuel gain (economizer)							-11,900	-20,000	-11,900	-20,000
Incremental fan energy							7,600	7,600	7,600	7,600
TOTAL:	142,000	233,000	57,100	79,200	159,000	126,000	81,600	86,800	57,600	62,800

For a case such as that given in Table 5.3, in which conditioning is economically competitive with low temperature operation via air dumping, some consideration must be given to the relative operational advantage of the low temperature procedure. Clearly, less maintenance and reliability problems would be expected from the operation of a fan-damper combination than with an SO_3 conditioning plant. The experience at Plant 6 with low temperature operation using this procedure has revealed no unexpected problems.

In summary, the use of a hot precipitator, SO_3 conditioning, or low temperature operation offers potential solutions to the problem of high dust resistivity. Each option has undergone some degree of successful operation in full-size installations, and the relative economics of the options are strongly influenced by local conditions. Low temperature operation and conditioning require less capital expenditure than a hot precipitator, but the capital saving is partially offset by the operating costs involved with these procedures. For installations in which low temperature operation via air dumping is compatible with basic boiler design requirements and where resistivity data are available, this method offers the simplest, and in some cases, the most economical solution to the resistivity problem.

G.   Bibliography - Section 5

1.   Oglesby, S. and Nichols, G. B., A Manual of Electrostatic Precipitator Technology - Part II, prepared for the National Air Pollution Control Administration under Contract CPA 22-69-73 by Southern Research Institute, Birmingham, Alabama (August 1970).

2.   McLean, K. J., "Some Effects of High Resistivity Fly Ash on Electrostatic Precipitator Operation," Paper II-A, Proceedings of the Electrostatic Precipitator Symposium, Birmingham, Alabama (February 1971) sponsored by the Air Pollution Control Office, Environmental Protection Agency.

3.   Southern Research Institute, Final Report on Contract CPA 70-149 (A Study of Resistivity and Conditioning of Fly Ash) to Division of Control Systems, Office of Air Programs, Environmental Protection Agency (in preparation).

4.   Berube, D. T., "Low Gas Temperature Solution to High Resistivity Ash Problems," Paper II-E, Proceedings of the Electrostatic Precipitator Symposium, Birmingham, Alabama (February 1971) sponsored by the Air Pollution Control Office, Environmental Protection Agency.

SECTION 6. LOW TEMPERATURE CORROSION AND FOULING

A.   Introduction

Reducing precipitator inlet gas temperatures to the 220 to 250°F range offers a promising method of lowering the high fly ash resistivity which occurs with the combustion of most low sulfur coals. However, operation at such low temperatures has caused corrosion and fouling of air heater elements in some installations, while others have experienced no difficulty with air heater exit temperatures as low as 220°F. An understanding of the factors which cause corrosion and fouling problems is therefore required if low temperature operation is to be considered as a means of lowering resistivity and increasing precipitator performance.

The purpose of this study, then, is to relate corrosion to fly ash and flue gas composition, fly ash resistivity, and temperature. If a basic understanding of this relationship could be gained, a decision on the advisability of low operating temperature could be made on the basis of fly ash and flue gas analytical data.

B.   Sulfuric Acid Occurrence in Flue Gas

1. SO_x, H_2O, and H_2SO_4 equilibria

A knowledge of the SO_3 concentration in the air heater and precipitator region of power plant exhaust systems is important from a standpoint of both corrosion and fly ash resistivity. The principal cause of corrosion in air heaters, and the most important factor in determining fly ash resistivity, is sulfuric acid, which results from the reaction of SO_3 with water vapor.

Most of the sulfur in power plant flue gases appears as SO_2, with typical SO_3 levels ranging from 1 to 2.5% of the SO_2. However, as Figure 6.1 shows, the equilibrium constant for the reaction

$$SO_2(g) + \tfrac{1}{2}O_2(g) = SO_3(g)$$
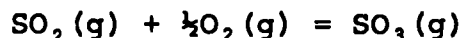
strongly favors the formation of SO_3 at temperatures below 1000°F with 3% oxygen. This graph was calculated from data cited by Hedley.[1] The kinetics of the reaction are, of course, unfavorable in the absence of a catalyst, but it is thermodynamically feasible

---

[1]Refer to the Bibliography at the end of this section.
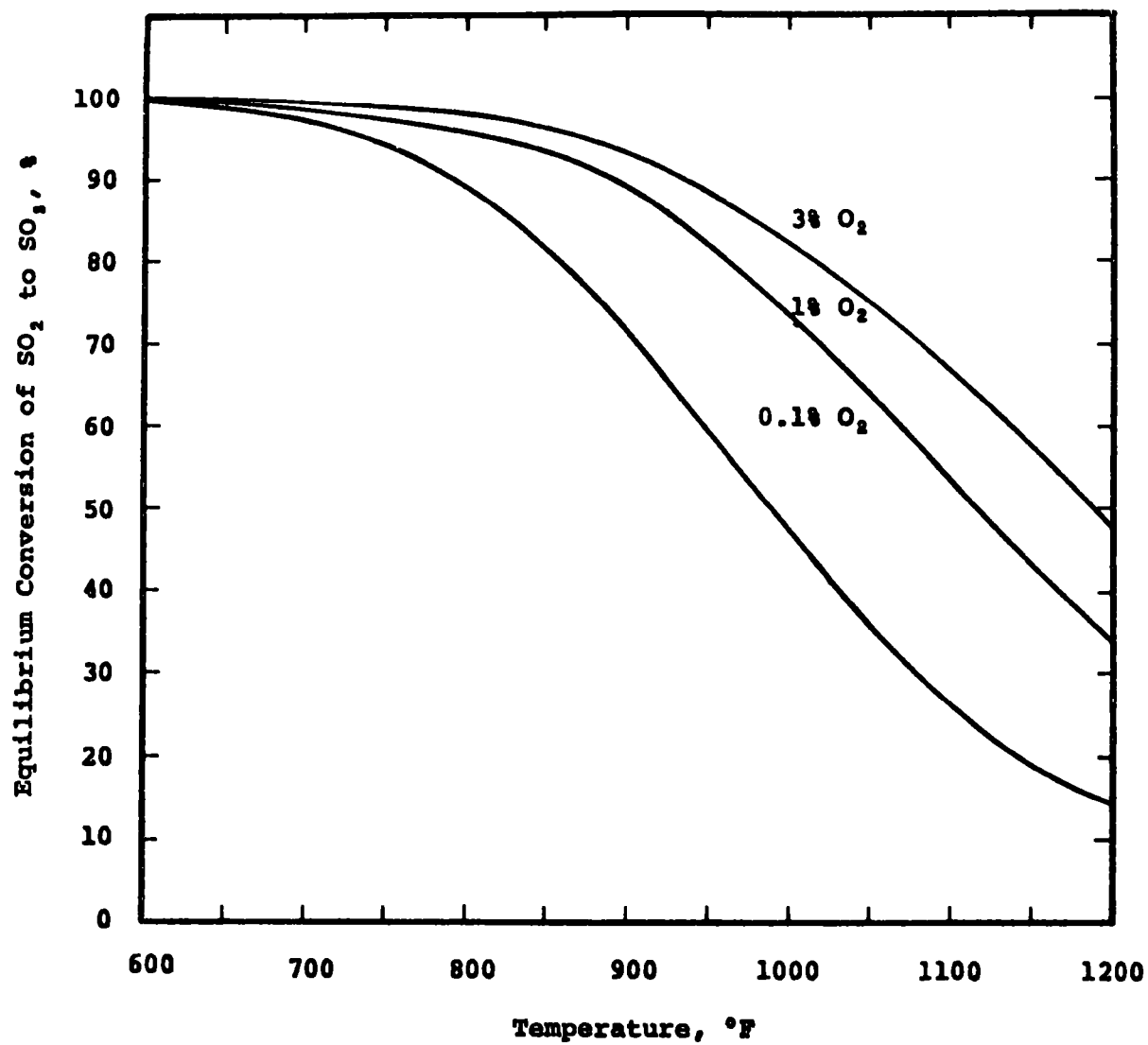
Figure 6.1. Equilibrium Conversion of SO_2 to SO_3

for SO_3 concentrations to exist at levels much greater than those normally encountered. Ratios of SO_3 to SO_2 as high as 0.1 have been reported.[2] Thus, since the formation of SO_3 is controlled by catalytic effects as well as the amount of excess air present, the concentration of SO_3 resulting from the combustion of a particular fuel can only be estimated in the absence of direct measurements.

The reaction between water vapor and SO_3 is given by

$$H_2O(g) + SO_3(g) = H_2SO_4(g).$$
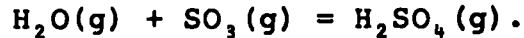
Figure 6.2 shows the equilibrium conversion of SO_3 to H_2SO_4 as a function of temperature for a typical flue gas water concentration of 8%. At temperatures below 400°F, essentially all of the SO_3 present is converted to H_2SO_4 at equilibrium. In contrast to the formation of SO_3, the formation of H_2SO_4 occurs rapidly in the thermodynamically feasible temperature range.[3] Thus, all SO_3 below the air heater in a power plant will exist as H_2SO_4, either in the vapor or liquid state. Since corrosion problems are associated with the presence of liquid phase sulfuric acid, the determination of the condensation characteristics of sulfuric acid from flue gas containing sulfuric acid and water vapor is a necessary step in evaluating the corrosion potential of a particular stack gas.

2.   Determination of the sulfuric acid dew point

Fly ash particles can influence the apparent dew point, or saturation temperature of H_2SO_4 in flue gas, but experience has shown that one commits practically no error by neglecting the presence of other gases and considering only the system sulfuric acid - water.[4] A thermodynamic analysis of the sulfuric acid - water - flue gas system, ignoring for the present the effect of fly ash, provides a theoretical basis for predicting acid dew points and condensate composition from vapor-liquid equilibria data.

For the case of ideal or quasi-ideal binary solutions, dew points of vapor mixtures composed of the binary solution vapor and noncondensible gases can easily be calculated from a knowledge of the pure component vapor pressures as a function of temperature. The H_2SO_4-H_2O system presents special problems because:

- the H_2SO_4 and water undergo chemical reaction to form the various hydrates of sulfuric acid, and therefore the equilibrium relationships are
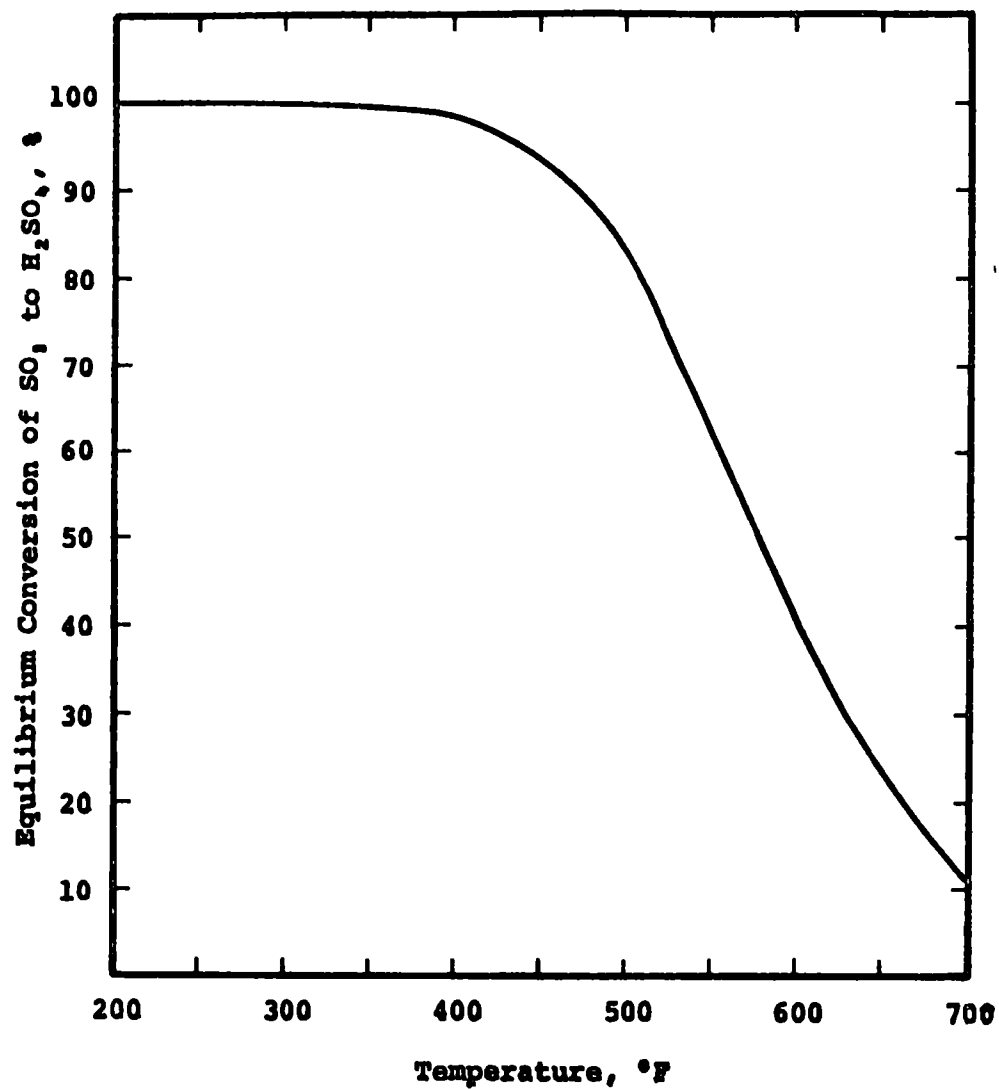
Figure 6.2. Equilibrium Conversion of SO_3 to H_2SO_4 at 8.0 vol % H_2O in Flue Gas

strongly composition-dependent, and

- H_2SO_4 has a very low pure component vapor pressure, thus making direct measurements extremely difficult.

The total vapor pressure of H_2SO_4 at low temperature is essentially the partial pressure of water above the acid solution, and this is available from the existing literature. In order to determine the dew point, however, the H_2SO_4 partial pressure at low temperature must be known, and the literature lacks such data.[4]

As a result of the experimental difficulties encountered in low temperature vapor pressure measurements, efforts have been made to calculate the partial pressures from liquid phase thermodynamic data. Abel[5] was the first to derive a relationship enabling the calculation of H_2SO_4, H_2O, and SO_3 partial pressures from standard state values of enthalpy, entropy, and heat capacity; and partial molal values of enthalpy, entropy, free energy, and heat capacity. Müller,[4] using Abel's calculated data, computed dew points of gases with low H_2SO_4 concentrations. Gmitro and Vermuelen[6] utilized thermodynamic data, which are claimed to be more recent and more complete, to calculate H_2SO_4, SO_3, and H_2O partial pressures from -50 to 400°C with solutions ranging from 10 to 100 weight percent H_2SO_4. Snowden and Ryan[3] have used Gmitro and Vermuelen's partial pressure data to construct a chart which gives the dew point temperature of a gas as a function of H_2SO_4 and H_2O partial pressures. The composition of the acid condensate occurring at a given dew point is also provided.

The dew points predicted from Abel's data are about 30°F higher than those arrived at with Gmitro and Vermuelen's data. The difference in these two works lies mainly in the data available for the calculation of the partial pressures. Gmitro and Vermuelen had access to much more accurate data and should have obtained the more accurate results. However, their results do not agree with direct dew point measurements by the condensation technique, whereas Abel's partial pressures have been verified in part by use of this method.

A suspect assumption common to predictions of acid dew points based on both the Abel and Gmitro calculations is that the vapor state is an ideal gas, and that the vapor solution is also ideal. A gas mixture may behave nearly ideally volumetrically, but a component present in small amounts may exhibit significant departure from ideality if that component is associated in the vapor state.

Among the limitations of some presentations in the litera-
ture of the Müller correlation with 10% water vapor is that they
do not indicate the effect of variations in the water vapor concen-
tration on sulfuric acid dew points. The concentration of the
condensate is also not provided. Figures 6.3 and 6.4 were
prepared to present this information.

Figure 6.3 is a sulfuric acid - water dew point chart
prepared from Abel's H_2SO_4 partial pressures and Greenewalt's[7]
water partial pressures above sulfuric acid solutions. The
partial pressure data were calculated by computer from the follow-
ing equations:

$$P_{H_2SO_4} = \exp\left[2.303\left(A + \frac{B}{T} + \frac{D(\ln T)}{2.303} + E \cdot T\right)\right] \qquad 6.1$$

and

$$P_{H_2O} = \exp\left[2.303\left(A' - \frac{B'}{T}\right)\right] \qquad 6.2$$

where T is in degrees Kelvin and partial pressures are in mm Hg.
The constants in these equations are given by Abel and Greenewalt
for various sulfuric acid concentrations. It should be noted that
the range of uncertainty indicated by Abel for the constant B in
Equation 6.1 results in a dew point uncertainty of 8°F at 10% water
vapor.

The information contained in Figure 6.3, if it were accurate,
would be of value in assessing the corrosion potential of a flue
gas. The dew point temperature can be predicted from an analysis
of H_2SO_4 and water vapor content, and if the gas is cooled to some
temperature below the dew point, the equilibrium concentration of
condensate and the amount condensed can be obtained. It should
be pointed out, however, that the amount of condensate predicted
from the use of a dew point chart such as Figure 6.3 is actually
a prediction of the amount available for condensation. The amount
of condensate depositing on a metal surface may differ from the
chart prediction because of mass transfer considerations.

As an example of the use of the chart, consider a flue gas
containing 10 ppm H_2SO_4 and 10% H_2O. Condensation would occur
at about 275°F, and the condensate composition at that point
would be about 79% H_2SO_4 by weight. If the gas were cooled to
250°F, 85% of the H_2SO_4 should be removed from the gas phase, and
an insignificant amount of the water vapor would also be condensed.
The condensation, therefore, follows the 10% water line, result-
ing in a condensate which would be the equilibrium composition of
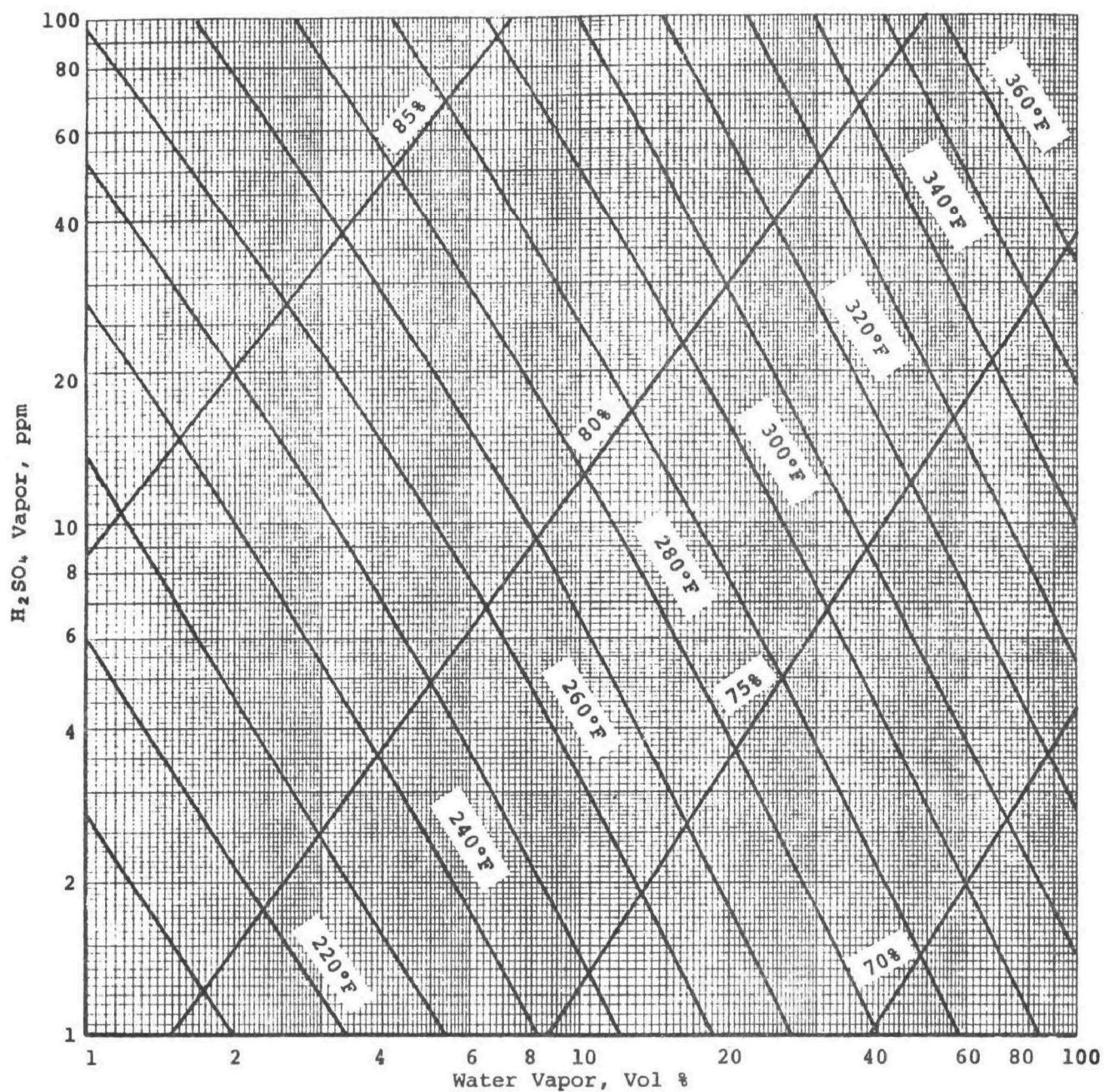
Figure 6.3. Dew Point and Condensate Composition for Vapor
Mixtures of H_2O and H_2SO_4 at 760 mm Hg Total
Pressure (Abel and Greenewalt)
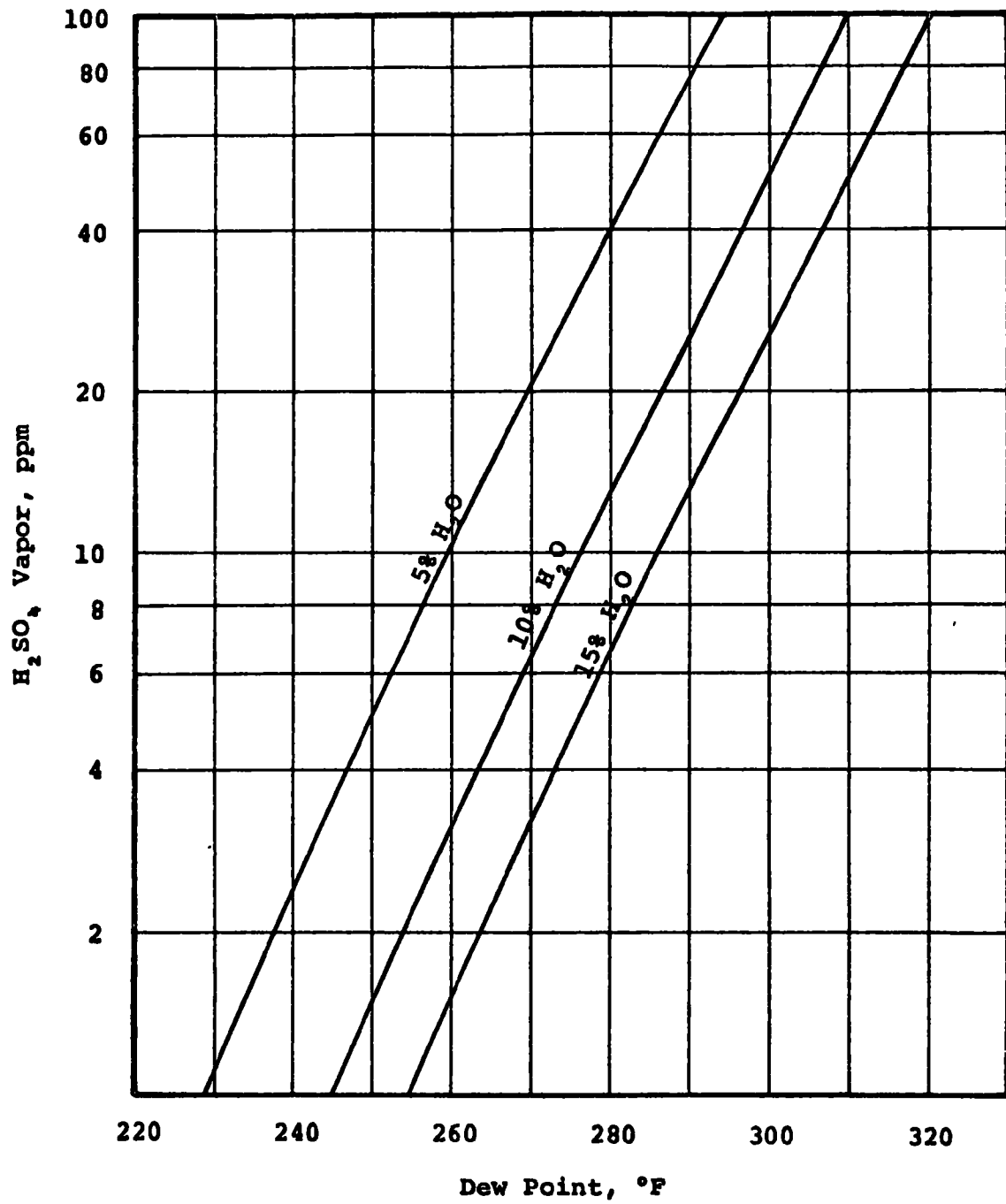
Figure 6.4. H_2SO_4 Dew Points for Typical Flue Gas Moisture Concentrations

the condensate at 250°F, assuming the vapor phase is in equilibrium with the total liquid condensed. The composition change of the liquid is small over the temperature interval given as an example, ranging from 79% at 275°F to 75% at 250°F.

It is apparent from Figure 6.3 that a knowledge of water vapor concentration is of fundamental importance. Appreciable changes in this variable can have a rather significant effect on the predicted sulfuric acid dew point, and if a gas is saturated with H_2SO_4, the condensate composition is determined by the water vapor content and temperature. Thus, if a surface is maintained at a known temperature lower than the sulfuric acid dew point, but higher than the water dew point, the concentration of acid condensate which occurs can be predicted from Figure 6.3 if the water vapor content of the gas is known.

In addition to the procedure based on calculated partial pressures, a number of efforts have been made to determine sulfuric acid dew points using instrumental and chemical procedures. Two methods will be discussed briefly: the condensation method and an electrical conductivity method.

The problem of measuring SO_3 concentration and acid dew point has been studied since Johnstone[8] examined the problem in 1929. Many papers[9-20] have been presented which employ the electrical conductivity method which Johnstone originated. The British Coal Utilization Research Association (BCURA) designed an instrument which has found widespread usage employing Johnstone's concept. This instrument, known as BCURA dew point meter, has been described in detail by Flint.[9] It is a portable instrument which measures the conductivity of a condensing film. The detector element is glass and contains two electrodes mounted flush with the surface. A tube inside the glass probe transports compressed air which is used to maintain the glass surface of the probe at the desired temperature. A thermocouple provides a readout of the glass surface temperature.

If an electrically conductive film forms on the detector element, a current will flow that is proportional to the magnitude of the externally impressed voltage and the conductivity of the condensing film. The current flow is measured with a microammeter. A dew point is determined by inserting the detector element into a gas stream with the instrument temperature held at some value above the dew point. The element temperature is then alternately increased and decreased slowly to establish the exact temperature at which the increase in conductivity, and thus the dew point, occurs.

The condensation method is widely used for determinations of SO_3 in stack gases. The basic procedure employed consists of pumping the flue gas through a condenser coil maintained below the dew point of sulfuric acid, but above the normal water dew point. A heated sampling probe is used to obtain the flue gas samples, and a filter is inserted at the probe entrance to exclude particulate matter. A fritted glass filter follows the condenser to serve as a spray trap. When the sampling period is concluded, the H_2SO_4 is washed from the condenser, and the washings are collected and titrated.[21]

The condensation of a binary vapor mixture from a noncondensible gas is normally path-dependent, and the composition of the vapor leaving a condenser is not fixed merely by stating that the gas is saturated at a particular temperature. This is true because the degree of fractionation occurring during condensation depends on conditions which exist in the condenser. For the case of H_2SO_4-H_2O vapor mixtures in flue gas, however, the water vapor is in large excess, and no appreciable change in its concentration occurs until the water dew point is reached. The composition of the gas is, therefore, not path-dependent, and the state of the system is fixed if the gas is saturated with H_2SO_4 at a certain temperature and water vapor content. As a result, the condensation method can be used to obtain dew points of H_2SO_4-flue gas mixtures. Since the gas leaving the condenser is saturated with H_2SO_4 at the condenser exit temperature, the concentration of the exit vapor represents the dew point, or saturation temperature, of the gas.

Figure 6.5 presents the results obtained for flue gas dew points as a function of H_2SO_4(g) content by various investigators. To make an exact comparison, all of the curves should be for a gas of the same volume percent water vapor. However, reference to Figure 6.3 will indicate that a variation in water vapor concentrations from 7 to 10% can cause only about a 5 to 8°F change in the dew point. Taylor's results were obtained with the BCURA dew point meter in a mixture of air, water vapor, and sulfuric acid.[20] Lisle's data were obtained using the condensation method, again with a mixture of air, water vapor, and sulfuric acid.[21] The dew point curves of Gmitro, Müller, and from Figure 6.3, are based on the previously discussed calculated partial pressures.

It is obvious from Figure 6.5 that, except for Lisle and Sensenbaugh's checks of the data based on Abel's sulfuric acid partial pressures (Müller's data and Figures 6.3 and 6.4), there is little agreement between the results of the various investigators. The data obtained from calculated partial pressures agree
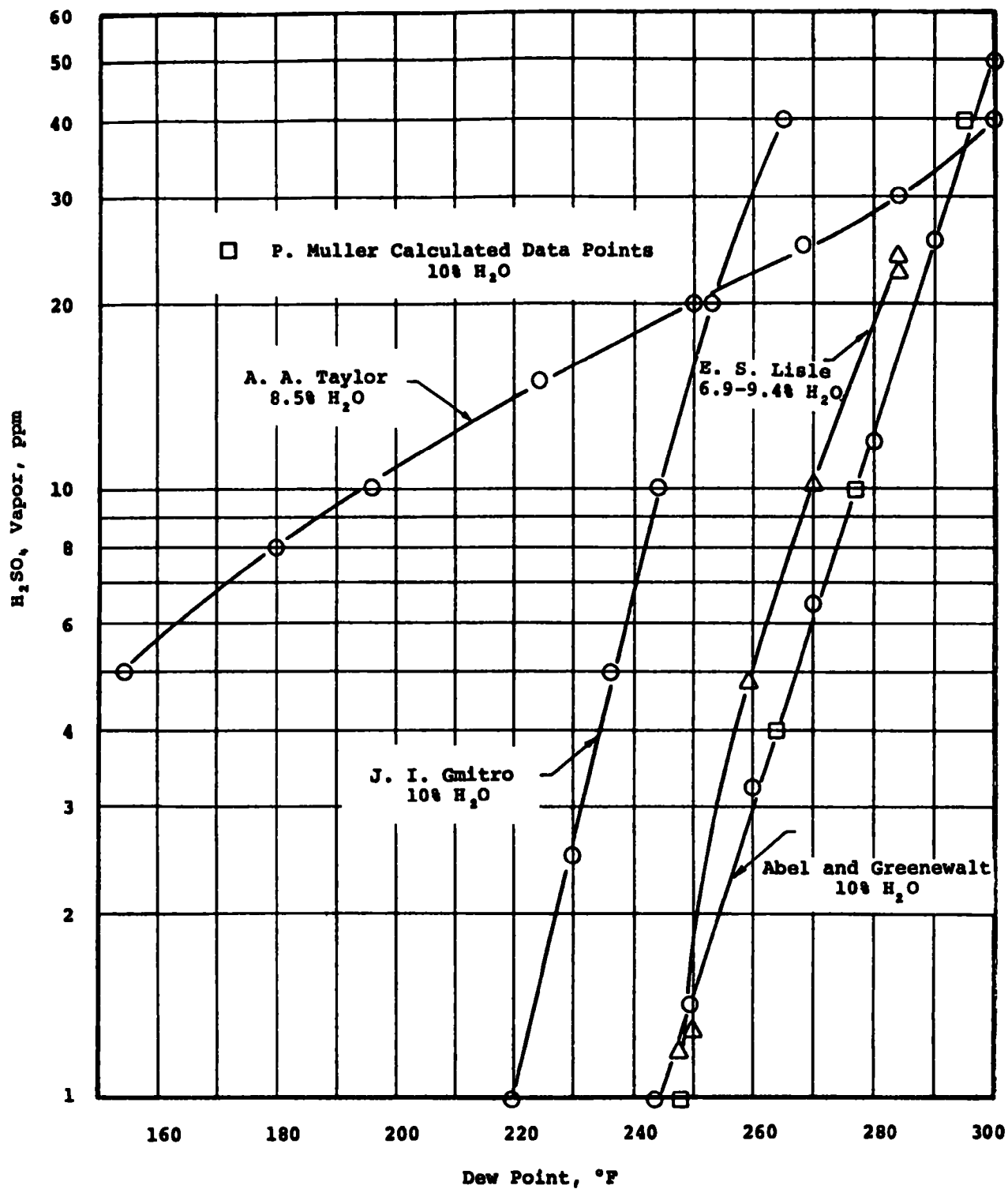
Figure 6.5. H_2SO_4 Dew Point Obtained by Various Investigators.

in form, which is to be expected since the equations used to calcu-
late the partial pressures are also of the same form. The nature
of the disagreement between the calculated dew point and those
obtained with the dew point meter suggest there is a sensitivity
problem with the instrument at low sulfuric acid partial pressures.

In view of the difficulties with calculations based on
liquid phase thermodynamic properties and the probable inaccuracy
of dew point meters at low acid partial pressure, we have con-
cluded that the only reliable method of correlating sulfuric acid
dew points with water and H_2SO_4 vapor concentration is a carefully
planned experimental program based on the condensation method
employed by Lisle and Sensenbaugh. In the absence of such data,
the dew points based on Abel's partial pressure data will be used,
since they have been verified in part by experiment and by the
operational experience of several power plants. A resolution of
the difference between the two sets of thermodynamic data (Abel's
and Gmitro's) is needed, but is beyond the scope of the present
study.

3.   Condensation characteristics

As stated previously, the amount of acid condensate predicted
from the use of a chart such as Figure 6.3 as a result of cooling
to a temperature below the sulfuric acid dew point is a prediction
of the amount available for condensation. Figure 6.6 shows that
the predicted percentage of H_2SO_4 condensed increases and asymp-
totically approaches 100% as the temperature is lowered below the
dew point. However, peak values of acid deposition rates at temper-
atures between the water and acid dew points have been observed by
numerous investigators.

The occurrence of such a peak in the condensation rate may
be caused by a change in the diffusivity of the H_2SO_4 in the
region close to the condensing surface. The rate of condensation
is dependent on the diffusion rate of H_2SO_4 and water vapor to the
surface. Small droplets of H_2SO_4 will form in the cooled gas ad-
jacent to the surface, and the size of these droplets is likely to
increase with decreasing temperature. The growth of the droplets
would slow their diffusion to the surface and increase the proba-
bility that they would be carried forward in the gas stream. Thus,
a temperature can be reached at which the slowed diffusion becomes
dominant over the increased amount of condensate available for
collision with the surface. This explanation is similar to one
offered by Flint and Kear.[14] A typical condensate rate curve,
obtained in a spiral condenser with a vapor mixture consisting of
7.5 vol % H_2O, 69 ppm H_2SO_4, and the balance air, is shown in Figure
6.7.[22]
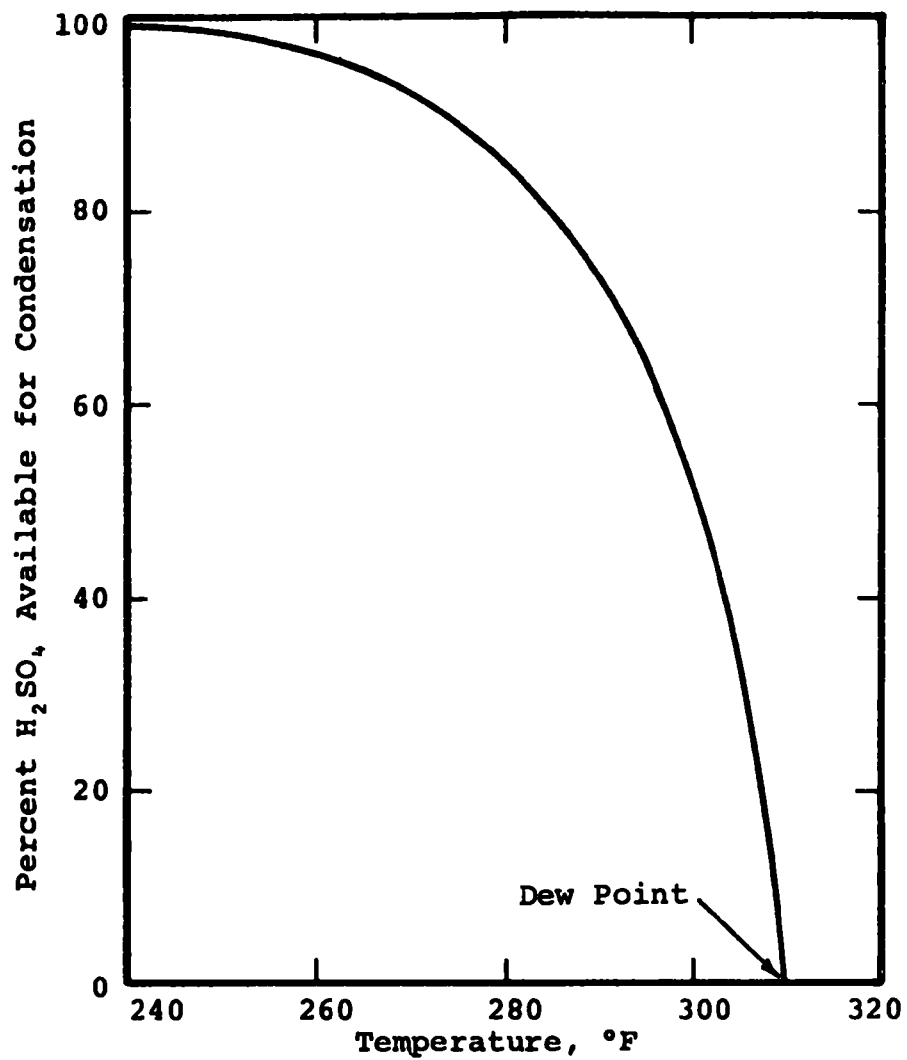
Figure 6.6. Percent H_2SO_4 Available for Condensation for Flue Gas of 100 ppm H_2SO_4 and 10% H_2O Vapor (Calculated from Figure 6.3)
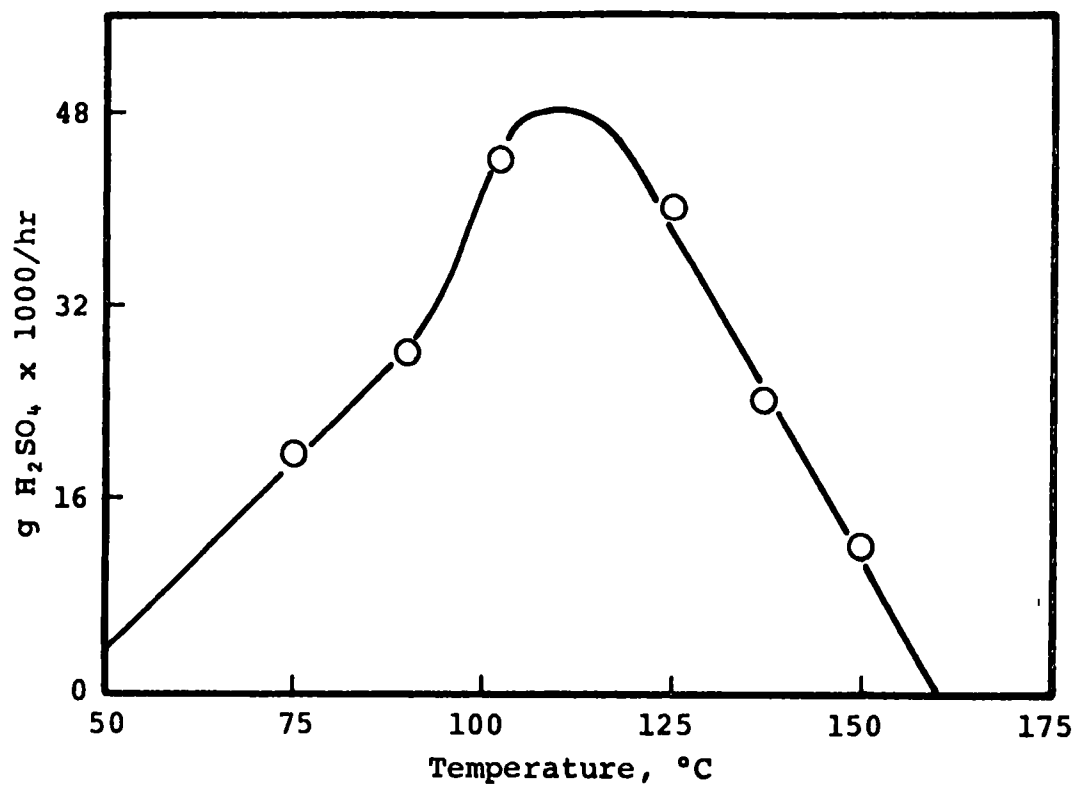
Figure 6.7. Variation in Condensation Rate with Surface Temperature (From H. D. Taylor)

C.   Factors Influencing Corrosion Rates

1.   Acid strength

If a flue gas is known to be saturated with H_2SO_4 vapor at a temperature below the acid dew point, it is possible to predict the initial condensate composition as a function of the water vapor partial pressure and temperature. Since data are available in the literature concerning the corrosion rates of various materials as a function of acid concentrations, it is of interest to determine whether there is any relationship between corrosion rates measured in flue gas and the acid condensate strength predicted from a gas analysis.

A study of flue gas corrosion of low alloy steels by Piper and Van Vliet[23] provides data which illustrate the difficulty encountered in predicting corrosion rates of metals from acid condensate strength alone. The compositions of the low alloy steel specimens used in this study are given in Table 6.1. The corrosion tests were conducted by inserting specimens maintained at known temperatures into stack gas produced from a pulverized-fuel-fired steam generator. The average H_2SO_4 content of the stack gas was about 30 ppm. Figure 6.8 gives the predicted sulfuric acid condensate compositions for the range of stack gas water vapor concentrations experienced during the study.

Figure 6.9 shows the average corrosion rate of selected steel specimens as a function of predicted H_2SO_4 condensate strength. The condensate strengths shown in Figures 6.8 and 6.9 were obtained from the computer printout of partial pressure for the H_2SO_4-H_2O system, using Greenewalt's equation (Equation 6.2) for the partial pressure of water over sulfuric acid solutions. The widths of the surface in Figure 6.9 indicate the possible acid concentrations at each temperature over the range of water vapor partial pressures encountered in the stack gas.

Figure 6.10 is a plot of corrosion rates of steel given by M. G. Fontana[24] at 75°F as a function of acid concentration. The corrosion rates for steel specimens immersed in acid are orders of magnitude higher than those observed by Piper. Since corrosion increases with temperature, the differences between the Fontana and Piper data are even greater than indicated because the latter's data were obtained at high temperatures.

Table 6.1. Composition, Percent by Weight, Spectrographic
Analysis of Specimens Tested
(from Piper and Van Vliet[10])

Name	Mn	Si	Cu	Ni	Cr	Zr
Cor-ten	0.40	0.38	0.23	0.29	0.61	--
NAX-A	0.85	0.90	0.07	<0.1	0.59	Present
NAX-B	0.82	0.79	0.29	<0.1	0.60	Present
NAX-C	0.53	0.54	0.07	<0.1	<0.1	Present

The low alloy steels used in the Piper study would not be
expected to exhibit greatly different corrosion rates in sulfuric
acid solution than the ordinary carbon steel on which Fontana's
data are based. Therefore, the orders of magnitude differences
in corrosion rates indicated are largely a reflection of the
differences in environment between the two situations. Another
contributing factor is the parabolic nature of the corrosion-time
relationship usually found in corrosion work. Thus, because of
the effects of fly ash and condensate deposition rates, it is not
practical to predict or correlate corrosion rates of materials in
flue gas solely on the basis of equilibrium condensate compositions.

2.   Acid deposition rate

The corrosion rate of metal surfaces in flue gas at tempera-
tures well above the water dew point is more strongly related to
the amount of condensate deposited than to the concentration of
the condensate. Consider, for example, a steel surface at 260°F
exposed to a flue gas with a bulk gas phase concentration of
10 ppm sulfuric acid vapor and 10% water vapor. A condensate
strength of 77% H_2SO_4 would be expected, and if fly ash neutral-
izing ability is ignored, some non-zero rate of corrosion would
be expected. If the same steel surface were exposed to a similar
flue gas with 80 ppm sulfuric acid vapor, the predicted conden-
sate strength would remain at 77% H_2SO_4, but the corrosion rate
would be greater because of the increased quantity of acid conden-
sate depositing on the metal. In both cases, decreasing the metal
surface temperatures to a value approaching the water dew point
(100 to 110°F) of the flue gas would result in increased corrosion
rates because of the highly corrosive dilute acid formed at these
temperatures.
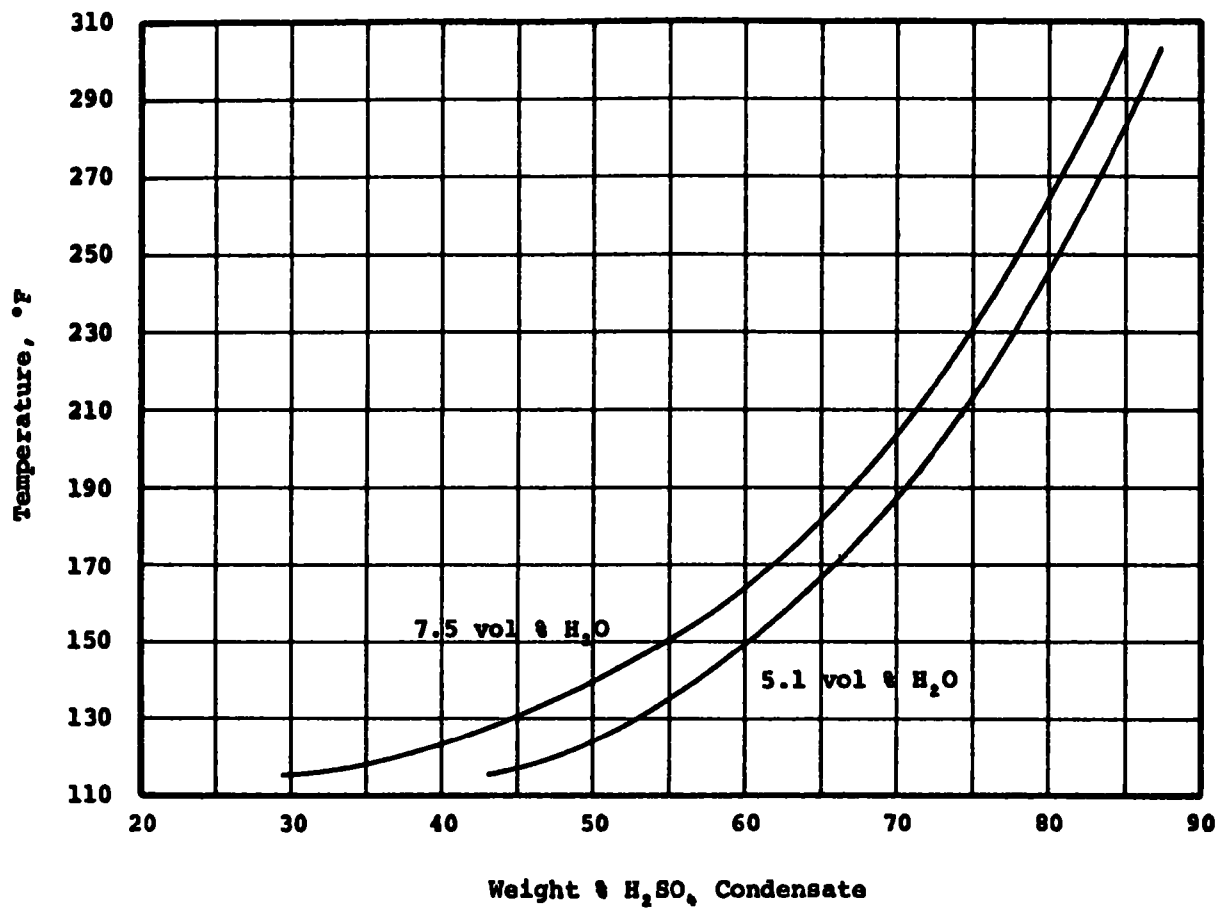
Figure 6.8. Equilibrium Sulfuric Acid Condensate
Composition
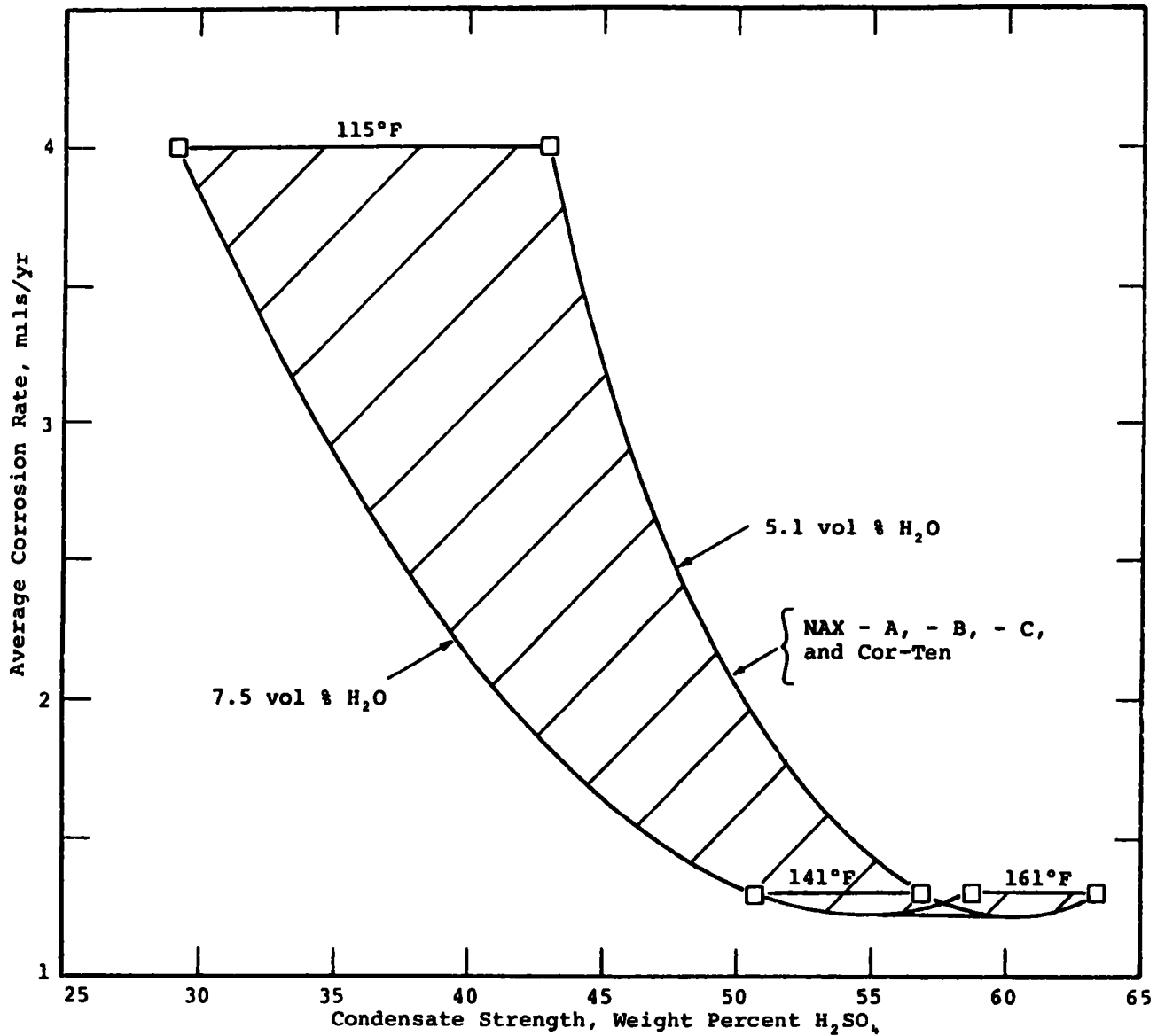
Figure 6.9. Corrosion of Steel in Flue Gas as a Function of Calculated H_2SO_4 Condensate Strength (Corrosion Data from Piper and Van Vliet; H_2SO_4 Data from Greenewalt)
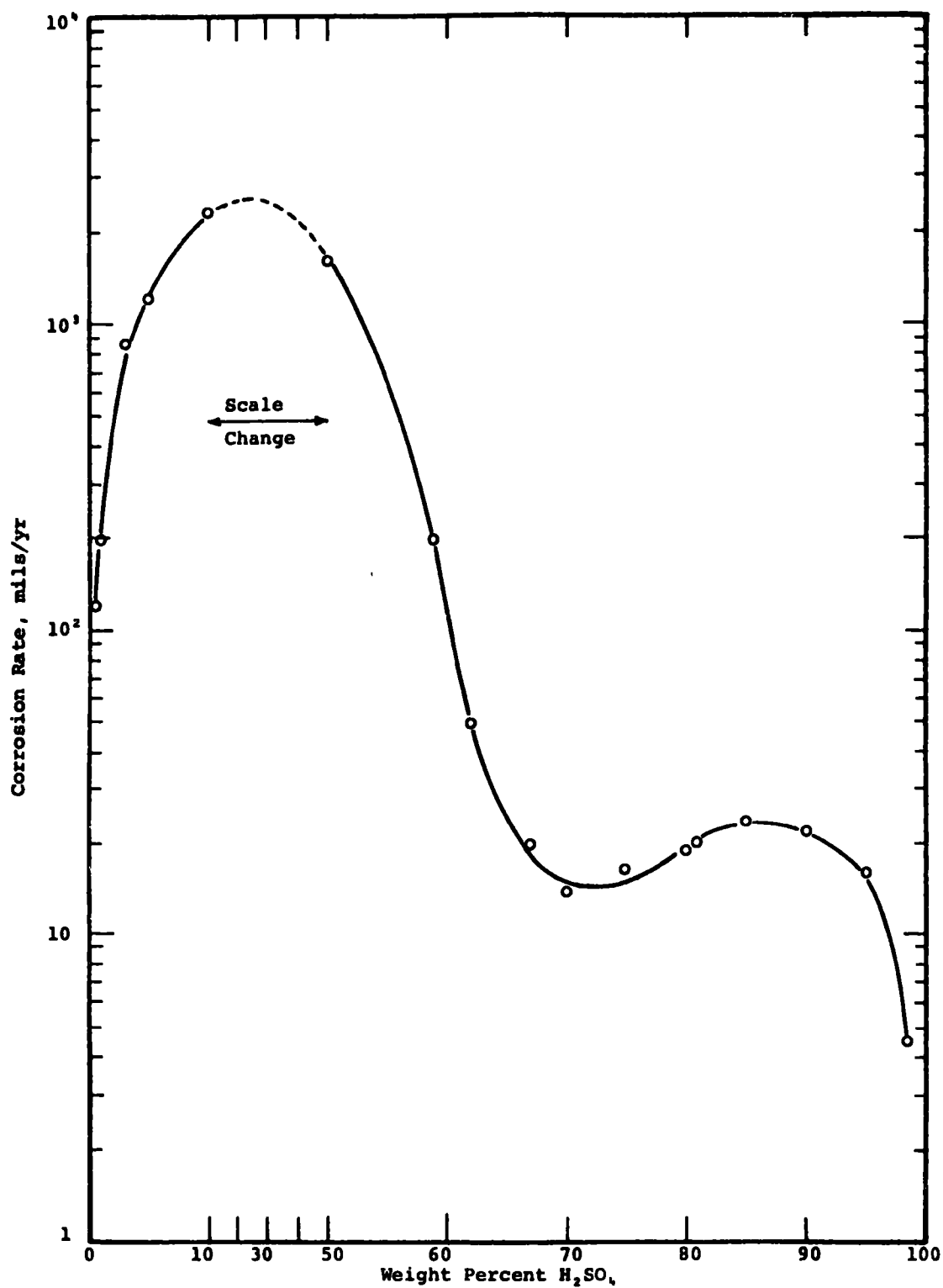
Figure 6.10. Corrosion of Steel as a Function of
H_2SO_4 Concentration at 75°F

The temperature at which the maximum condensation rate of acid occurs has been correlated with the temperature of maximum corrosion in flue gases. Figure 6.11 was taken from a study by G. G. Thurlow, in which an air-cooled corrosion probe was exposed to flue gas produced from burning a 0.8% sulfur coal.[25] The rate of sulfate deposition shows a peak at the same surface temperature as the corrosion rate. This peak rate effect is often not observed with coal firing, but Black[18] and Clark[19] have found this phenomenon quite useful in correlating corrosion of air preheaters in oil fired units. The sulfur content of the fuel used in these studies ranged from 1.4 to 4.0%.

Black and Clark's work was done with the BCURA dew point meter, and the peak rate of acid deposition was indicated by a peak rate of increase in current, measured as microamps per minute. The maximum corrosion rate is expected to occur in a regenerative air preheater at the point where the average metal temperature corresponds to the peak rate temperature indicated by the BCURA meter. By superimposing a plot of the dew point meter readings in the region of the peak over lines of average metal temperature, it was possible to match the peak rate temperatures with actual corrosion experience.

The above authors also found that the BCURA indication of the acid dew point was a poor indicator of flue gas corrosion potential, particularly when oil and gas mixtures are fired. This observation is not surprising since, as Figure 6.3 indicates, the dew point alone does not specify how much acid is available for condensation. The accuracy of the dew point meter may also be an important factor, because instructions for use of the meter state[26] that changes in dew point readings of less than 20°F are not to be regarded as significant. Referring again to Figure 6.3, a change of dew point at 10% water vapor from 270 to 290°F indicates a 370% increase in the H_2SO_4 vapor content of the flue gas.

Studies conducted by Lee, Freidrich and Mitchell,[16] in which the BCURA meter was employed with flue gas produced from burning low sulfur lignite, showed that the meter was unable to detect acid dew points with low sulfur coals. In one experiment, no acid dew point was detected by the meter in the presence of sulfuric acid vapor levels as high as 27 ppm. The author's explanation for this is that the condensed acid was completely neutralized by basic constituents in the fly ash.

Thus, since high fly ash resistivity is associated with low sulfuric acid vapor concentrations, the BCURA meter is not likely to be of value in assessing the low corrosion potential associated with a flue gas containing high resistivity fly ash.
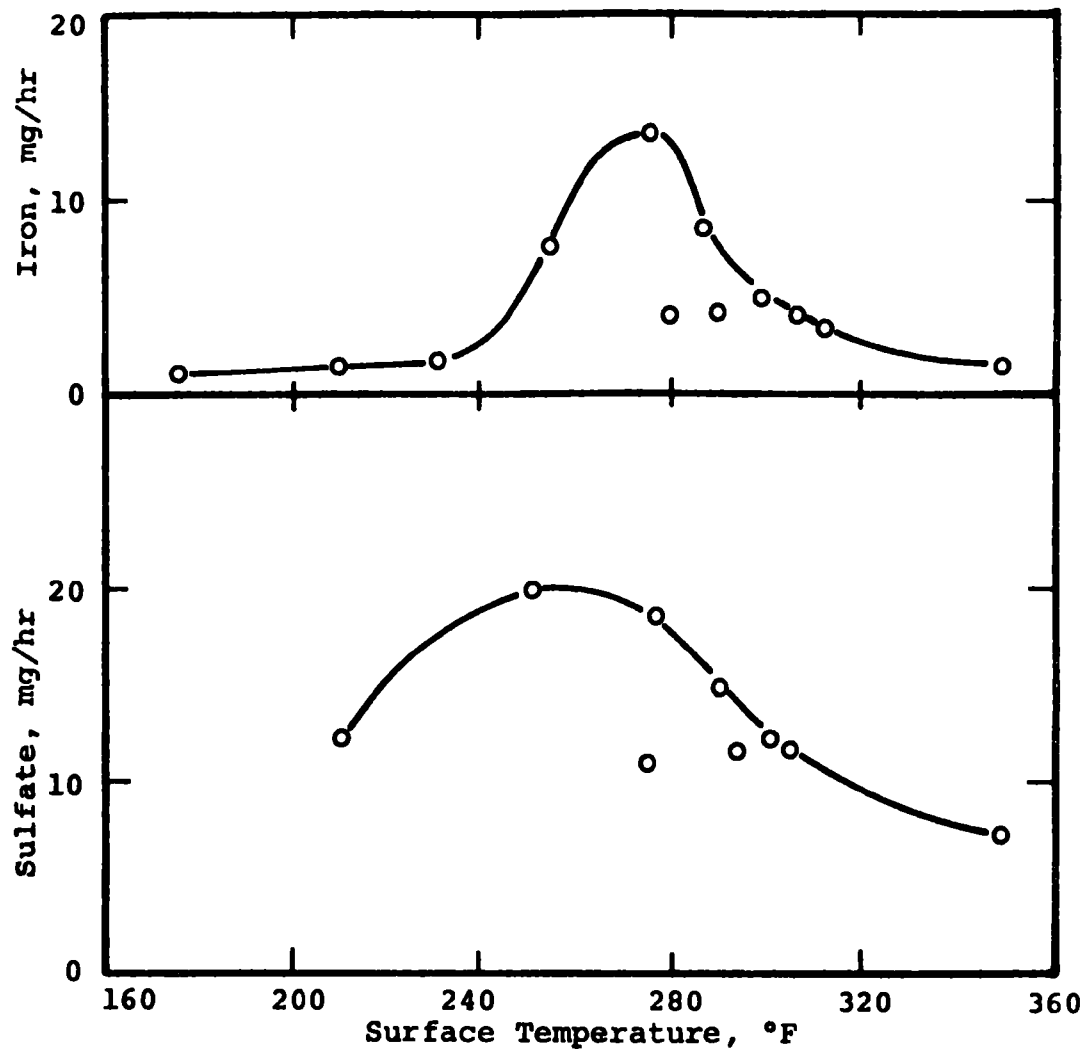
Figure 6.11. Variation of Condensation and Corrosion with Surface Temperature (Data from Thurlow)

3. **Fly ash alkalinity**

Although fly ash can cause severe plugging problems in air-heaters, it is well established that alkaline ashes can neutralize a portion of the SO_3 and H_2SO_4 occurring in stack gases, thereby acting to reduce corrosion. Lee provides data which illustrate the interaction of acid condensate with fly ash. Figure 6.12 illustrates the effect of surface temperature on acid condensation rate when burning a 7% sulfur coal with 3% excess oxygen. The RBU plotted on the y axis in the upper graph is a measure of the rate of acid condensation when the BCURA dew point meter is maintained at the indicated temperatures. Data for the lower graph were obtained by isokinetically sampling the flue gas and collecting the fly ash and acid condensate in a Teflon vial maintained at 180, 212, 245, and 275°F. The contents of the vial were then extracted, and the extract was analyzed for acid or base content. If the extract pH was less than 7, the solution was titrated with sodium hydroxide, and the results were reported as a negative cation content. If the extract was basic, the solution was titrated with HCl, and the results were reported as an excess cation content, indicating that the condensed sulfuric acid had been completely neutralized.

The acid neutralizing ability of fly ash with various base contents is illustrated in Figure 6.13 for a flue gas with a typical dust loading of 5 gr/scf. The parallel lines each represent a base content of fly ash, expressed as milliequivalents reactive base per gram fly ash. Data obtained on Contract CPA 70-149 (A Study of Resistivity and Conditioning of Fly Ash) indicate that fly ash produced from burning a high sulfur coal has as much as 0.6 milliequivalents soluble base (1.7% CaO) per gram fly ash.[27] This quantity of base is capable of neutralizing 80 ppm H_2SO_4 in the gas phase, assuming that the flue gas has an ash concentration of 5 gr/ft^3. This is not to say that complete neutralization will occur, since the degree of neutralization obtained in the flue gas is a function of the rate of transfer of H_2SO_4 to the fly ash particles and the rate of reaction occurring on the particle surface.

4. **Hydrochloric acid**

Sulfur, chlorine, and alkali metal compounds are associated with high temperature corrosion in coal-fired boilers, but low temperature corrosion is usually thought of only in terms of sulfuric acid. However, metals with surface temperature below the moisture dew point would be subjected to HCl attack if the chlorine
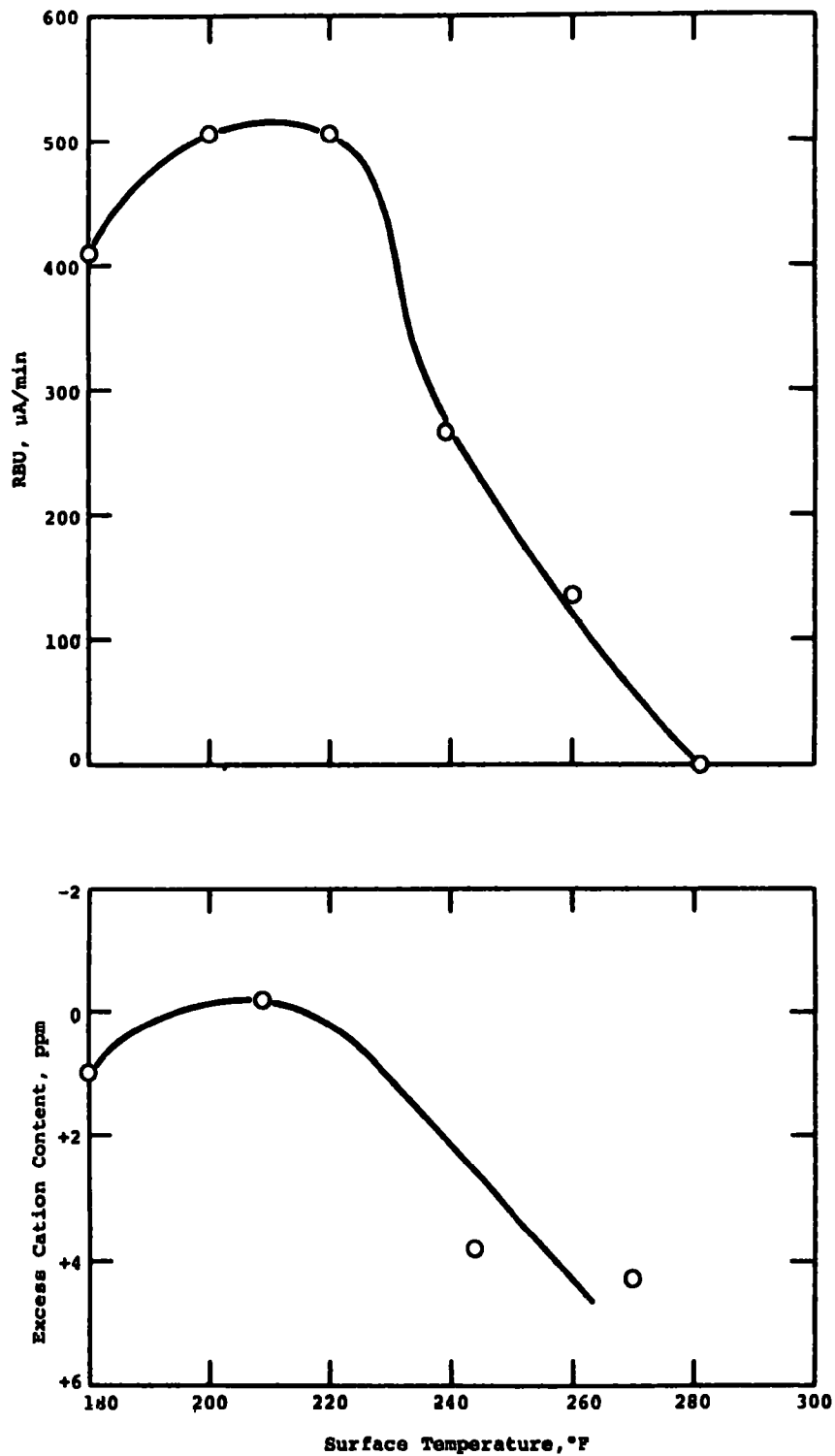
Figure 6.12. Variation in Rate of Acid Buildup
(RBU) and Excess Cation Content of
Fly Ash as a Function of Surface
Temperature. Coal Contains 7% Sulfur
with 3% Excess O_2 (Data from Lee)
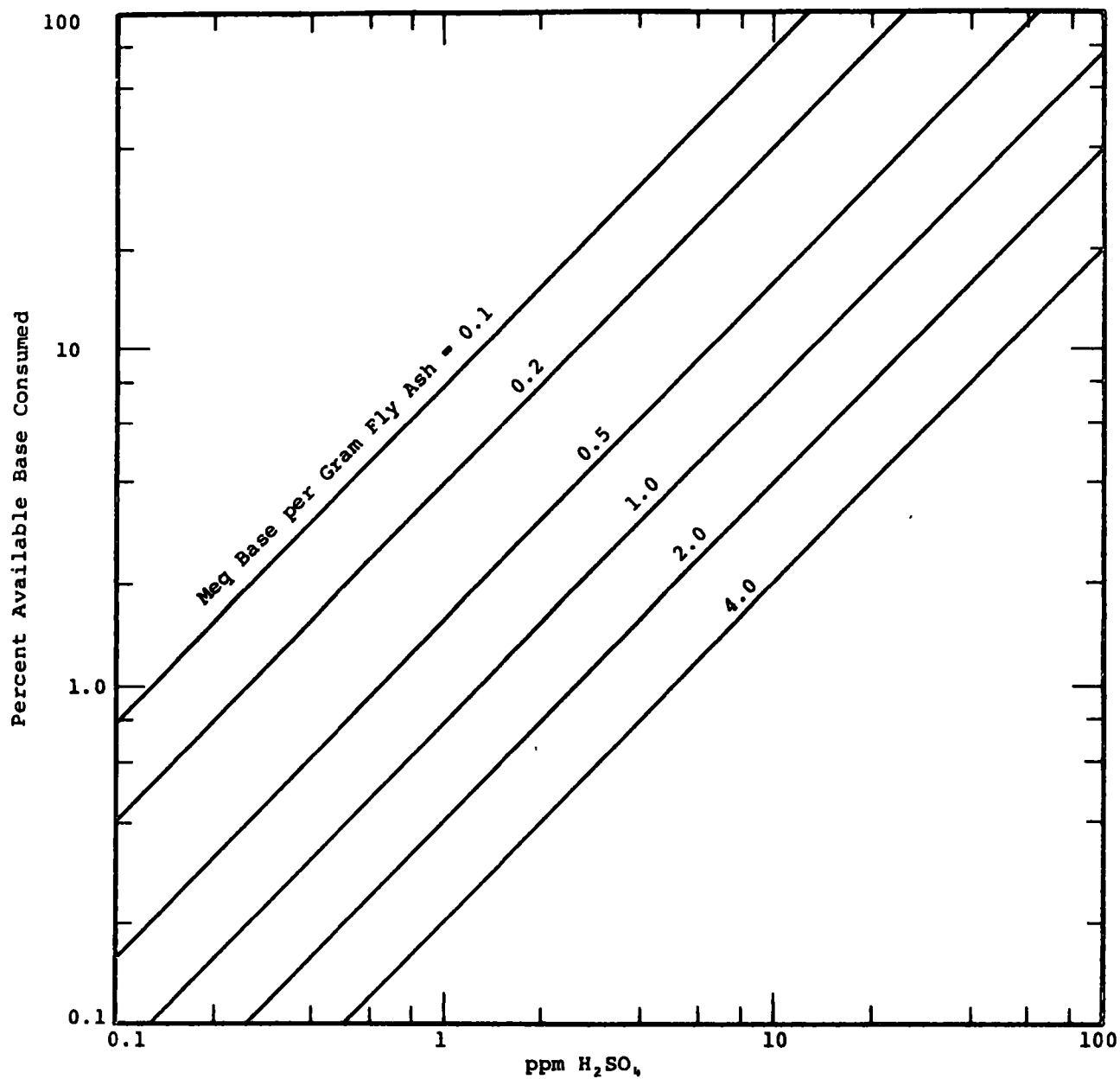
Figure 6.13. Consumption of the Available Base on Fly Ash as a Function of the Concentration of Neutralizing Acid in Flue Gas with 5 gr/scf Fly Ash

content of the coal is converted to HCl. Although not all of the chlorine in coal appears as NaCl, it is of interest to examine the chemical reactions undergone by NaCl in the combustion process. The following discussion is taken from a study by Halstead[28] in which chloride and sulfate deposit formations were examined with probe tests and by thermodynamic calculations.

In pulverized coal firing, the NaCl can be expected to evaporate and undergo some degree of vapor phase hydrolysis.

$$NaCl(g) + H_2O(g) = NaOH(g) + HCl(g)$$

The reactions of the chloride and NaOH with SO_2 to form Na_2SO_4 are, however, of greater importance. They are

$$2NaCl(g) + H_2O(g) + SO_2(g) + \tfrac{1}{2}O_2(g) = Na_2SO_4(g) + 2HCl(g)$$

$$2NaOH(g) + SO_2(g) + \tfrac{1}{2}O_2(g) = Na_2SO_4(g) + H_2O(g)$$
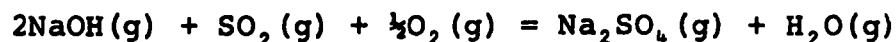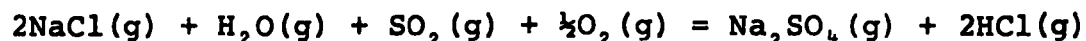
Halstead calculated the equilibrium partial pressures of Na_2SO_4 and NaCl in flue gases produced from burning the coals listed in Table 6.2 at 5% O_2 excess, stoichiometric O_2, and 2% O_2 deficient. These calculations, together with deposition studies conducted with a cooled probe, indicate that almost total conversion of NaCl to Na_2SO_4 takes place with 3 to 5% excess oxygen in large boilers with good mixing of fuel and air. With lower oxygen levels, and when poor mixing and short residence times are encountered, the conversion of NaCl to Na_2SO_4 may be incomplete.

Table 6.2. Sulfur and Chlorine Concentrations
in Flue Gas (from Halstead[16])

Sulfur in coal %	Chlorine in coal %	Sulfur compounds[a] in flue gas vol ppm	Chlorine compounds[a] in flue gas vol ppm
0.8	0.8	750	680
1.2	0.4	1100	340
1.8	0.07	1700	60

a. Calculated by assuming complete volatization of all sulfur and chlorine in coal and one atom of sulfur or chlorine present in each gas molecule.

Thus, it can be seen that significant concentrations of HCl are likely to result from the combustion of chlorine-containing coal. The subject of HCl corrosion in flue gases has received comparatively little attention in the literature because it is not likely to occur unless temperatures near the water dew point are encountered. Air preheater elements, however, can drop below the moisture dew point if excessive water vapor, such as would occur from a steam leak, is present.

Figure 6.14, taken from a study by R. W. Kear,[29] illustrates the effect of HCl in a flue gas on corrosion of a test probe. This experiment was conducted using an apparatus which produced a synthetic flue gas by addition of SO_2 and Cl_2 to the fuel supply of a small laboratory burner. Analysis of the flue gas indicated that all chlorine was converted to HCl, resulting in 400 ppm HCl by volume. It should be noted, however, that corrosion could be caused by the presence of chlorine gas. The assumption that Figure 6.14 is an illustration of the effect of HCl gas is therefore dependent upon Kear's conclusion that all chlorine is converted to HCl in the burner flame. The SO_3, or H_2SO_4, content of this gas was reported as 36 ppm. The temperature at which the corrosion rate accelerates corresponds to the water dew point of the synthetic flue gas, which is about 7% by volume water vapor. When the metal surface temperature is above the water dew point, the presence of HCl has no effect on corrosion, but it can be seen from Figure 6.14 that drastic increases in corrosion occur due to HCl as the metal surface falls below the water dew point. The corrosion probe was exposed for a 30-minute period in each experiment.

Data obtained by Piper and Van Vliet[23] confirm Kear's results. Piper's data were obtained by exposing metal condensers, which could be cooled to selected temperatures, to flue gas produced from burning a 0.066% chloride coal. Analysis of the flue gas showed that HCl concentrations ranged from 16 to 82 ppm, and the sulfuric acid vapor concentration averaged 30 ppm. The relative rates of corrosion of low alloy steel specimens maintained at 161, 141, 115, and 87°F for 2-month exposures were 1, 1, 3, and 66, respectively. The water dew point of the flue gas during the exposure period ranged from 91 to 104°F. It is thus apparent that the rate of attack greatly accelerated below the water dew point. This corrosion is a result of both H_2SO_4 and HCl, but the importance of the effect of HCl is indicated by the fact that at the water dew point, the chemical equivalents of chloride exceeded those of sulphate. Another important observation of the Piper study was that a vitreous enamel coating on Cor-Ten, which was used in a pilot-plant air preheater, was considerably attacked at temperatures below the water dew point.
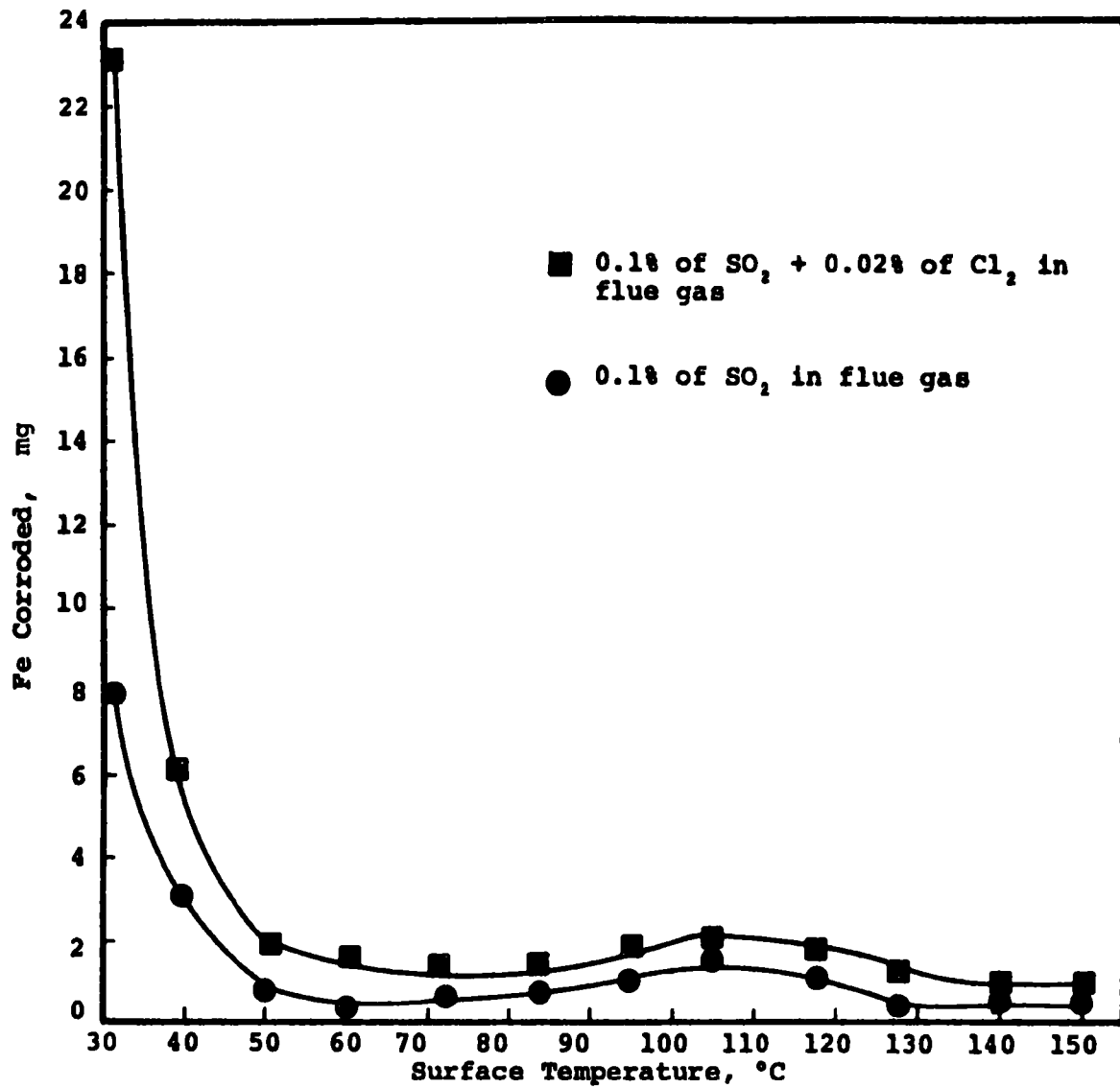
Figure 6.14. The Effect of Chlorine Addition on Corrosion of Mild Steel in a Synthetic Flue Gas (from R. W. Kear)

Since high resistivity fly ash usually occurs in the absence of sulfuric acid vapor, it is of interest to consider such a situation in which appreciable concentrations of HCl exist. Piper analyzed the vapor-liquid equilibria data for the system HCl-H_2O, and concluded that, with an HCl vapor concentration of 82 ppm, the hydrochloric acid dew point would be 7°F above the water dew point. A similar analysis of the water-SO_2 system indicated that the sulfurous acid dew point, for a stack gas with about 1900 ppm SO_2 and typical water vapor concentrations, would be the same as the water dew point.

D. Fouling of Low Temperature Surfaces

Deposit formation, or fouling, in air heater elements is a combination of chemical and physical processes. At 600 to 700°F, which is the range of temperature normally encountered at the hot end of regenerative air heaters, the saturation partial pressure of the mineral components of fly ash is extremely low. Thus deposit formation in this region is not a result of condensation from the vapor phase, but is instead a mechanical process in which slag and refractory material are carried by the flue gas into the air heater elements. These particles can lodge within the passages of hot end elements and thereby accumulate additional deposits of finer dust particles.[30] Procedures are reported in the literature for removing such deposits.

If the flue gas contains appreciable amounts of H_2SO_4, corrosion and deposit buildup will occur simultaneously in the cooler regions of the air heater.[31] The following reaction will occur on steel surfaces which are below the H_2SO_4 dew point.

$$Fe + H_2SO_4 \rightarrow FeSO_4 + H_2$$

The ferrous sulfate can then oxidize to form ferric sulfate.

$$4FeSO_4 + 2H_2SO_4 + O_2 \rightarrow 2Fe_2(SO_4)_3 + 2H_2O$$
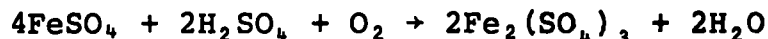
An extensive study of regenerative air heater deposits by the Bureau of Mines[32] found that deposits built up in thickness at the cold end of the air heater, and that this area was the principal region of corrosion and destruction of the element. All deposits found in this area exhibited the following characteristics: partial solubility in water, presence of sulfates, and acidity. The solubilities in water of these deposits varied over a wide range——13 to 98%. Deposits with highest solubities were found on preheater test plates which were most severely

attacked by acid. Some of the variations in deposit solubility were attributed to variations in the ability of the deposits to trap fly ash.

Reaction of the ferrous and ferric salts formed during corrosion with alkaline compounds sometimes used in washing air heaters can produce compounds that will result in additional fouling. Ferric sulfate, for example, can undergo the following reactions.[31]

$$Fe_2(SO_4)_3 + 3Ca(OH)_2 \text{ (lime)} \rightarrow 2Fe(OH)_3 + 3CaSO_4$$

$$Fe_2(SO_4)_3 + 6NaOH \rightarrow 2Fe(OH)_3 + 3Na_2SO_4$$

$$Fe_2(SO_4)_3 + 3Na_2CO_3 \text{(soda ash)} + 3H_2O \rightarrow 2Fe(OH)_3 + 3Na_2SO_4$$
$$+ 3CO_2$$
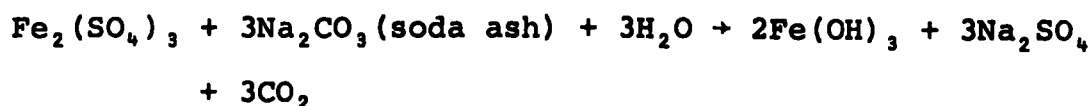
The $Fe(OH)_3$ (ferric hydroxide) is undesirable because it is a sticky, gelatinous precipitate which can cause severe fouling. The above reactions indicate that, in washing air heater elements or tubes, removing the soluble sulfates with a neutral water wash is desirable prior to a caustic wash.

It is important to note that deposit formation can occur in air heater elements in the absence of significant amounts of H_2SO_4. Chemical analysis of deposits from air heaters installed in some lignite-burning power stations has revealed no chemical evidence for deposition.[33] In one instance, moisture from steam cleaning action was found to be responsible for trapping ash deposits. Deposits formed in this manner are similar to cement and very difficult to remove.

In the absence of moisture and acid condensate problems, the nature of the fouling mechanisms discussed herein suggests that lowered cold end temperature would not result in increased deposit formation.

E.   Laboratory Corrosion Studies

Samples of fly ash were obtained for corrosion studies from the precipitator hoppers of two plants with high dust resistivity problems. These ash samples have widely different soluble base contents, as can be seen from Table 6.3. Sulfur contents of the coal burned in the two plants range from 0.6 to 1.0%. Laboratory experiments were conducted to determine whether deposited layers of these ashes exhibit differing capabilities for neutralizing

Table 6.3. Fly Ash Properties

	pH of suspension	Soluble sulfate wt %	Soluble base as CaO		Mass median particle diameter, μ
			meq/g	wt %	
Neutral (from Plant 1)					
As received	6.70	0.31	0	0	38
Following experiment (Experiment 4, Table 6.4)	1.69	23.4	0	0	–
Basic (from Plant 6)					
As received	12.25	1.2	2.7	7.6	18
Following experiment (Experiment 3, Table 6.4)	8.72	23.1	Not determined		–

acid and inhibiting corrosion.

A schematic diagram of the apparatus used for the experiments is given in Figure 6.15, and data obtained are presented in Tables 6.3 and 6.4. The corrosion specimen was a 1 in. diameter mild steel disc, and the amount of corrosion occurring as a result of exposure to H_2SO_4 was determined by measuring the weight loss.

The experiments in Table 6.4 can be divided into two groups. In Experiments 1 through 4, the acid condensation rate on the disc was relatively low, but high condensation rates were achieved in Experiments 5 through 10 by increasing the strength of oleum used as an SO_3 vapor source and by lowering the temperature of the water bath. Water vapor concentrations of 2 - 2.5% by volume were provided by the water spargers. Since the air streams bearing H_2O and SO_3 vapor mix in the heated glass "T," a saturated mixture of air and H_2SO_4 is formed, and the condensation rate will depend on the temperature of the condensing surface and the concentration of H_2SO_4 in the gas phase. For both sets of experimental conditions, an examination of the corrosion rates (meq basis) and acid deposition rates in Table 6.4 shows that an excess of acid was present with respect to the amount of iron corroded in all experiments.

For the experiments with fly ash, the ash was deposited in the sample container in such a manner that the disc was covered to a thickness of approximately 0.2 mm. Acid did not sufficiently penetrate the ash to reach the underside of the disc in Experiments 3 and 4, and the penetration rates were calculated on the basis of one side only. Corrosion was observed on both sides in all other experiments; therefore, the total area of both disc surfaces was used as a basis of calculation.

A comparison of data from Experiment 3 with those from Experiment 4 indicates that the basic fly ash was more effective in reducing corrosion than the neutral ash. The equilibrium pH values of the ash samples prior to and following these experiments are given in Table 6.3. As would be expected, the neutral ash slurry is much more acidic than that of the basic ash after both have experienced an equivalent sulfate gain due to H_2SO_4 condensation. The fact that the basic ash produced a pH greater than 7 following the experiment shows that it was capable of neutralizing all of the condensed acid. Complete neutralization did not occur until the acid-ash mixture was slurried in water, however, as evidenced by the measurable degree of corrosion which occurred in Experiment 3.
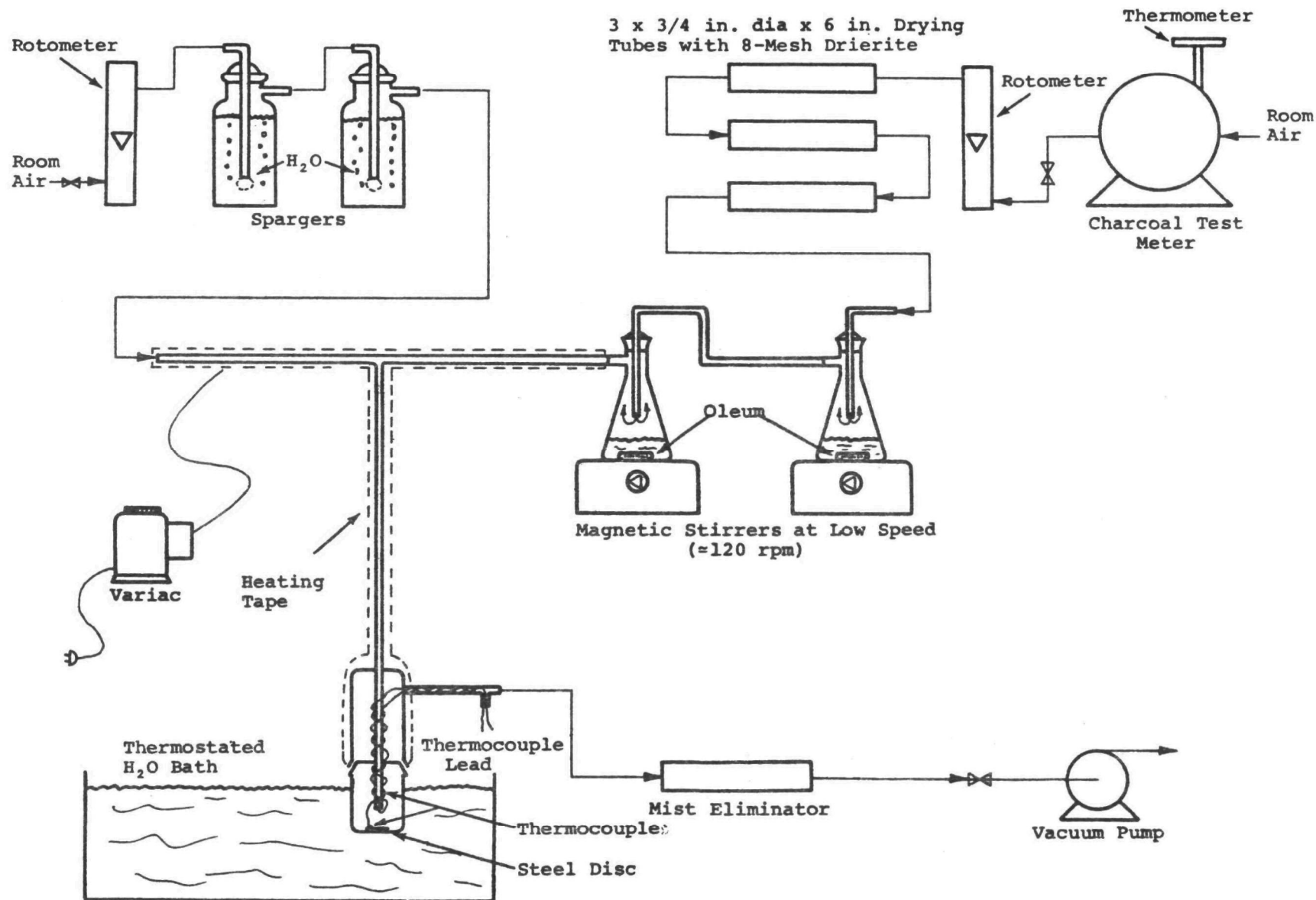
Figure 6.15. Schematic Diagram of Apparatus Used in Corrosion Experiments

Table 6.4. Corrosion Rate Experiments

Experiment No.	H_2SO_4 vapor generator, % Acid used	Duration hr	Condensate composition wt % H_2SO_4	Temperature, °F			H_2SO_4 Condensate rate meq/hr	Apparent corrosion rate			Ash layer	H_2SO_4 Reacting with disc wt %
				gas	water bath	disc surface		mg/hr	meq/hr[b]	mils/yr		
1	104	2.0	56	383	78	--	--	1.05	0.056	46	None	--
2	104	1.9	52	379	84	--	1.3	0.90	0.048	39	None	3.7
3	104	2.1	—	388	79	—	1.5	0.20	0.011	17[a]	Basic	0.7
4	104	2.0	--	412	79	—	1.6	0.40	0.022	34[a]	Neutral	1.4
5	107	1.0	36	349	37	90	5.0	32	1.7	1400	None	34
6	107	1.0	40	374	39	77	6.0	32	1.7	1400	None	28
7	107	1.0	--	388	37	95	10.1	18	0.97	790	Basic	10
8	107	1.0	--	392	37	86	8.6	17	0.91	740	Basic	11
9	107	1.0	--	390	36	86	12.4	53	2.8	2300	Neutral	23
10	107	1.0	--	388	39	81	12.4	41	2.2	1800	Neutral	18

a. Based on exposure of one side of disc to acid rather than both sides as in all other runs.

b. Assuming formation of $Fe_2(SO_4)_3$.

-144-

For the experiments with low acid condensation rates, both the neutral and basic ash deposits reduced the weight loss rate of the disc, but the penetration rate calculated for Experiment 4 (neutral ash) is not significantly different from those of Experiments 1 and 2 (no ash). These results are to be expected, since the neutral character of the material from Plant 1 indicates that any corrosion inhibiting value which it exhibits is likely to be the result of physical rather than chemical factors.

High corrosion rates were obtained in Experiments 5 through 10 due to increased acid condensation rates and decreased condensate composition. The high percentage of H_2SO_4 reacting with the disc in these experiments is an indication of the greater corrosiveness of acid in the 36 - 40 wt % range. Some difficulty was encountered in maintaining constant experimental conditions, as indicated by variations in the disc surface temperatures and the acid condensation rates. Once again, the data suggest that the neutral ash has little corrosion inhibiting value, but significantly lower corrosion rates were obtained with the basic substance. In contrast to the conditions of Experiment 3, an excess of acid was present with respect to the base content of the ash layer for Experiments 7 and 8. If it is assumed that the same amount of base reacts per unit weight of basic ash in both sets of experiments, it can be shown that less than 30% of the condensing acid could have been neutralized in Experiments 7 and 8. The principal mechanism by which corrosion rates were reduced in Experiments 7 and 8 appeared to be the formation of a cement-like deposit which reduced the amount of acid reaching the metal surface. Such deposits would be likely to cause plugging of air heater elements in plant operation.

Generalizations concerning the direct effect of basic and neutral fly ashes on corrosion rates from these experiments are hazardous because of the complex nature of the corrosion process. However, it is possible to draw some conclusions regarding the interaction of the fly ash with condensing acid.

The reduced corrosion rate obtained in Experiment 3 indicates that the basic fly ash from Plant 6 neutralized a major portion of the acid as it condensed. This is an important observation because data obtained under Contract CPA 70-149 has revealed the presence of unreacted acid on the surface of fly ash containing amounts of water soluble base substantially in excess of the apparent surface acidity. Thus, basic ash deposited on metal surfaces could conceivably present an acidic, and hence corrosive, environment to a metal surface and exhibit little or no neutralizing capability. A layer of $CaSO_4$, formed by reaction

between H_2SO_4 and CaO, apparently can prevent the underlying soluble base from being utilized. The ash from Plant 6 contained appreciable sulfate when received from the precipitator hoppers (1.2%), but the experimental data presented here indicate that the sulfate did not present an impermeable barrier to the liquid condensate.

The neutral ash from Plant 1 would not be expected to provide a significant degree of protection from condensing acid, and the experimental data tend to confirm this. However, even a neutral ash can reduce the amount of acid available for corrosion in a flue gas by adsorbing SO_3. The small amount of sulfate (0.31%) present on the ash from Plant 1 when received indicates that some adsorption of SO_3 at high temperatures occurred. The operating temperature of the precipitator at Plant 1 is about 320°F, which is well above the H_2SO_4 dew point.

In conclusion, then, the data from these experiments indicate that a basic ash such as that from Plant 6 can be of significant value in neutralizing condensed acid and reducing air heater corrosion rates. However, in the presence of an excess of condensing acid, serious deposit formation problems could be expected. The neutral ash was of little or no apparent value in reducing corrosion rates, but it exhibited a lesser tendency to form cement-like deposits than did the basic material. The most important benefit to be expected from the presence of a basic fly ash from the standpoint of corrosion is the consumption of SO_3 by the basic material in the high temperature region prior to the air heater. Unfortunately, this also creates a high resistivity problem for precipitators operating in the 300°F range.

F.   Summary of Field Experience

1.   Discussion with Air Preheater Company

A conference with Mr. Norman D. Clark, Manager of Technical Services of the Air Preheater Company, was held concerning low temperature corrosion and fouling problems. Mr. Clark has authored a number of papers concerning corrosion of regenerative air heaters in various types of service.

The Air Preheater Company is of the opinion that low temperature air heater corrosion and fouling will not be a limiting factor in low temperature operation with low sulfur coals. No problems with corrosion have been reported from installations burning low sulfur coals, but fouling, caused principally by moisture from steam leaks or steam cleaning, can cause plugging

problems. Usually, no effort is made to maintain air heater element temperatures above the acid dew point due to the loss of boiler efficiency which this would involve, but the water dew point (~110°F) is to be avoided because of potential fouling and corrosion from acids other than sulfuric acid.

Typical air heater element lifetimes were given as follows.

- Gas firing - almost never replaced

- Coal firing - 3 to 5 years

- Oil firing - 2 to 3 years under normal conditions, but severe corrosion can cause destruction after only a few months of service.

2.   Plant data

Table 6.5 is a compilation of available data from a number of power plants concerning fly ash, flue gas and coal composition, and fly ash resistivity. The data reported in this table were either obtained by SRI personnel under Contracts CPA 70-149 and CPA 70-166 or made available to SRI by the utility companies.

Of all the plants listed in Table 6.5, only Plants 10 and 9 have experienced significant air heater corrosion problems. As the following discussion will indicate, the factors that result in high resistivity fly ash usually indicate that no corrosion problems are to be expected.

The ash samples for which analyses are given in Table 6.5 were either collected from the precipitator hoppers or obtained with a resistivity apparatus at the precipitator inlet. The values of pH and free acid obtained in a 95% ethanol slurry, which are given for selected samples, are an indication of acid present on the surface of the ash. Samples which show an acidic pH in 95% ethanol generally exhibit a minimum pH in water, followed by a rise to a basic equilibrium value as the water soluble base is dissolved. The presence of significant amounts of unreacted acid on the ash surface is thought to be an indication that the fly ash has been "conditioned" by sulfuric acid.

Data for SO_2 - SO_3 were obtained by SRI personnel using procedures described elsewhere.[27] Resistivity data were also obtained by SRI using either a point-plane or cyclone resistivity

Table 6.5. Properties of Flue Gas and Fly Ash for Various Coal-Fired Boilers

Plant designation	Coal analysis (dry basis) sulfur %	ash %	Fly ash analysis water slurry pH	sol base as CaO %	sol SO₄ %	ethanol slurry pH	free acid as H₂SO₄ %	Flue gas analysis precip. inlet (wet basis) SO₂ vol ppm	H₂SO₄ vapor vol ppm	H₂O vol %	Typical fly ash resistivity Ω-cm	temp °F
6	0.7–1.0	8.5	12.2	7.6	1.2	>9.1	0	--	--	10.7	1.9×10^{11} 1.0×10^{10}	302 220
1	0.6	12	8.2	Negligible	0.23	4.6	0.008	375	<1	7.7	1.9×10^{12}	320
2[a]	0.5	5.9	11.1	2.10	1.50	8.1	0	387	<1	8.9	3.8×10^{12}	275
11	0.5	15–25	11.2	1.50	0.17	--	--	--	--	--	4.5×10^{11}	230
8-3[a]	0.5	8.6	9.4	0.35	0.77	--	--	365	<1	7.7	1.0×10^{12}	309
5	0.95–1.90	15.8–16.0	9.4	0.19	0.41–0.47	--	--	610–1030	0.8–4.4	7.0	3×10^{11}–1.5×10^{12}	256–319
7[a]	2.1	21.9	5.1	0	0.36	--	--	1650	8.7	5.7	1.0×10^{12} 2.0×10^{11}	319 300
4	3.6	16.4	11.0	1.65	0.77	3.8	0.037	2680	15	8.0	1.0×10^{10}	287
9[a,b]	~3.5	~14	9.8	0.35	1.15	3.9	0.088	--	--	--	1.0×10^{9}	290
10[a,b]	3.2	11.2	6.4	0	0.40	4.4	0.02	--	--	--	--	--

a. Precipitator preceded by mechanical collector.

b. Corrosion of air heater has occurred.

apparatus, with the exceptions of Plants 6 and 11. For these two plants, the data were given to SRI by the operating utilities.

Plant 6 has successfully overcome a high dust resistivity problem by lowering the precipitator operating temperature to about 220°F at full load. An inspection of the low temperature zone of this installation was conducted while the unit was off the line for routine maintenance. This plant had nine months of operation with low gas temperatures.

The areas examined for evidence of corrosion were the cold and intermediate zones of the air heater elements, the plates and wires in the precipitator, and the sides of the duct encompassing the precipitator assembly. No evidence of corrosion was found in the air heater elements. Thin deposits were noted in some areas of the cold-end elements, but these were insufficient to cause measurable draft losses. Minor corrosion was observed on the perforated plate distributors at the precipitator inlet. The rusted areas corresponded to regions of low gas velocity caused by duct geometry. The only significant corrosion in the entire assembly was found on the under side of the top plate of the precipitator housing. The top side of this plate is exposed to streams of low temperature bleed air from the plant exterior, and it is probable that temperatures below the water dew point were reached. The purpose of the bleed air is to maintain a positive pressure for prevention of dust buildup on the rapper bushings.

We have no direct measurement of SO_3 at Plant 6, but measurements from Plant 2, which uses a similar fuel, show that SO_3 levels above and below the air heater are less than 1 ppm. The soluble sulfate content of fly ash taken from the precipitator hoppers of Plant 6, if a dust concentration of 1.5 gr/ft^3 is assumed, is equivalent to an SO_3 concentration of 10 ppm. It is possible, however, that a portion of the sulfate originated from oxidation of SO_2 on the ash surface rather than from SO_3 in the bulk gas phase. Figure 6.3 shows that the dew point of a flue gas with 10 ppm SO_3 and 10.7% water vapor is estimated as 275°F. The minimum cold end average temperature of the air heater at Plant 6 is 140°F. It is therefore probable that some acid condensation, and possibly corrosion, would have occurred if the basic ash had not been present to combine with the SO_3 in the high temperature zone prior to the air heater, thus preventing the formation of H_2SO_4 vapor in the air heater region. Furthermore, the data in Tables 6.3 and 6.4 and the lack of surface acidity indicated in Table 6.5 show that any H_2SO_4 which may form in the air heater region is likely to be neutralized.

In view of the known dependence of fly ash resistivity on temperature and the presence of H_2SO_4 on the fly ash surface, the hypothesis of negligible H_2SO_4 in the low temperature zone at Plant 6 may seem inconsistent with the decrease in resistivity with temperature which occurs at this installation. This apparent inconsistency can be qualitatively resolved by attributing the resistivity behavior to increasing adsorption of water vapor on the fly ash surface with decreasing temperature. It is also possible that oxidation of SO_2 to SO_3 occurs on the ash surface, and provides surface H_2SO_4 for conditioning for a brief time period, after which the acid is neutralized. The following reaction sequence may be used to represent this hypothesis.

$$SO_2(g) + \tfrac{1}{2}O_2(g) \rightarrow SO_3(g)$$

$$SO_3(g) + H_2O(g) \rightarrow H_2SO_4(g) \leftrightarrow H_2SO_4(l)$$

$$H_2SO_4(g \text{ or } l) + CaO(s) \rightarrow CaSO_4(s) + H_2O(g)$$
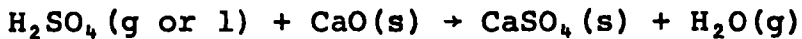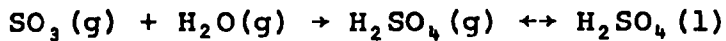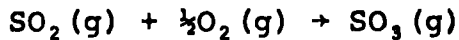
Thus, by adsorption of water and/or surface formation of SO_3, it is possible to explain the lowering of resistivity with decreasing temperature in the absence of appreciable SO_3 concentrations in the bulk gas phase.

Plant 11 and Plant 10 are the other plants listed in Table 6.5 with lowered cold-end temperatures. Plant 11 operates with a low sulfur coal which produced a highly basic fly ash with a high resistivity. No corrosion problems have been experienced at this installation, as would be expected. Precipitator inlet temperatures range from 230-253°F.

Plant 10 has operated with precipitator inlet temperatures from 228-246°F. Excessive deterioration of air heater cold end elements occurred when gas temperatures were lowered to 228°F, and as a result, operating temperature has now been raised to 243-246°F. The reason for lowering the exit temperature was said to be a desire to increase boiler efficiency rather than a need to lower fly ash resistivity. Fly ash and coal samples supplied to SRI were analyzed and are reported in Table 6.5. However, the sulfur content of the coal normally used was reported by the utility to be 1.2-1.35%. Analysis of the fly ash indicates a neutral ash similar to that from Plant 1, and little or no acid neutralizing ability would be expected. The low sulfate content indicates that, in spite of the high sulfur content of the coal and the relatively low temperature at which the ash was collected, a comparatively small amount of H_2SO_4 is collected by the ash. From the ash content of the coal, the grain loading at Plant 10 is estimated, prior to the mechanical collector, as 3 gr/scf,[34] and the sulfate content of the fly ash is equivalent to only 6.4 ppm H_2SO_4. It is therefore probable that most of the H_2SO_4

formed from the combustion of this relatively high sulfur coal remained in the gas phase and was available for condensation.

Although we have no resistivity measurements from Plant 10, it is possible to infer from the coal and fly ash analysis that a low resistivity fly ash (significantly less than 2×10^{10} Ω-cm) is probable at this installation at the precipitator operating temperatures. It has been shown from studies of H_2SO_4 conditioning under Contract CPA 70-149 at Plant 1 that a sulfate gain of only 0.1-0.2% due to adsorption or condensation of H_2SO_4 is sufficient to lower resistivity by two orders of magnitude for a neutral fly ash.

Plants 9 and 4 normally operate with a high sulfur coal, and typical air heater exit temperatures for both units range from 275-285°F. These plants have low fly ash resistivities at normal operating temperatures, and at times the resistivity value at Plant 4 has been too low for proper precipitator operation with high gas velocity. The cold-end portion of the air heaters at both of these installations operates below the acid dew point, but the corrosion experience has been somewhat different. Plant 4 has an average cold-end temperature of about 200°F, and Figure 6.3 shows that most of the H_2SO_4 vapor is available for condensation at this temperature. Furthermore, measurements of SO_3 before and after the air heater have indicated, on at least one occasion, a significant drop in SO_3 concentration across the heater. It is therefore probable that significant amounts of H_2SO_4 are condensed, either on the ash in the cool boundary layer adjacent to the metal surface, or on the metal surface itself. In spite of this fact, the cold-end baskets (made of low-alloy steel) have been in service for at least ten years at Plant 4 without requiring replacement. Table 6.5 shows that the fly ash at this unit is highly basic, and would be expected to have significant acid neutralizing ability. However, the presence of surface acidity, as indicated by data obtained in a 95% ethanol slurry, suggests that a sulfate layer on the ash is preventing a portion of the water soluble base from being utilized.

Plant 9 has required some replacement of cold-end air heater elements, but not at an excessive rate. The data in Table 6.5 indicates that the fly ash from Plant 9 is less basic than that from Plant 4, but the presence of a mechanical collector at Plant 9 makes a direct comparison of the two fly ash analyses difficult because of the difference in particle size distribution. It is, however, reasonable to conclude that without the presence of the basic fly ashes at both installations, corrosion would have been more severe.

Plant 7 operates at high air heater exit temperatures with an intermediate sulfur coal. The resistivity values indicated in Table 6.5 for this plant would be classified as high, but the near-neutral character of the ash, together with the presence of appreciable concentrations of H_2SO_4 vapor in the gas phase and the slope of the resistivity temperature curve, suggest that acceptable resistivity values would occur at about 280°F. With an 80°F inlet air side temperature, this would give a cold-end average of 180°F for the air heater. The Air Preheater Company's cold-end temperature and material selection guide gives a suggested minimum average cold-end temperature of about 160°F for a coal of 2.1% sulfur content and corrosion-resistant, low-alloy steel cold end elements.[35] Some degree of corrosion may occur because the cold-end metal temperatures fall appreciably below the acid dew point, and because the neutral ash at Plant 7 could be expected to have no significant acid neutralizing ability. However, the experience of the Air Preheater Company as represented by their materials and temperature guide, and the lack of excessive H_2SO_4 vapor concentrations found at 300-320°F are indications that a severe corrosion problem should not occur at Plant 7 with the presently used fuel if air heater exit temperatures as low as 280°F were employed.

The corrosion experience of Plant 5 (Unit 1) is of interest because the average air heater exit temperature is about 260°F. Sulfur content of the coal normally burned at this unit is approximately 1%, and a typical dust load would be 3.7 gr/scf. Coal composition varied during the time period in which resistivity data were taken, and possibly as a result, the resistivity data show considerable scatter and no strong variation with temperature. Nonetheless, the relatively high resistivity values are to be expected on the basis of the coal sulfur content and the moderately basic character of the fly ash. No corrosion problems have occurred at this unit, and none would be expected with the relatively low H_2SO_4 vapor concentrations which were measured.

Plants 8-3 and 2 are typical of installations burning very low sulfur coal; that is, no appreciable H_2SO_4 vapor concentrations are found in the bulk gas phase, the fly ash produces a basic water slurry, and the resistivity is unfavorably high in the normal operating temperature range of 275-300°F.

If the design of these plants were such that operation in the 220-240°F range were possible, no corrosion problems would be expected because of the absence of H_2SO_4 vapor. Unfortunately, there is not a sufficient quantitative knowledge of the relationship between resistivity and temperature to predict with confidence that

low temperature operation at these installations would produce resistivity below the critical value of 2×10^{10} Ω-cm. The fact that the flue gas water concentrations at Plants 2 and 8-3 are about 30% lower than that at Plant 6 is an unfavorable condition for achieving lowered resistivity. However, the fly ashes from Plants 2 and 8-3, and in particular, that from Plant 8-3, are less basic than the ash produced at Plant 6. Data obtained under Contract CPA 70-149 indicate that a highly basic ash requires a greater gain of H_2SO_4, either by condensation or adsorption, to lower resistivity than does a neutral ash. Thus, if lowering of resistivity is due to the combined effects of water adsorption and the formation of SO_3 on a fly ash surface discussed earlier, it could be argued that the resistivity of the extremely basic ash of Plant 6 would show less sensitivity to decreasing temperature than the fly ash at Plants 2 and 8-3. Since the variables of ash composition and flue gas water concentrations indicate opposing effects when comparing Plant 6 with Plants 2 and 8-3, it would be hazardous to equate the resistivity-temperature experience of Plant 6 with the other two installations.

G.   Methods of Assessing Corrosion Tendencies of Flue Gases

A comprehensive discussion of methods developed in England for assessing the corrosion and fouling potential of flue gases is given in a bulletin entitled, "Testing Techniques for Determining the Corrosive and Fouling Tendencies of Boiler Flue Gases" published by the Boiler Availability Committee.[26] The following discussion is a brief summary of the purpose and method of operation of those procedures which relate to low temperature corrosion and fouling.

1.   Corrosion probes

The purpose of corrosion probes is to measure the amount of corrosion produced by acid condensed on metal surfaces in a flue gas environment. These probes provide a means of supporting a prepared metal test specimen in flue gas streams at a selected temperature. The BCURA probe is an air-cooled device in which the surface temperature of the test specimen is monitored with a thermocouple brazed to the body of the probe. Exposure periods of 15-30 minutes are recommended, and the amount of corrosion is determined by measuring weight loss of the specimen.

Probes designed for short term experiments are of value for comparing relative effects of variations in operating parameters, such as temperature and fuel composition. However, for

prediction of actual corrosion rates over extended periods, long term tests of 100 hours or more are desirable. A liquid-cooled probe has been designed by the Shell Petroleum Company, Ltd., for such extended experiments.[36]

2. Acid deposition probes

An indirect measurement of the rate of acid deposition on a cooled surface is given by the BCURA dew point meter, which has been described previously. Since the conductivity readings of the dew point meter can be influenced by substances other than sulfuric acid, it is of interest to consider a direct means of measuring acid deposition rates.

Alexander[37] has described an air-cooled deposition probe which accomplishes this purpose. The probe consists of an air-cooled, one-inch diameter stainless steel tube in which the cooling air passes through the tube and discharges into the flue gas. The amount of acid depositing on test areas of the probe, the surface temperature of which is known, is determined by analysis of deposits obtained from the test surfaces.

3. Gas and ash analysis

An analysis of flue gas for SO_3, SO_2, H_2O, and dust loading, along with analysis of the fly ash for soluble components, is necessary for a qualitative assessment of the flue gas corrosion potential. Procedures used by SRI for these analyses are described in the final report from Contract CPA 70-149.[27]

H. Summary and Conclusions

It has been established that the principal cause of corrosion in the low temperature zone of power plant exhaust systems is condensation of sulfuric acid, either directly onto metal surfaces or onto fly ash particles which subsequently come in contact with the metal. Other acids, in particular hydrochloric acid, can be responsible for corrosion at temperatures approaching the water dew point of flue gas, but such temperatures are not normally encountered.

Fouling in the low temperature zone of air heaters is primarily caused by reaction of sulfuric acid with fly ash and the metal surfaces of the heat exchanger. A basic fly ash can neutralize appreciable quantities of SO_3 upstream from the air heater region, but laboratory experiments suggest that reaction of highly basic fly ashes with high concentrations of H_2SO_4 in the low

temperature zone can result in problems with deposit formation.
This conclusion is supported by the experience of the Central
Electricity Generating Broad of England, in which medium sulfur
coals with alkaline ashes have produced fouling,[38] but little
air heater wastage accompanied the deposit formation. It is also
possible to have deposit formation in the low temperature zone
in the absence of sulfuric acid if excessive moisture from steam
leaks or soot blowing is present.

Severe corrosion and fouling problems in regenerative air
heaters are associated with the temperature at which peak rates
in acid deposition occur. These peak rates often are not observed
with coal firing due to the presence of fly ash, but in any case,
the existence of such a peak is a manifestation of relatively
high concentrations of free H_2SO_4 vapor. Thus, the resistivity
of fly ash, due to the presence of excessive H_2SO_4, would be
expected to be lower than desirable for proper precipitator oper-
ation with high gas velocity under these conditions. Resistivity
data taken at plants burning high sulfur coals with alkaline fly
ashes have demonstrated that resistivity values below the critical
2×10^{-6} Ω-cm are obtained at temperatures above 280°F. Therefore,
lowering precipitator operating temperatures is neither necessary
nor desirable for the case of high sulfur coals, which produce
relatively high concentrations of H_2SO_4 vapor.

An analysis of the factors which cause corrosion, and the
operating experience of at least two power plants, has demonstrated
that low temperature operation of precipitators (220-250°F) will
not cause low temperature corrosion and fouling problems with a
flue gas containing a basic fly ash and no appreciable concen-
trations of sulfuric acid vapor. The occurrence of corrosion and
high fly ash resistivity thus tend to be mutually exclusive phe-
nomena. A possible exception to the rule would be a stack gas with
high (over 100 ppm) HCl concentration.

For the case of a plant burning a low to medium sulfur
coal which produces a near-neutral, high resistivity ash at
approximately 300°F and low concentrations of H_2SO_4 vapor, the
occurrence of some degree of corrosion as a result of lowered
cold-end temperatures cannot be rigorously excluded. However,
data obtained under Contract CPA 70-149 have shown that amounts
of sulfuric acid sufficient to "condition" a neutral ash can be
adsorbed at temperatures well above the sulfuric acid dew point.
It is therefore probable that an acceptable fly ash resistivity
could be obtained at a temperature sufficiently high to avoid
appreciable condensation of sulfuric acid on the cold-end elements
of an air preheater. A quantitative evaluation of resistivity

and corrosion under such circumstances would require fly ash resistivity data and relative corrosion rates (obtained with a corrosion probe such as described in Section G) as a function of temperature in the flue gas.

I.   Bibliography — Section 6

1.   Hedley, A. B., in The Mechanism of Corrosion by Fuel
      Impurities (H. R. Johnson & D. L. Littler, editors),
      Butterworth, London, p 204 (1963).

2.   Cuffe, S. T., Gerstle, R. W., Orning, A. A., and
      Schwartz, C. H., J. Air Poll. Control Assoc. 14, p 353
      (1964).

3.   Snowden, P. N., and Ryan, M. H., "Sulfuric Acid Condensation
      from Flue Gases Containing Sulfur Oxides," J. Inst. Fuel 42,
      p 188 (1969).

4.   Mueller, Peter, "Study of the Influence of Sulfuric Acid
      on the Dew Point Temperature of the Flue Gas," Chemie -
      Ing.-Tech. 31, p 345 (1959).

5.   Abel, Emil, "The Vapor Phase Above the System Sulfuric
      Acid - Water," J. Phys. Chem. 50, p 260 (1946).

6.   Gmitro, J. I., and Vermuelen, T., "Vapor-Liquid Equilibria
      for Aqueous Sulfuric Acid," Univ. of California Radiation
      Laboratory Report 10866, Berkeley, California (June 24,
      1963).

7.   Greenewalt, C. H., "Partial Pressure of Water Out of
      Aqueous Solutions of Sulfuric Acid," Ind. and Eng. Chem.
      17, pp 522-523 (May 1925).

8.   Johnstone, H. F., "An Electrical Method for the Determination
      of the Dew Point of Flue Gases," Univ. of Illinois Eng. Exp.
      Station, Circular 20 (1929).

9.   Flint, D., "The Investigation of Dew Point and Related
      Condensation Phenomena in Flue Gases," J. Inst. Fuel 21,
      p 248 (1948).

10.   Burnside, W., Marshall, W. G., and Miller, J. M., "The
      Influence of Superheater Metal Temperature on the Acid Dew
      Point of Flue Gases," J. Inst. Fuel 29, p 261 (1956).

11.   Corbett, P. F., and Flint, D., "The Influence of Certain
      Smokes and Dusts on the SO_3 Content of the Flue Gases in
      Power Station Boilers," J. Inst. Fuel 25, p 410 (1953).

12. Dooley, A., and Whittingham, G., "The Oxidation of Sulfur Dioxide in Gas Flames," _Trans. Faraday Soc._ 42, p 354 (1946).

13. Whittingham, G., "The Influence of Carbon Smokes on the Dew Point and Sulfur Trioxide Content of Flame Gases," _J. Appl. Chem._ 1, p 382 (September 1951).

14. Flint, D., and Kear, R. W., "The Corrosion of a Steel Surface by Condensed Films of Sulfuric Acid," _J. Appl. Chem._ 1, p 388 (1951).

15. Lee. G. K., Friedrich, F. D., and Mitchell, E. R., "Effect of Fuel Characteristics and Excess Combustion Air on Sulfuric Acid Formation in a Pulverized-Coal-Fired Boiler," Department of Energy, Mines, and Resources, Mines Branch (Canada), 9p (1967).

16. Friedrich, F. D., Lee, G. K., and Mitchell, E. R., "Combustion and Fouling Characteristics of Two Canadian Lignites," Department of Energy, Mines, and Resources, Mines Branch (Canada), Research Report R208, 31p (August 1969).

17. Kear, R. W., "The Influence of Carbon Smokes on the Corrosion of Metal Surfaces Exposed to Flue Gases," _J. Appl. Chem._ 1, p 393 (September 1951).

18. Black, A. W., Stark, C. F., and Underwood, W. H., "Dew Point Meter Measurements in Boiler Flue Gases," ASME Paper No. 60-WA-285 (December 1960).

19. Clark, N. D., and Childs, G. D., "Boiler Flue Gas Measurements Using a Dew Point Meter," _Trans ASME_ 87(A-1), p 8 (1965).

20. Taylor, A. A., "Relation Between Dew Point and the Concentration of Sulfuric Acid in Flue Gases," _J. Inst. Fuel_ 16, p 25 (1942).

21. Lisle, E. S. and Sensenbaugh, J. D., "The Determination of Sulfur Trioxide and Acid Dew Point in Flue Gases," _Combustion_ 36 (1), p 12 (1965).

22. Taylor, H. D., "The Condensation of Sulfuric Acid on Cooled Surfaces Exposed to Hot Gases Containing Sulfur Trioxide," _Trans. Faraday Soc._ 47, p 1114 (1951).

23. Piper, John D. and Van Vliet, H., "The Effect of Temperature Variation on Composition, Fouling Tendency, and Corrosiveness of Combustion Gas from Pulverized-Fuel-Fired Steam Generators," Trans. ASME 80, p 1251 (August 1958).

24. Fontana, M. G., Corrosion: A Compilation, The Press of Hollenback (1957).

25. Thurlow, G. G., "An Air Cooled Metal Probe for the Investigation of the Corrosive Nature of Boiler Flue Gases," J. Inst. Fuel 25, pp 252-255 and 260 (1952).

26. The Boiler Availability Committee (London), "Testing Techniques for Determining the Corrosive and Fouling Tendencies of Boiler Flue Gases," (Bulletin No. MC/316), p 18 (March 1961).

27. Southern Research Institute, Final Report on Contract CPA 70-149 (A Study of Resistivity and Conditioning of Fly Ash) to Division of Control Systems, Office of Air Programs, Environmental Protection Agency (in preparation).

28. Halstead, W. D., "The Behavior of Sulfur and Chlorine Compounds in Pulverized-Coal-Fired Boilers," J. Inst. Fuel 42, p 344 (September 1969).

29. Kear, R. W., "The Effect of Hydrochloric Acid on the Corrosive Nature of Combustion Gases Containing Sulfur Trioxide," J. Appl. Chem. 5, p 237 (May 1955).

30. Canady, B. L., "High Pressure Jetting of Regenerative Air Preheaters," Combustion, p 55 (February 1955).

31. Roddy, Charles P., "Sulfur and Air Heater Corrosion," Power Engineering, p 40 (January 1968).

32. Barkley, J. F., et al., "Corrosion and Deposits in Regenerative Air Heaters," U. S. Bureau of Mines Report of Investigations 4996, 23 pp (August 1953).

33. Brownell, Wayne E., "Analysis of Fly Ash Deposits from Hoot Lake Station," Report to The Air Preheater Corp., Wellesville, New York, 12 pp (December 1961).
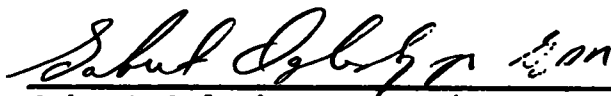
34. IGCI/ABMA Joint Technical Committee Survey, "Criteria for the Application of Dust Collectors to Coal-Fired Boilers," (April 1965).

35. Clark, Norman D., "Higher Efficiency Through Lower Stack Temperature," The Air Preheater Corp., Wellesville, New York.

36. Kear, R. W., "A Constant Temperature Corrosion Probe," J. Inst. Fuel 32, p 267 (1959).

37. Alexander, P. A., Fielder, R. S., Jackson, P. J., and Raask, E., "An Air-Cooled Probe for Measuring Acid Deposition in Boiler Flue Gases," J. Inst. Fuel 33, p 31 (1960).

38. CERL (private communication).

Respectfully submitted:

Grady B. Nichols, Head
Particulate Control Section

John P. Gooch
Research Chemical Engineer

Approved:

Sabert Oglesby, Jr., Director
Engineering Research

Birmingham, Alabama
July 6, 1972
2500-XIII
SORI-EAS-74-344

APPENDIX 1: LIST OF SYMBOLS

APPENDIX 2: COMPUTER PRINTOUT

APPENDIX 1.
LIST OF SYMBOLS

A = Collection electrode area or specific area of an object
C = Constant or coefficient
C_p = Current to charge particulate
D = Dust concentration or diffusion coefficient
E_0, E_a, E_p = Electric field, starting, charging, at collecting plate
F = Force, Farad
K = Aspect ratio, constant
$L_p L_w$ = Length of precipitator or corona wire
N = Densities of various quantities - number per units volume
P = Perimeter, probability
Q = Quality factor or quantity
R = Radius - specific dimension
S = Surface area per gm of dust, circumference
V = Voltage, ionization potential
W = Weight of dust
X = Fraction of molecules ionized.

a = Radius corona wire or dust particle
b = Radius collection pipe, wire and pipe precipitator
d = Air density, relative
e = Electronic charge
f = Wire roughness factor, reentrainment factor
h = Height of plates, velocity head
i = Current, per unit length
j = Current, per unit area
k = Boltzmann's constant, coefficient
$\ln$ = Natural logarithm
n = Number of items per unit time
p = Velocity pressure
q = Electrical charge
r = Radius or reduction factor
t = Time , thickness
v = Velocity
v_g = Volume flow rate
w = Migration velocity or precipitation rate parameter

LIST OF SYMBOLS (Continued)

α = Ionization coefficient, acceleration, erosion coefficient
β = Constant erosion coefficient
γ = Secondary emission coefficient
δ = Boundary layer thickness
Δ = Increment
$\varepsilon, \varepsilon_0$ = Relative dielectric constant, permittivity of free space
η = Collection efficiency, viscosity
μ = Mobility
ρ = Resistivity, space charge density, gas density
σ = Conductivity
Σ = Summation
τ = Time constant
χ = Concentration ratio
∇^2 = Laplacian operator

APPENDIX 2.
COMPUTER PRINTOUT FOR
ELECTROSTATIC PRECIPITATOR MODEL

.

PAGE   1   *ESP*

// JOB   *ESP*

```
LOG DRIVE     CART SPEC     CART AVAIL    PHY DRIVE
   0000          0002          0002          0002
                               0001          0001


V2 M10    ACTUAL 16K    CONFIG 16K

// FOR
*LIST SOURCE PROGRAM
*ONE WORD INTEGERS
*IOCS(CARD,1132 PRINTER,PLOTTER)

C*****************************************************************************
C*      ELECTROSTATIC PRECIPITATOR MODEL.                                   *
C*****************************************************************************
C          PRECIPITATOR PARAMETERS
C
C
C          A  = COLLECTION AREA   FT2 --- M2
C          VG = GAS FLOW RATE   FT3/SEC --- M3/SEC
C          VO = APPLIED VOLTAGE   VOLTS --- VOLTS
C          TC = TOTAL CURRENT   AMPS --- AMPS
C          DL = DUST LOAD   GR/FT3 --- KG/M3
C          WL = LENGTH OF CORONA WIRE   FT --- M
C          AC = CORONA WIRE RADIUS   IN --- M
C          B  = PLATE SPACING   IN --- M
C          PL = LENGTH OF PRECIPITATOR   FT --- M
C          V  = GAS VELOCITY   FT/SEC --- M/SEC
C        ETAO = DESIGN EFFICIENCY (STATED EFF)
C          DD = DUST DENSITY   KG/M3
C         RHO = DUST RESISTIVITY   OHM-M
C          RF = ROUGHNESS FACTOR-CORONA WIRE
C         DEL = RELATIVE AIR DENSITY
C          W  = WEIGHT OF DUST   KG
C          U  = MOBILITY   M2/(VOLT-SEC)
C         EPS = DIELECTRIC CONSTANT(RELATIVE)
C          CD = CURRENT DENSITY   AMPS/M2
C          E  = CHARGE ON AN ELECTRON   COU
C          ET = ELECTRIC FIELD IN DEPOSIT   VOLT/M
C          CL = CURRENT PER  M. OF CORONA WIRE   AMP/ M
C          EO = STARTING ELECTRIC FIELD   VOLTS/M
C          NS = NUMBER OF PARTICLE SIZES
C         FID = FREE ION DENSITY   NUMBER/M3
C         VIS = GAS VISCOSITY   KG/(M-SEC)
C          NF = NO OF .3 METER INCREMENTS IN PL METERS OF PRECIPITATOR
C          DV = DUST VOLUME
C        ZMFP = MEAN FREE PATH
C        FPLT = ELECTRIC FIELD AT PLATE
C         CCF = CUNNINGHAM CORRECTION FACTOR
C        AFID = AVERAGE FREE ION DENSITY
C        PSAT = FRACTION OF SATURATION CHARGE
C         ZMD = INTERPOLATED MMD OF COLLECTED DUST
C       ROVRI = RATIO OF TOTAL TO IONIC SPACE CHARGE
C        ZMDL = INTERPOLATED MMD OF EFFLUENT DUST
C          WT = WEIGHT OF DUST COLLECTED IN EACH INCREMENT
C        FRRI = F(ROVRI)
```

```
PAGE   2    *ESP*
C        DER = D(ERAVG)/D(ROVRI)
C        DFRI = D(FRRI)/D(ROVRI) * F'(ROVRI)
C        DRRI = -F(ROVRI)/F'(ROVRI)
C
C
C
C    ITL(K) = NAME OF PLANT - IDENTIFICATION
C
C      DW(I) = AMOUNT OF MATERIAL REMOVED EACH INCREMENT
C
C   DIAM(J) = DIAMETER OF PARTICLES   M
C   PCNT(J) = PERCENTAGE OF PARTICLES OF DIAM(J)
C    VOL(J) = VOLUME PER PARTICLE   M3
C    XNO(J) = NO. PER   M3 EACH SIZE RANGE
C   QSAT(J) = SATURATION CHARGES
C      Q(J) = CHARGE ON EACH PARTICLE
C    ONO(J) = INITIAL NO. OF PARTICLES IN EACH SIZE RANGE
C    DXS(J) = TOTAL NO. OF PARTICLES REMOVED IN EACH SIZE RANGE
C    RAD(J) = RADIUS OF PARTICLES   M
C
C
C
C
      DIMENSION DIAM(11),VOL(11),XNO(11),QSAT(11),Q(11),
     $ ONO(11), DXS(11), PCNT(11), RAD(11)
      DIMENSION DW(27), ITL(40)
      DIMENSION WS(11)
      DIMENSION WSL(20),CCF(20)
C
C    CONSTANTS
C
      PI = 3.1415927
      E = 1.6E-19
      U = 2.2E-4
      EPS = 100.
      RF=0.90
      EPSO = 8.85E-12
      VIS = 1.8E-5
C
C
      READ(2,5) NS,(DIAM(I),I=1,NS)
    5 FORMAT(I2/(10F8.0) )

      DO 3 I = 1,NS
      DIAM(I)=DIAM(I)*1.E-06
      RAD(I) = DIAM(I) / 2.
    3 CONTINUE

C
      WRITE(3,17)
   17 FORMAT('1')

C
      READ(2,4) (PCNT(I),I=1,NS)

      DO 7412 I = 1,NS
      PCNT(I) = PCNT(I) * 1.E-2
 7412 CONTINUE
```

```
PAGE   3    *ESP*

 1000 READ(2,7) ITL
    7 FORMAT(40A2)
      LK=0


      READ(2,4)A,VG,VO,TC,DL,WL,AC,B,PL,V,ETAO,DD,RHO,X,TEMP,P
    4 FORMAT(10F8.0)

      PL = PL * 0.305
      NF = PL / .3 + .5
      IF( NF ) 9999,9999,8

C
C         CONVERSION
C
    8 A = A * 9.3E-02
      VG = VG * 4.73E-4
      DL = DL * 2.29E-03
      WL = WL * 0.305
      AC = AC * 2.54E-2
      B  = B * 2.54E-2
      RHO = RHO * 10.**(X-2.)
      DV = DL / DD
      V = V * 0.305

      WRITE(3,3010) ITL
 3010 FORMAT('0',40A2/)

C
      T = 1. / V
C
C
      DO 1 I = 1 ,NS
      VOL(I) = PCNT(I) * DV
    1 CONTINUE
C
C COMPUTE WEIGHT OF DUST
C
      W = DL * VG
C
C COMPUTE CURRENT DENSITY
C
      CD = TC / A
C
C COMPUTE ELECTRIC FIELD IN DEPOSIT
C
      ET = CD * RHO
C
C COMPUTE CURRENT PER  M. OF CORONA WIRE
C
      CL = TC / WL
C
C COMPUTE STARTING ELECTRIC FIELD
C
      PO=1.0
      TO=293.*1.8
      TEMP=TEMP+459.
      DEL=(TO/TEMP)*(P/PO)
```

```
PAGE   4    *ESP*

C CALCULATE MEAN FREE PATH
      TDK=TEMP/1.8
      ZMV=8.205E-05*TDK/P
      ZMFP=ZMV/(1.414*PI*(1.6E-19)*(6.02E+23))
      EO = 3.E6 * RF * DEL * (1.+.03  *(DEL/AC)**.5)
C
C   COMPUTE VALUE OF EXPONENT IN DEUTSCH EQUATION FOR THE STATED EFF.
C
  305 X=ALOG(100./(100.-ETAO))
C
      DO 9 I = 1, NS
      DXS(I) = 0.0
      XNO(I) = VOL(I)/ ( 4./3. * PI * RAD(I)**3 )
      ONO(I) = XNO(I)
    9 CONTINUE
C
C
C   COMPUTE EFFICIENCY PER 0.3 METER INCREMENT
C
      ETAPF = 1.-EXP(-0.3*X/PL)
C
C   COMPUTE AMOUNT OF MATERIAL REMOVED PER INCR.ON A TOTAL WEIGHT BASIS
C
      SW = 0.0
C
      DO 700 I=1,NF
      DW(I) = (W - SW) * ETAPF
      SW = SW + DW(I)
  700 CONTINUE
C
C        PRINT INPUT PARAMETERS
      IF(LK)111,111,160
C
  111 WRITE(3,10)PL,NF,A
   10 FORMAT(' PPR LENGTH =',E11.4,1X,'METERS',T41,'NO. OF INCREMENTS ='
     $,I3,T81,'COLLECTION AREA =',E11.4,1X,'M2')
C
      WRITE(3,11) VG, VO, TC
   11 FORMAT(' GAS FLOW RATE =',E11.4,' M3/SEC',T41,'APPLIED VOLTAGE =',
     $E11.4,' VOLTS',T81,'TOTAL CURRENT =',E11.4,' AMPS' )
C
      WRITE(3,12) DL, WL, AC
   12 FORMAT(' DUST LOAD =',E11.4,' KG/M3',T41,'CORONA WIRE LENGTH =',
     $ E11.4,' M',T81,'CORONA WIRE RADIUS =',E11.4,' M' )
C
      WRITE(3,13) B, V, ETAO
   13 FORMAT(' PLATE SPACING =',E11.4,' M',T41,'GAS VELOCITY =',E11.4,
     $'  M/SEC',T81,'DESIGN EFFICIENCY =',F6.2,' PERCENT')
C
      WRITE(3,14) DD, RHO, DV
   14 FORMAT(' DUST DENSITY =',E11.4,' KG/M3',T41,'DUST RESISTIVTY =',
     $ E11.4,' OHM-M',T81,'DUST VOLUME =',E11.4,' M3/M3')
C
      WRITE(3,15) W, CD, ET
   15 FORMAT(' DUST WEIGHT =',E11.4,' KG/SEC',T41,'CURRENT DENSITY =',
     $E11.4,' AMP/M2',T81,'DEPOSIT E FIELD =',E11.4,' VOLT/M' )
C
      WRITE(3,16) CL,EO,DEL,RF
```

```
PAGE  5    *ESP*
   16 FORMAT(' CURRENT/M =',E11.4,' AMP/M',T41,'STARTING E FIELD =',
     1 E11.4,' VOLT/M',T81,'REL. AIR DENSITY=',F7.4,
     2/' ROUGHNESS FACTOR=',F6.3)
C
C
  160 X=ETAPF*100.
      WRITE(3,161)X
  161 FORMAT(/' INPUT EFFICIENCY/INCREMENT=',F6.2)
      WRITE(3,4322)
 4322 FORMAT(//T5,'ROVRI',T16,'ERAVG',T31,'EPLT',T43,'PSAT',T53,'TOAVG',
     1T63,'TEFF',T76,'MMD',T89,'WEIGHT',T101,'SECTION NO.'/)
C********************************************************************
C
C     START   INCREMENTAL ANALYSIS OF PRECIPITATOR
C
C********************************************************************

      LK=1
      PSAT = 0.0
      ZWT=0.
      ZCA=(12.*PI*EPSO*EPS)/(EPS+2.)
      ROVRI=10.
      DO 3000 I=1,NF
C CONVERGE ON CORRECT ROVRI USING NEWTON'S METHOD
      ZC=200.*(DW(I)/W)*(FLOAT(NF)/TC)*VG
  500 CALL EVSR(AC,EO,CL,U,B,ERAVG,DER,ROVRI,EPSO,PI)
      DFRI=0.
      SUM=0.
      DO 1300 L=1,NS
      QSAT(L)=ZCA*ERAVG*1.4*RAD(L)**2
      SUM=SUM+QSAT(L)*XNO(L)
 1300 DFRI=DFRI+(ZC*ZCA*DER*1.4*RAD(L)**2)*XNO(L)
      DFRI=DFRI-1.0
      FRRI=ZC*SUM+1.0-ROVRI
      DRRI=-FRRI/DFRI
      ROVRI=ROVRI+DRRI
      TEST=0.05
      IF(ABS(DRRI)-TEST)510,500,500
  510 FID=CD/(E*U*ERAVG)
C   COMPUTE AVERAGE CHARGING TIME CONSTANT
C
      RATIO=1./ROVRI
      AFID=FID*RATIO
      TOAVG = (4. * EPSO)/(AFID*E*U)
C
C   COMPUTE CHARGING TIME CONSTANT IN THIS INCREMENT
C
C
      TEFF=(TOAVG*PSAT)/(1.-PSAT)
C
      ZL=0.305
      PSAT=1./(1.+((TOAVG)/(TEFF+T*ZL)))
C
C
C********************************************************************
C
C         START PARTICLE SIZE LOOP
C
```

```
C***********************************************************************
C
      WT = 0.
      DO 2900 J = 1. NS
C
C   COMPUTE CHARGE ON EACH PARTICLE AFTER ONE INCREMENT OF TRAVEL
C
      Q(J) = QSAT(J) * PSAT
C
C
C
C
C   COMPUTE MIGRATION VELOCITY FOR EACH SIZE RANGE
C
      A2EO2=AC*AC*EO*EO
      B2=B*B
      AC2=AC*AC
      EPLT=((1.-(AC2/B2))*ROVRI*CL/(2.*PI*EPSO*U)+A2EO2/B2)**.5
      EMV=(Q(J)*EPLT)/(6.*PI*RAD(J)*VIS)
      CCF(J)=1.+0.86*ZMFP/RAD(J)
      EMV=CCF(J)*EMV
C
C   COMPUTE EFFICIENCY FOR EACH SIZE RANGE
C
      X = (-A*EMV*0.3) / (VG*PL)
C
      EFF =  1. - EXP( X )
C
C   COMPUTE NUMBER OF PARTICLES REMOVED IN EACH SIZE RANGE
C
      DXNO = XNO(J) * EFF
      DXS(J) = DXS(J) + DXNO
C
C   SUM WEIGHT OF PARTICLES REMOVED
C
      WS(J)=DXNO*(1.33333*PI*RAD(J)**3)*DD
      WT=WT+WS(J)
C
C
C   COMPUTE NEW SIZE DISTRIBUTION INTO NEXT SECTION
C
      XNO(J) = XNO(J) - DXNO
C
C
C
 2900 CONTINUE
      ZWT=ZWT+WT
C
C   CALCULATE MMD AND WEIGHT COLLECTED FOR EACH INCREMENT
      ZTM=0.
      DO 2901 J=1,NS
      ZTM=ZTM+WS(J)
      CZA=ZTM/WT
      IF(CZA-0.5)2901,2901,2902
 2901 CONTINUE
 2902 CZB=(ZTM-WS(J))/WT
      TL1=CZA-CZB
      TL2=0.50-CZB
      KJ=J-1
```

PAGE   7   *ESP*

```
         IF(KJ)2910,2910,2911
 2910 ZMD=DIAM(J)
         GO TO 2912
 2911 ZMD=DIAM(KJ)+(TL2/TL1)*(DIAM(J)-DIAM(KJ))
 2912 WRITE(3,4323)ROVRI,ERAVG,EPLT,PSAT,TOAVG,TEFF,ZMD,WT,I
 4323 FORMAT(T5,F6.3,T13,E11.4,T27,E11.4,T41,F7.4,T51,F7.4,T60,F7.3,T71,
     1E11.4,T86,E11.4,T105,I2)
 3000 CONTINUE
C
         ETC=(ZWT/DL)*100.
         DIFF=ETC-ETAO
         DIFF=ABS(DIFF)
         IF(DIFF-0.5)60,300,300
  300 ETAO=ETC
         GO TO 305

C        PRINT DIAM., PERCENT, AND EFFICIENCY FOR EACH SIZE RANGE

   60 WRITE(3,18)
   18 FORMAT('0PARTICLE SIZE RANGE STATISTICS'/)
         WRITE(3,19)
   19 FORMAT(5X,'DIAMETER-METERS',5X,'PERCENT OF TOTAL',4X,'EFFICIENCY'
     1,7X,'CCF')
C
         X = 0.0

         DO 2990 I=1,NS
         EFESR     = DXS(I) / ONO(I)
         X = X + EFESR * PCNT(I)
         XY=PCNT(I)*100.
         XEP=EFESR*100.
          WRITE(3,2291)DIAM(I),XY,XEP,CCF(I)
 2291 FORMAT(2X,E17.7,T29,F10.6,T45,F10.6,T61,F7.4)
         SL=(1.0-EFESR)*ONO(I)
         WSL(I)=SL*(1.33333*PI*RAD(I)**3)*DD
 2990 CONTINUE

         X = X * 100.
         WRITE(3,2292) ETAO, X
 2292 FORMAT('0',4X,'EFFICIENCY - STATED = ',F5.2,5X,'COMPUTED =' ,F6.2
     S,5X,'CONVERGENCE OBTAINED')
C
C
C CALCULATE MMD OF EFFLUENT
         WTL=(1.-(X/100.))*DL
         ZTM=0.
         DO 2995 I=1,NS
         ZTM=ZTM+WSL(I)
         CZA=ZTM/WTL
         IF(CZA-0.5)2995,2995,2996
 2995 CONTINUE
 2996 CZB=(ZTM-WSL(I))/WTL
         TL1=CZA-CZB
         TL2=0.50-CZB
         KJ=I-1
         IF(KJ)2980,2980,2981
 2980 ZMDL=DIAM(I)
         GO TO 2982
```

PAGE   8   *ESP*

```
 2981 ZMDL=DIAM(KJ)+(TL2/TL1)*(DIAM(I)-DIAM(KJ))
 2982 WRITE(3,2997)ZMDL
 2997 FORMAT(5X,'MMD OF EFFLUENT=',E11.4//)
C
      GO TO 1000

 9999 CALL EXIT
      END
```

FEATURES SUPPORTED
 ONE WORD INTEGERS
 IOCS

CORE REQUIREMENTS FOR
 COMMON   0 VARIABLES   566 PROGRAM   2150

END OF COMPILATION

// XEQ

PAGE   1   *EVSR*

// JOB   *EVSR*

LOG DRIVE   CART SPEC   CART AVAIL   PHY DRIVE
   0000   0002   0002   0002
                               0001   0001

V2 M10   ACTUAL 16K   CONFIG 16K

// DUP

*DELETE   EVSR
CART ID 0002   DB ADDR 20ED   DB CNT   0011

// FOR
*ONE WORD INTEGERS
*LIST SOURCE PROGRAM
```
C*********************************************************************
C*    THIS SUBROUTINE CALCULATES ELECTRIC FIELD AND DE/D(ROVRI) AS    *
C*    A FUNCTION OF RADIUS. OUTPUT IS A SPACE AVERAGE.                 *
C*********************************************************************
      SUBROUTINE EVSR(AC,EO,CL,U,B,EAVG,DER,ROVRI,EPSO,PI)
      A2EO2=AC*AC*EO*EO
      EAVG=0.0
      DER=0.0
      R=AC
      DR=(B-4.*AC)/50.
      J=0
      AC2=AC*AC
      ZKL=ROVRI*CL/(2.*PI*EPSO*U)
      DO 100 I=1,200
      R2=R*R
      ZKM=(1.-(AC2/R2))*ZKL
      E=(ZKM+A2EO2/R2)**.5
      DET=0.5*(1./E)*(ZKM/ROVRI)
      IF(R-B)45,45,90
   45 EAVG=EAVG+E
      DER=DER+DET
      R=R+DR
      J=J+1
  100 CONTINUE
   90 EAVG=EAVG/FLOAT(J)
      DER=DER/FLOAT(J)
      RETURN
      END
```

FEATURES SUPPORTED
 ONE WORD INTEGERS

CORE REQUIREMENTS FOR EVSR
 COMMON   0 VARIABLES   22 PROGRAM   218

RELATIVE ENTRY POINT ADDRESS IS 0025 (HEX)

END OF COMPILATION

// DUP

TECHNICAL REPORT DATA
(Please read Instructions on the reverse before completing)

1 REPORT NO EPA-650/2-74-132	2	3. RECIPIENT'S ACCESSION NO.
4 TITLE AND SUBTITLE An Electrostatic Precipitator Performance Model		5 REPORT DATE July 1972
		6. PERFORMING ORGANIZATION CODE
7 AUTHOR(S) Grady B. Nichols and John P. Gooch		8 PERFORMING ORGANIZATION REPORT NO. SORI-EAS-74-344
9 PERFORMING ORGANIZATION NAME AND ADDRESS Southern Research Institute 2000 Ninth Avenue South Birmingham, Alabama 35205		10. PROGRAM ELEMENT NO. 1AB012; ROAP 21ADJ-026
		11. CONTRACT/GRANT NO. CPA 70-166
12. SPONSORING AGENCY NAME AND ADDRESS EPA, Office of Research and Development NERC-RTP, Control Systems Laboratory Research Triangle Park, NC 27711		13. TYPE OF REPORT AND PERIOD COVERED Final; Through 7/6/72
		14. SPONSORING AGENCY CODE

15 SUPPLEMENTARY NOTES

16. ABSTRACT The report gives results of: a review of the design details of a pilot precipitator; and particle concentration profile studies. It also reviews discussions of resistivity measurement and correlations between resistivity and precipitator operation. Objectives of the study covered by the report were: to extend the precipitator model to include factors not included in the first model influencing its accuracy; to design and build a pilot precipitator for further studies of the factors influencing precipitation processes; to review limitations to precipitator performance due to back corona and sparking; to investigate the particle concentration profile in the interelectrode space; to obtain data from both field and pilot plant tests to attempt to verify the computer model; and to analyze potential for optimizing precipitator performance by design or operating modifications.

17. KEY WORDS AND DOCUMENT ANALYSIS

a DESCRIPTORS	b.IDENTIFIERS/OPEN ENDED TERMS	c. COSATI Field/Group
Air Pollution Mathematical Models Electrostatic Precipitators Resistance Measurement	Air Pollution Control Stationary Sources	13B 12A 14B

18. DISTRIBUTION STATEMENT Unlimited	19. SECURITY CLASS *(This Report)* Unclassified	21. NO OF PAGES 184
	20. SECURITY CLASS *(This page)* Unclassified	22 PRICE

EPA Form 2220-1 (9-73)